TECHNICAL MEMORANDUM

NUREG/CR-2773
ANL-CT-82-14

COMMIX-1A THREE-DIMENSIONAL IN-VESSEL SIMULATION OF THE FFTF TRANSIENT THERMAL HYDRAULICS

by

S. P. Vanka, H. M. Domanus, and W. T. Sha

Prepared for the

Office of Nuclear Regulatory Research
U. S. NUCLEAR REGULATORY COMMISSION
under Interagency Agreement DOE 40-550-75

The facilities of Argonne National Laboratory are owned by the United States Government. Under the terms of a contract (W-31-109-Eng-38) among the U. S. Department of Energy, Argonne Universities Association and The University of Chicago, the University employs the staff and operates the Laboratory in accordance with policies and programs formulated, approved and reviewed by the Association.

MEMBERS OF ARGONNE UNIVERSITIES ASSOCIATION

The University of Arizona
Carnegie-Mellon University
Case Western Reserve University
The University of Chicago
University of Cincinnati
Illinois Institute of Technology
University of Illinois
Indiana University
The University of Iowa
Iowa State University
The University of Kansas
Kansas State University
Loyola University of Chicago
Marquette University
The University of Michigan
Michigan State University
University of Minnesota
University of Missouri
Northwestern University
University of Notre Dame
The Ohio State University
Ohio University
The Pennsylvania State University
Purdue University
Saint Louis University
Southern Illinois University
The University of Texas at Austin
Washington University
Wayne State University
The University of Wisconsin-Madison

Available from

GPO Sales Program
Division of Technical Information and Document Control
U. S. Nuclear Regulatory Commission
Washington, D.C. 20555

and

National Technical Information Service
Springfield, Virginia 22161

ARGONNE NATIONAL LABORATORY
9700 South Cass Avenue
Argonne, Illinois 60439

ERRATUM FOR

NUREG/CR-2773
ANL-CT-82-14

COMMIX-1A THREE-DIMENSIONAL IN-VESSEL SIMULATION OF THE FFTF TRANSIENT THERMAL HYDRAULICS

by

S. P. Vanka, H. M. Domanus, and W. T. Sha

The attached figure should replace Fig. 17f on page 79.

July 1982

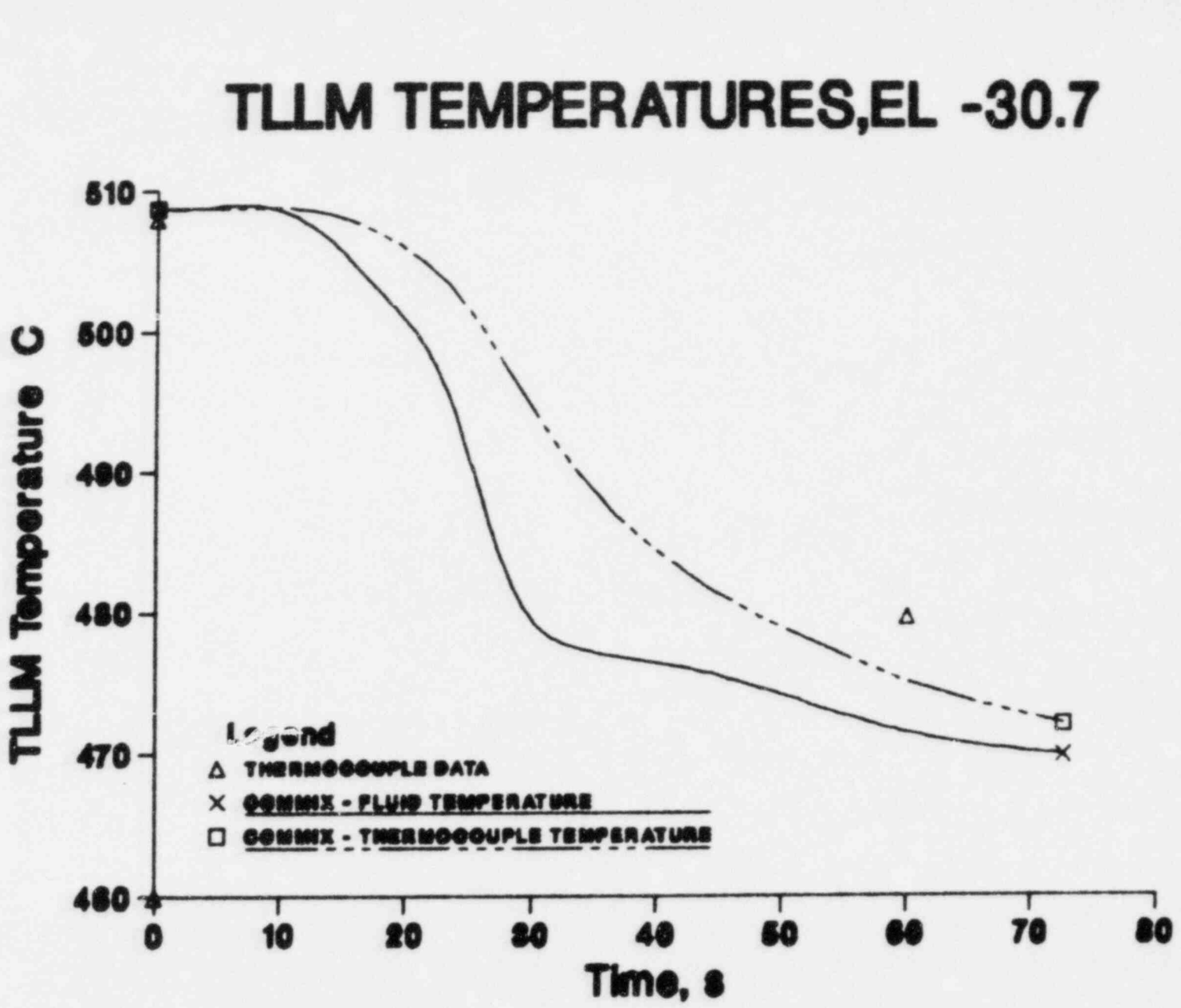

Fig. 17f. Comparison of Calculated and Measured TLLM Temperatures at Elevation -30'7" (-9.32m)

TECHNICAL MEMORANDUM

NUREG/CR-2773
ANL-CT-82-14
(Distribution
Code: R7)

ARGONNE NATIONAL LABORATORY
9700 South Cass Avenue
Argonne, Illinois 60439

COMMIX-1A THREE-DIMENSIONAL IN-VESSEL SIMULATION OF THE FFTF TRANSIENT THERMAL HYDRAULICS

by

S. P. Vanka, H. M. Domanus, and W. T. Sha

Components Technology Division

May 1982

Prepared for the
Division of Reactor Safety Research
Office of Nuclear Regulatory Research
U. S. NUCLEAR REGULATORY COMMISSION
Washington, D. C. 20555
under Interagency Agreement DOE 40-550-75
NRC FIN No. A2045

COMMIX-1A THREE-DIMENSIONAL IN-VESSEL SIMULATION OF THE FFTF TRANSIENT THERMAL HYDRAULICS

by

S. P. Vanka, H. M. Domanus, and W. T. Sha

Abstract

The three-dimensional flow and temperature fields occurring in the FFTF during a flow transient followed by a reactor scram have been simulated by the COMMIX-1A computer code. The transient simulated corresponds to the tests conducted at the Hanford Engineering and Development Laboratory. The COMMIX-1A code employs the porous media formulation in which the concepts of volume porosity, surface permeability, distributed resistance, and distributed heat source are used to model a flow domain with internal structures. The governing equations for conservation of mass, momentum, and energy are solved as a boundary-value problem in space and as an initial-value problem in time. The present report presents the calculated results for the steady-state reactor full-power operation and for a transient from full flow down to natural circulation combined with a power scram. The results are compared with experimental measurements, where applicable. Thermal stratification is observed in the upper plenum, together with eddy-type recirculation. In addition, we observe that the core flow is strongly coupled with the flow phenomena in the upper plenum. Comparisons of measured flow rates, temperatures exiting the core, and temperatures in the upper plenum with experimental data have been satisfactory.

NRC FIN #

A2045

Title

3-D Time-dependent Code Development

TABLE OF CONTENTS

List of Tables

Abbreviations used in this Report

FOTA	Fuel Open Test Assembly
TLIM	Temperature and Liquid Level Monitor
PTP	Proximity Test Plug

List of Figures

EXECUTIVE SUMMARY

In the present work, the steady-state and transient in-vessel thermal hydraulics of the FFTF have been simulated by the use of the COMMIX-1A computer code. The transient simulated is a flow coast down from full flow to natural circulation in combination with a reactor scram from full power. The COMMIX-1A computer code is a general-purpose program which solves the transient three-dimensional forms of the conservation equations for mass, momentum, and energy. The porous-medium formulation is employed through the concepts of volume porosity, surface permeability, distributed resistances, and distributed heat sources. The effects of heat capacity of internal structures are explicitly taken into account. The differential forms of the equations are expressed as finite differences and are solved by an iterative technique.

The geometrical details and the flow conditions pertinent to the FFTF operation have been taken from the FFTF design documents and from material supplied by Hanford Engineering Development Laboratory. A 120° sector of the vessel was simulated. The results of the calculations have been compared with the measured data. The quantities compared are the exit temperatures and flows from the fuel and reflector assemblies, the temperatures in the upper plenum as measured by the Temperature and Liquid Level Monitors (TLLMs), and the temperature at the Proximity Test Plug (PTP). The calculations compare satisfactorily with the data.

The important observations from this study are the complex flow and temperature patterns during the transient and the thermal stratification in the upper plenum. It is seen that the hot fluid is trapped in the top portion of the plenum, and the cold fluid (after the power shutdown) bypasses the hot fluid, flowing directly from the core exit to the outlet. Because of this, the thermal liner of the vessel walls is subjected to a large temperature gradient. We also observe that the flow from the core is strongly coupled with the thermal hydraulics of the upper plenum.

1. Introduction

In an earlier report [1], we considered the steady-state behavior of the in-vessel thermal hydraulics of the Fast Flux Test Facility. The COMMIX-1A computer code [2] was used to model the three-dimensional flow geometry, and the governing fluid flow and energy equations were solved with a finite-difference technique. The complete details and the capabilities of this computer code have been reported earlier by Sha et. al [2,3]. Briefly, the computer code solves the transient three-dimensional Navier-Stokes and energy equations for single-phase flows in Cartesian or cylindrical polar-coordinate systems. It also has a unique way of treating internal obstacles and porous objects through the concepts of surface permeability and volume porosity. The computer code also models the thermal-structure response to temperature and flow transients.

In the present study, we have considered the transient in-vessel thermal hydraulics of the FFTF, following a pump trip from full flow and a reactor scram from 100 % power. Such a test was recently conducted at Westinghouse Hanford Engineering and Development Laboratory [4] on the commissioned FFTF reactor. The intent of the present study has been to calculate the flow and temperature fields during such a transient, with special emphasis being placed

on a) thermal stratification in the plenum; b) prediction of maximum coolant temperature, and thus cladding temperature, in the core; and, c) inclusion of the thermal inertia of the core structures and other solid objects placed in the core and plena. Further, we have considered the entire in-vessel geometry including the inlet plenum, the reactor core, the leakage path, the suppression plate, and the upper plenum.

In the following sections, first, a brief description of the reactor geometry is given. A brief description of the COMMIX-1A code specifying its capabilities is given in Section 3. Section 4 describes the steady-state results, and compares of calculated values with experimental data, where applicable. Section 5 describes the results of the transient. The calculated temperatures at the exit of the FOTA (Fuel Open Test Assembly), a typical reflector, and the TLLMs have been compared with data measured by Hanford Engineering Development Laboratory. The details of the input data and of the geometry are discussed in the appendices.

The present report is basically an extension of our earlier work [1] with some minor changes. First, we consider only a 120° sector, which makes the computations faster, without loss in essential generality of the results. Second, we have used a more advanced version (version 8.0) of COMMIX-1A. We have, in addition, modified the flow resistances in the reflector region based on new measured temperature data available in the reflector region from HEDL [5]. The transient results are, however, presented for the first time.

2. Description of the Geometry

2.1 General

The complete details of the FFTF system have been earlier documented in the design reports of FFTF. The FSAR (Final Safety Analysis Report)[6] also contains a description of the reactor vessel and the complete plant. The following material has been excerpted from the relevant sections of the FSAR, with appropriate changes for consistency and sequence with the rest of the material in this report.

The primary function of the reactor is to provide the capability of testing candidate materials for the fast breeder program in environments approximating those to be found in commercial fast breeder power reactors. The core provides the neutron flux, establishes the power density and operating temperature, and houses test specimens.

The reactor system components (Fig. 1) are:

1. Driver Fuel Assembly

2. Nuclear Control Components
   a. Control Rod Components
   b. Control Rod Drive Mechanism (CRDM)
   c. CRDM Shield Plug and Enclosure Cap
   d. Control Rod Disconnect Driveline
   e. Absorber Assembly

3. Open Test Assemblies

4. Core Special Assemblies
   a. In-Core Shim Assembly
   b. Simulated Core Assembly
   c. Materials Surveillance Assembly

5. Radial Reflector

6. Core Radial Restraint

7. Radial Shield

8. Core Support Structure

9. Instrument Tree

10. Low Level Flux Monitor (Mechanical)

11. Baffle/Liner Interface Seal

12. Horizontal Baffle

The assembly of these components within the reactor vessel is shown in Fig. 1. The initial core has an active height of 0.9144 m (36 in.), a volume of 1.034 m^3, and at the design power of 400 MWt has a peak flux of 7 x 10^{15} n/cm^2-sec. The average fuel burnup is 45,000 MWd/MT (and maximum burn up = 80,000 MWd/MT) at nominal coolant temperatures of 315.5°C (600°F), inlet, and 482.2°C (900°F), core outlet. The initial core design is capable, also, of operating at nominal core coolant inlet and outlet temperatures of 414°C (777°F) and 580.5°C (1077°F), respectively, at reduced burnup.

The driver fuel is composed of mixed plutonium-uranium oxides (PuO_2/UO_2), with compositions of 22.43 and 27.37 wt% Pu/(U + Pu) for the inner and outer enrichment zones, respectively. Natural uranium is used, and the plutonium used has a fissile content of about 88 wt% (Pu-239 + Pu-241). Future reload driver fuel may deviate from these compositions because of changing operational requirements and feed-material assays.

2.2 Core Arrangement

The reactor core consists of a hexagonal array of vertical elements arranged as shown on the Core Map (Fig. 2). The initial active core, which consists of 91 positions, is surrounded radially by a reflector region, containing three rows of reflector assemblies with additional locations available in the inner row (Row 7, where fixed shim or additional movable control-rod assemblies may be inserted in the future), and the radial shield region, which is composed of shield segments. All these components are supported and located by the core support structure. The core restraint mechanisms, which are mounted on the core barrel, position the core and control-core configuration including the reflector region. In-vessel storage for irradiated fuel assemblies and other components is provided between the core-support-structure barrel and the reactor-vessel thermal liner. The instrument trees are hung from plugs in the vessel head and laterally supported by the core-support-structure barrel.

Each of the core-basket lattice positions that comprise the hexagonal core and reflector regions have the same nominal lattice spacing of 0.120 m (4.730 in.) (room temperature). The available eight test positions are located in a Y-shaped pattern of three radial corridors extending from the center of the flats of the hexagonal arrangement. Assemblies in these corridors extend to the reactor head for contact instrumentation (open test assemblies) and optional sodium coolant inlet/outlet connections to a closed loop system (closed loop in-reactor assemblies). Other driver fuel positions in the core may also be used as test positions. Contact instrumentation, however, is not possible in these positions. The trisected design is compatible with the refueling system, which uses three in-vessel handling machines, each of which services a 120° segment of the core.

2.3 Thermal/Hydraulic Characteristics

2.3.1 Core Assembly Orificing

Core assembly orificing is used to optimize thermal performance and to limit the maximum cladding temperature. Cladding temperatures are reduced by increasing the flow in the high-power assemblies above the average and reducing the flow in the lower-power assemblies below the average while maintaining the same total core flow rate. The method used to orifice the FFTF fuel assemblies adjusts the flow rate so that the maximum steady-state cladding inside temperature which occurs in each orificing zone is as nearly equal as possible.

The three orificing zones used are:

Hexagonal Rows 1 to 4 of the core

Hexagonal Row 5

Hexagonal Row 6

Orificing is also used to regulate the flow to the control and safety rods, fixed shims, reflectors, shielding, and vessel thermal liner.

2.3.2 Coolant Flow Path (Fig. 3)

The coolant flow enters the reactor vessel through three 0.4064-m (16-in.)-ID inlet nozzles. The nozzles are spaced 120° apart and are located near the bottom of the reactor vessel. From the nozzles, the coolant enters a large inlet plenum, where the coolant is mixed before flowing through a flow-distribution system to the reactor core and outlet plenum. Finally, the coolant exits through three 0.711-m (28-in.)-ID outlet nozzles, which are spaced 120° apart.

2.3.3 Outlet Plenum

To ensure that fuel assemblies are fully immersed in sodium at all times while in the reactor vessel, the outlet plenum has been made deep enough so that the distance from the top of the core to the pool surface, 4.877 m (over 16 ft.), is greater than the sum of the length of a fuel assembly, 3.66 m (12 ft.), and the clearances needed to handle an assembly. The

design requirements placed on the outlet plenum have led to a plenum design which contains a large volume of sodium. This large volume of sodium ensures that thermal transients at the core outlet will be significantly attenuated before they affect the vessel outlet nozzles.

In addition, the outlet plenum design meets two requirements: 1) Cover-gas entrainment is limited by the use of a horizontal baffle below the coolant surface, and 2) adequate coolant volume is provided to fill the guard vessel in the event of a sodium leak, while still maintaining the reactor-coolant level above the minimum safe level.

2.4 Driver Fuel Assembly

The fuel assembly is basically a hexagonally shaped component, 0.116 m (4.575 in.) across outside flats and 3.657 m (12 ft.) long. The assembly comprises: a bundle of 217 fuel pins, 0.584-cm (0.230-in.)-OD, and containing the mixed oxide (PuO_2/ UO_2) pellets; a surrounding duct tube; and lower and upper end hardware. The pins are positioned in a triangular lattice and spaced by a 0.142-cm (0.056-in.)-dia. helical-wrapped wire. The fuel assembly is located radially by the core support structure and uses a hydraulic balance holddown system to maintain a fixed axial position during reactor operation.

2.5 Reactivity Control

The neutron flux level in the FTR is controlled by vertical movement of neutron-absorbing assemblies into and out of the core. The absorber assembly is a bundle of 61 stainless steel-clad B_4C pins (natural boron) housed in a duct similar to that of the driver fuel assembly. The reactor has the capability of accommodating up to nine in-core control rods and nine peripheral control rods. The initial core uses three in-core safety rods and six control rods, plus additional fixed shim control rods in the form of in-core shim assemblies and fixed shim assemblies.

2.6 Radial Reflector

The radial reflector consists of two types of reflector assemblies: inner and outer. The inner assemblies have an external hexagonal configuration and are the same length, 3.657 m (144 in.), as the driver fuel assembly and are supported by the core basket. The outer assemblies are about 0.3048 m (12 in.) shorter than the inner assemblies, 3.349 m (131.85 in.) and are supported by the inner radial shield assembly. The reflector assemblies are composed of a section of Inconel 600 and upper and lower shield sections of stainless steel. The Inconel section and the upper shield sections consist of blocks stacked on a vertical array of parallel coolant and structural tubes.

2.7 Radial Shield

The radial shield consists of six inner shield blocks and six outer shield blocks, which are arranged around the periphery of the radial reflector region. The inner and outer shield blocks are composed of vertical-standing stainless steel plates.

2.8 Core Support Structure

The core support structure positions the core components within the reactor vessel. The support structure is welded to the reactor vessel and is composed of the lower structure, support skirt, core barrel, core basket, horizontal thermal baffle, and in-vessel storage. The core basket is centrally located in the core support structure. The core barrel is welded to the lower structure and provides lateral support for the radial shield, the core restraint mechanisms, and the instrument tree. The horizontal thermal baffle on top of the core barrel provides thermal protection to the lower structure and the core barrel from the outlet plenum coolant. In-vessel storage is provided in three sections of the annular region between the core barrel and the reactor-vessel thermal liner. Each storage region provides 19 natural-convection-cooled receptacles for core components, and one transfer port position for the core component pot.

The core basket is centrally located within the core support structure and provides vertical support for the driver fuel assemblies, test assemblies, absorber assemblies, and inner reflector assemblies. The basket is a closed cylinder with 151 tubular receptacles connecting the upper and lower tube sheets. The cylindrical section of the basket has twelve rectangular flow slots, fitted with flow strainers, oriented to mate with comparable slots in the core support structure. Azimuthal orientation and vertical retention are provided by a locating pin and a breech-lock-type locking ring.

2.9 Instrument Tree

The instrument tree is mounted on the reactor head and positions the core outlet instrumentation sensors above the driver-fuel assemblies (temperature and flow) and control-rod assemblies (outlet temperature) and provides secondary holddown for them. The instrument tree also positions instrumentation over control-rod fixed shim assemblies and selected reflector assemblies. All instrumentation is routed through large and small openings in the instrument-tree columns. The drive assemblies for lift and rotation of the instrument tree are located in the head compartment. Each instrument tree also contains guide tubes for six control-rod drivelines. The FTR has three instrument trees, each covering a trisector of the core.

2.10 Horizontal Baffle

The horizontal baffle is mounted at the upper end of the core barrel and acts as a thermal insulator between the hot outlet plenum and the relatively cool fuel-storage annulus. In addition to limiting thermal conduction, the baffle limits outlet-plenum sodium from flowing into the fuel-storage annulus region.

The horizontal baffle, consisting of 42 plates 0.0508 m (2 in.) thick, has a trisector symmetry. Each plate is supported from a single standoff to permit unrestrained thermal distortion.

Complete details of the vessel geometry may be obtained from the design manuals and the FSAR.

3. Brief Description of the COMMIX-1A Code

The COMMIX-1A computer program is a general-purpose thermal-hydraulic code that can be used to analyze multidimensional steady/unsteady reactor component/multicomponent fluid-flow problems. The computer program has been under development at Argonne National Laboratory under sponsorship of the U. S. Nuclear Regulatory Commission. The general background and equations solved by COMMIX-1A have been reported earlier at various instances, but notably in Ref. 2 and 3. For completeness, we give brief details of the computer code and its capabilites.

The equations solved by COMMIX are the transient, three-dimensional forms of the equations for

a. Mass continuity,

b. Conservation of x momentum, y momentum, z momentum, and

c. Conservation of energy.

The above fluid and heat-transport equations are solved in the concept of volume porosity/surface permeability, which permits easy and realistic representation of partially open internal regions. The effects of heat capacity of internal structures are explicitly taken into account.

The equations are solved by a finite-difference calculation procedure originally based on the IMF procedure of Ref. 7, but improved for faster and more efficient computations. The version of the COMMIX code series currently used is VER 8.0, which is based on a fully implicit time-differencing option.

In addition to the above features, COMMIX has input features which permit easy simulation of complex geometries. As a result, COMMIX has been applied to study thermohydraulic conditions in reactor components such as plena, reactor cores, pipes, and heat exchangers, and in combinations of these components.

4. Steady-state Behavior of the FFTF for 100% Power

The present section describes the results of the steady-state behavior of the FFTF vessel at 100 % power. The present results for steady state display essentially the same behavior reported in Ref. 1, with some improvements in the reflector region temperature. As mentioned earlier, we have considered only a 120° sector of the geometry. This sector includes the row 2 FOTA, one inlet, one outlet, the instrument tree, and the in-vessel handling machine. All the details of the components have been prescribed to the code through the option for surface permeabilities and volume porosities. Appendix 4 gives a listing of the input data used for this simulation.

4.1 Details of the Computations

The reactor vessel trisector has been modeled as a number of discrete cells. In the present calculation 2334 cells were placed in the flow domain. The finite-difference grid is shown in Figs. 4a and b. The inlet to the domain is placed at K = 5, and the outlet is at K = 13. The inlet is

modeled as a prescribed velocity and temperature surface. At the outlet, a continuity-of-mass velocity boundary condition and a zero derivative temperature boundary condition are prescribed.

4.2 Presentation of the Results

The steady-state flow and temperature fields were calculated by going through a null transient. The steady state was determined when velocity changes between time steps was less than 5×10^{-5} times the maximum velocity. The enthalpy changes similarly were less than 1.0×10^{-5} times a nominal enthalpy.

The coolant flow path has been earlier sketched in Fig. 3. The inlet flow enters the inlet plenum, flows upwards to the core basket and the shield, and subsequently enters the outlet plenum. The outlet is placed midway in the 120° sector. The present calculations display this expected behavior.

The output from the calculations is a detailed description of the velocities and temperatures at the 2334 nodes in the trisector. Since it is difficult to present all the information concisely, we have plotted the flow patterns and temperature fields in axial and azimuthal planes. These are shown in Figs. 5 a-d, 6 a-d, and 7 a-d. The temperatures and flow rates exiting the assemblies have been compared with measured data. Table 1 compares assembly flow rates and temperatures, and Tables 2 and 3 show the temperatures in the plenum (TLLMs and the PTP). Overall, the agreement between measurements and calculations is reasonably good. The temperature contours are shown in Figs. 7 a-d for various planes. It can be seen from the results presented in the figures that the flow patterns and temperature contours are highly three-dimensional.

4.3 Discussion of the Results

The steady-state results obtained in the present calculations are similar to the results presented earlier in Ref. 1. The phenomena notable are: a) three-dimensionality (i.e., r, z, θ variations), b) vortex-type flow in the upper plenum, and c) thermal stratification in the upper plenum with interface close to the outlet nozzle. These features are exactly as reported earlier for the 360° simulation.

The comparison of the calculated and measured temperatures is reasonably good, but for some discrepancies. These discrepancies may be either due to some inaccuracies in the measurements or due to inexact prescription of the flow resistances. In some assemblies, however, where both flow and temperature differ in the same direction (both being under or over predicted), there appears to be some error either in the measurement or in the reported local power distribution. The FOTA temperature (cell I = 1, J = 1-4) is about 6°C below the measured value. It is, however, possible to slightly adjust the flow resistance to decrease the flow and thereby increase the temperature; but we have not done so. Overall, the agreement with the TLLM temperatures is reasonably good, but we observe the same discrepancy at the PTP, as observed in the earlier study. The discrepancy is attributed to insufficient mixing in the calculations in the upper plenum, and insufficient detailing in modeling the region near instrument tree exits. We have, however, accounted for the

gaps between the top of the fuel assemblies and the bottom of the instrument-tree tubes.

5. Transient Calculations

5.1 Transient Functions

The transient for which the calculations have been made is the initial part of the natural-circulation experiments performed at HEDL. These transients are composed of reductions in flow and power over very short time intervals. The transient functions used in the calculations (obtained from HEDL [5]) are shown in Figs. 8 a-c and are tabulated in Table 4. The power undergoes a sharp reduction from 100 % power to about 8 % in the first 2.5 sec and decays slowly from there on. The flow, on the other hand, decays from full flow to very low flow somewhat more slowly. Associated with the transient inlet flow is also a transient inlet temperature, which decreases slightly from the steady-state value. Further, two different power-transient functions are used, one for the fuel assemblies, and the other for the reflector assemblies.

5.2 Computational Aspects

The calculations for the transient were begun from the steady-state solution described in Sec. 4. The implicit solution scheme was employed. A time step size two times the Courant limit was arbitrarily chosen. It is felt that a larger time step can be used at the later portion of the transient so that computer running time can be reduced. Furthermore, since the fully implicit option is new, we do not have enough operating experience to take advantage of using "optimum" operating parameters. Because of the significant computer time required, it has been possible to simulate only the first 80 sec of the transient. At this time, the power and flow have decreased to low values, approximately 3 and 4 % of their initial levels respectively. The following sections describe some of the results from this transient calculation.

5.3 Fuel Assembly Temperatures

Accurate measurements of the transient temperatures of the Fuel Open Test Assembly were made by HEDL (8) at various locations in a fuel assembly (on several of the 217 pins) for 10-sec intervals. In our present calculations, however, we do not resolve the spatial temperature distribution within the assembly; hence, we have compared the calculations with a 'mean' value of the measured temperatures. (The mean calculated is the arithmetic average of the temperatures, although a mean weighted with local flow rates is more appropriate. Since the local flow rates within a fuel assembly are unknown, the arithmetic mean is calculated.)

Figure 9 compares the calculated FOTA temperatures with measurements at every 10 sec. The spread in the measurements is about 5°C. It is seen that we underpredicted slightly the 10-sec value, but for other temperatures the agreement is good. The discrepancy at 10 sec may be either due to inadequate thermal structure modeling in the FOTA (although we have considered here all the detailed material constructions, and heat sources), or due to error in the measurements of time or temperature during the rapid change.

5.4 Flow Patterns During the Transient

During the flow-reduction period, the momentum of the jets issuing from the core (fuel assemblies) is gradually reduced. Consequently, the jets become progressively weaker in penetrating the upper-plenum fluid. The cooling of the jets further promotes the stratification in the plenum. The heavy, cold jets progressively start to bend over the core, and the flow directly passes to the outlet. Figures 10 a-h, 11 a-h, and 12 a-h show the flow patterns at times t = 29.0, 53.0 and 79 sec from the steady state. It is seen from these figures that there is a reverse flow in the region above the core jets. This reverse flow is because of the following reason. When the core power was suddenly shut down with an appreciable flow still flowing through the core, the temperatures of the jets go through a minimum temperature. (This can be seen through the FOTA temperature plot of Fig. 9.) However, the momentum of the jets is still large enough to deposit this fluid in the upper region of the plenum. With further reductions in the flow with time, the assembly flows get hotter, but cannot penetrate the cold fluid above them. The cold fluid gradually sinks to the core top and mixes with the other flow, eventually exiting the vessel. Evidence to this behavior is seen in both the measured and the calculated PTP (Proximity Test Plug) temperatures shown in Table 3. The fluid trapped in the upper region is relatively hot and is stably stratified. The flow pattern shown in Figs. 12 a-h will persist for the remaining time of the natural circulation period, but for the natural diffusion of the interface with time. Based on these flow patterns, it is clearly seen that a strong coupling exists between upper plenum and core flows.

5.5 Thermal Field During the Transient

Figures 13 a-d, 14 a-d, and 15 a-d show the contours of equal temperatures at times t = 29.0, 53.0, and 79 sec respectively. The temperature contours are primarily a manifestation of the flow field, which is shown in earlier Figs. 10-12. In the steady state the contours show a stratified region at the top, but there is a radial variation of temperatures in the region above the core. This is simply a consequence of the jets issuing out of the core. However, as the transient progresses, the loss in momentum of the jets tends to flatten out the contours in the top, as seen in Figs. 13-15. At t = 79 sec, the temperature contours are nearly horizontal, showing a stratified region with a small temperature gradient. We believe this pattern will prevail for a long time during the natural-circulation transient, however altered somewhat by the diffusion processes across the interface.

Figures 16 and 17 a-f show the variation of the temperatures in the plenum with time. The measurements of TLLM temperatures have been made only at every 1-min intervals; hence, we could not compare the calculations extensively. There appears to be some problem in the measured TLLM temperatures at -27 ft 7 in and -28 ft 11 in (which show nonmonotonic temperature variations from top to bottom of the plenum). These TLLMs may be of a different 120° sector in the plenum. The PTP temperatures shown in Fig. 16 show discrepancies with measurements if considered as calculated. However, because the thermocouples have a lag of about 10 sec, we have calculated the thermocouple temperature from the calculated fluid temperature taking into account the thermocouple thermal inertia (see Appendix 5). The agreement between data and calculations is good after this adjustment. Figure 18 presents the time-

temperature variation of a typical reflector. The reflectors, because of their large thermal inertia and relatively low flow rate, do not cool down as fast as the core does, and the temperature stays nearly constant with time. This behavior agrees with similar calculations performed with the CORA code [5].

6. Summary

The present report has presented the results of in-vessel calculations for steady state and transient thermal-hydraulic behavior of the FFTF. The transient simulated is a pump trip from full flow, followed by a scram from a 100 % (full) power operation. The COMMIX-1A (version 8.0) has been employed to perform the calculations. The calculations have been compared with measurements where possible. The agreement of steady-state fuel assembly and reflector flows and temperatures has been reasonably good. The calculated transient FOTA (row 2) temperature agrees well with measurements (except at 10 sec). The calculated temperatures agree reasonably well with the measured TLIM and PTP data. Thermal stratification with temperature gradients is seen in the upper plenum. Strong thermal hydraulic coupling between upper plenum and core flows has been observed.

The calculated results can be improved by rigorously modeling the geometry just above the core with finer computational mesh. We plan to repeat the calculations at a later date after feedback is received from readers.

TABLE 1: COMPARISON OF STEADY STATE TEMPERATURES AND FLOWS AT THE TOP OF THE CORE

CELL (I,J) (r,θ)	CALCULATED TEMPERATURE (°C)	MEASURED TEMPERATURE (°C)	CALCULATED FLOW (gpm)	MEASURED FLOW (gpm)
1,1	541.3	547.9	164.4	164.2
1,2	541.3	547.9	164.4	164.2
1,3	541.3	547.9	164.4	164.2
1,4	541.4	547.9	164.4	164.2
1,5	544.3	548.3	162.5	155.4
1,6	544.3	548.3	162.5	155.4
1,7	544.3	548.3	162.5	155.4
1,8	544.3	548.3	162.5	155.4
2,1	526.5	529.9	423.3	410.0
2,2	526.4	529.9	423.3	410.0
2,3	527.1	527.1	423.3	429.2
2,4	527.1	527.1	423.3	429.2
2,5	515.6	516.4	560.3	551.2
2,6	515.6	516.4	560.3	551.2
2,7	510.5	515.9	559.3	541.2
2,8	510.5	515.9	559.3	541.2
3,1	522.1	520.6	517.7	527.5
3,2	522.1	520.6	517.7	527.5
3,3	529.6	528.2	517.7	520.0
3,4	529.6	528.2	517.7	520.0
3,5	516.2	512.7	269.9	256.2
3,6	516.2	512.7	269.9	256.2
3,7	515.3	514.9	269.9	256.2
3,8	515.3	514.9	269.9	256.2
4,1	502.8	499.5	317.1	312.5
4,2	502.8	499.5	317.1	312.5
4,3	535.6	547.5	528.5	522.9
4,4	535.6	547.5	528.5	522.9
4,5	526.0	540.0	497.0	512.6
4,6	527.4	540.0	497.0	512.6
4,7	525.5	532.5	497.0	512.0
4,8	525.5	532.5	497.0	512.0
5,1	428.5			
5,2	428.5	405.5		
5,3	428.5	405.5		
5,4	428.6			
5,5	424.3	438.9		
5,6	424.1			
5,7	422.7	412.7		
5,8	422.7	436.1		
6,1	406.6			
6,2	406.6	397.0		
6,3	421.5	397.0		
6,4	421.6	448.0		
6,5	427.7			
6,6	427.7	417.2		
6,7	420.7			
6,8	420.8	438.3		

TABLE 2: COMPARISON OF CALCULATED AND MEASURED TLIM TEMPERATURES

(Steady State)

TLIM ELEVATION (FT. IN.)	CALCULATED TEMPERATURE (°C)	MEASURED TEMPERATURE (°C)
- 19.7	518.6	507.12
- 24.0	518.6	509.0
- 26.5	518.5	510.0
- 27.7	518.4	508.0
- 28.11	516.2	509.0
- 30.7	508.75	509.0

(t = 1 min)

TLIM ELEVATION (FT. IN.)	CALCULATED TEMPERATURE (°C)	MEASURED TEMPERATURE (°C)
- 19.7	505.4	507.12
- 24.0	497.5	500.71
- 26.5	486.9	503.5
- 27.7	483.6	492.5
- 28.11	480.0	501.6
- 30.7	471.8	479.6

TABLE 3: COMPARISON OF PTP TEMPERATURES WITH MEASUREMENTS

TIME (mins)	CALCULATED TEMPERATURE (°C)	MEASURED TEMPERATURE (°C) CHANNEL* A	B	C
0.0	541.0	525.4	527.9	526.7
0.25	417.2	520.5	515.6	521.13
0.50	484.1	466.7	469.1	468.5
0.75	505.5	480.1	485.6	483.8
1.0	504.1	489.9	503.4	493.6
1.25	501.5	489.9	502.2	493.6
1.5		488.7	502.2	492.3

*Channels A, B, and C refer to three different measurement ports.

TABLE 4: TRANSIENT FLOW AND POWER FUNCTIONS USED IN THE SIMULATION

A. FLOW FUNCTION

time (s)	ratio
0.0	1.0
1.0	0.981
1.0	0.98i
3.0	0.7799
6.0	0.570
9.0	0.439
12.0	0.356
15.0	0.297
18.0	0.2516
21.0	0.2182
24.0	0.1923
27.0	0.1722
30.0	0.1534
35.0	0.1309
40.0	0.1124
45.0	0.0972
50.0	0.0854
59.0	0.0678
63.0	0.0642
70.0	0.0554
75.0	0.0487
85.0	0.0393

B. CORE POWER FUNCTION

time (s)	ratio
0.0	1.0
2.5	0.0795
3.0	0.078
5.0	0.0657
7.5	0.0572
10.0	0.0527
15.0	0.0468
50.0	0.0325
69.0	0.0293
119.0	0.0247

C. REFLECTOR POWER FUNCTION

time (s)	ratio
0.0	1.0
4.0	0.1062
9.0	0.0905
19.0	0.0804
39.0	0.0726
69.0	0.0671
119.0	0.0628

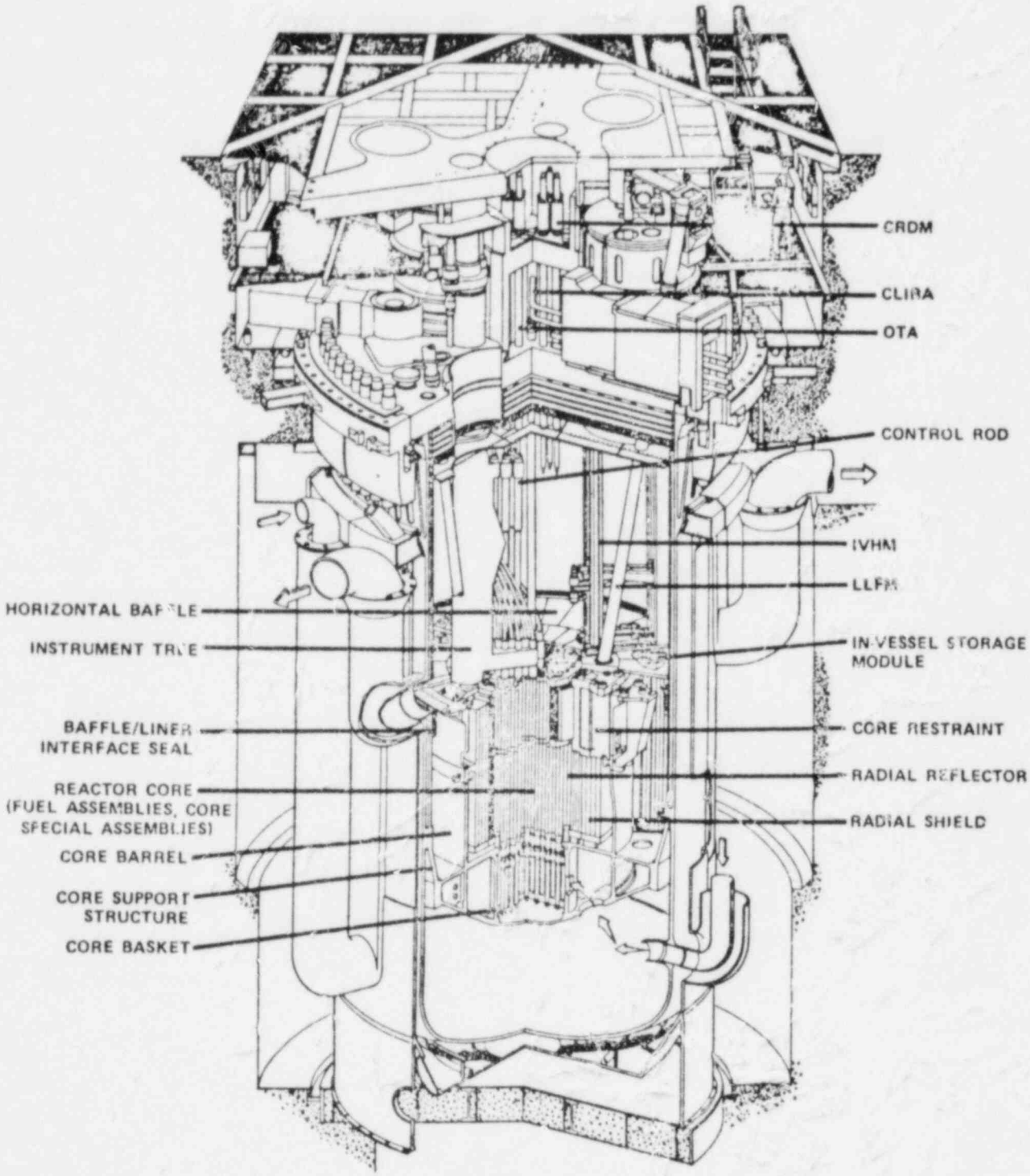

Fig. 1. Reactor Vessel and Internal Components Composite

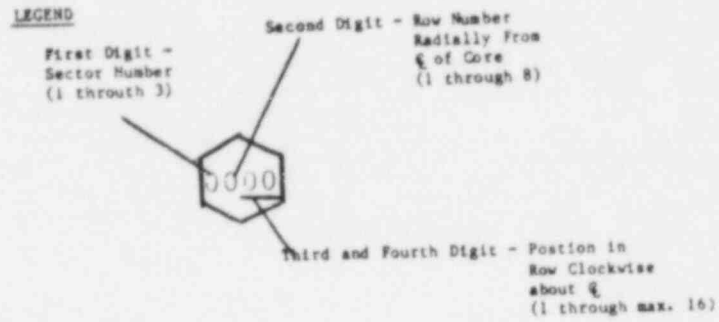

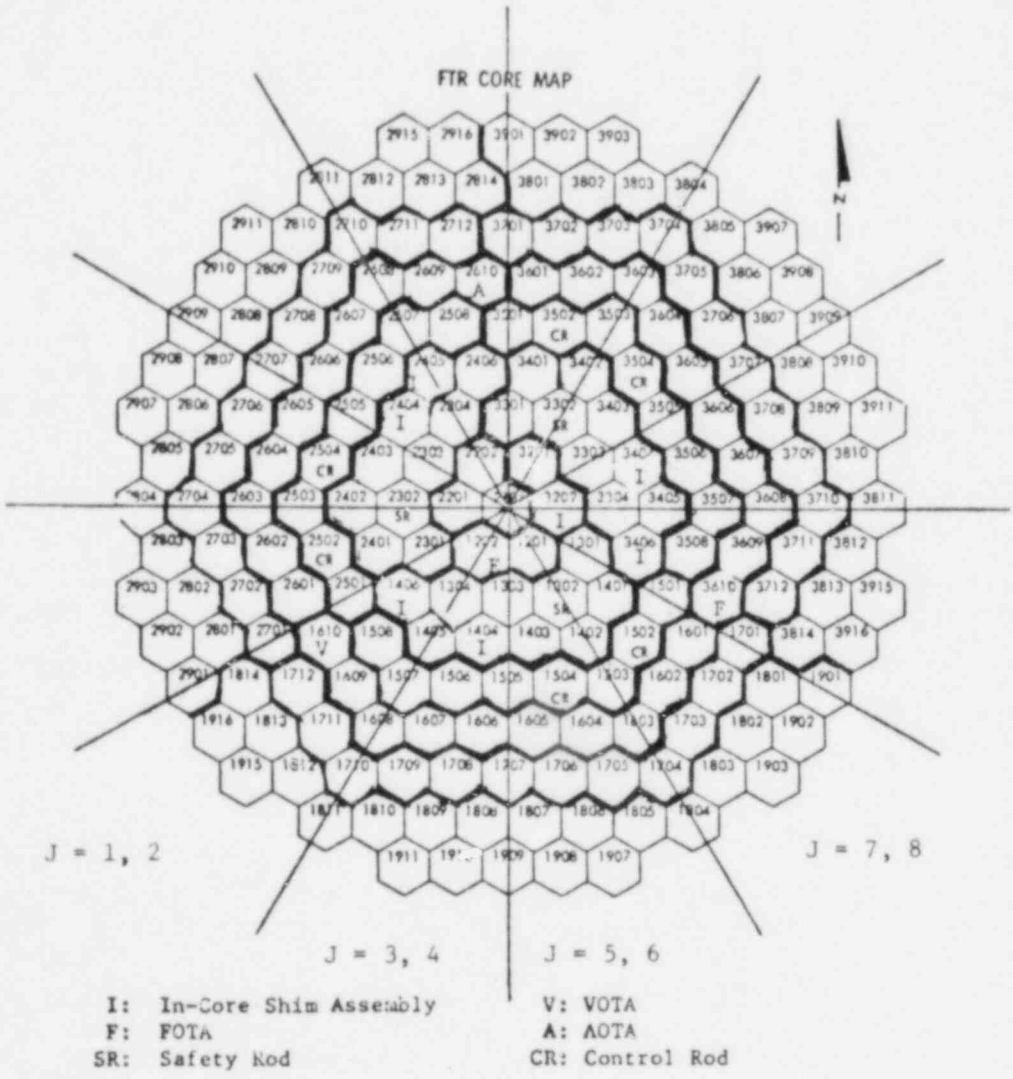

Fig. 2. Core Map

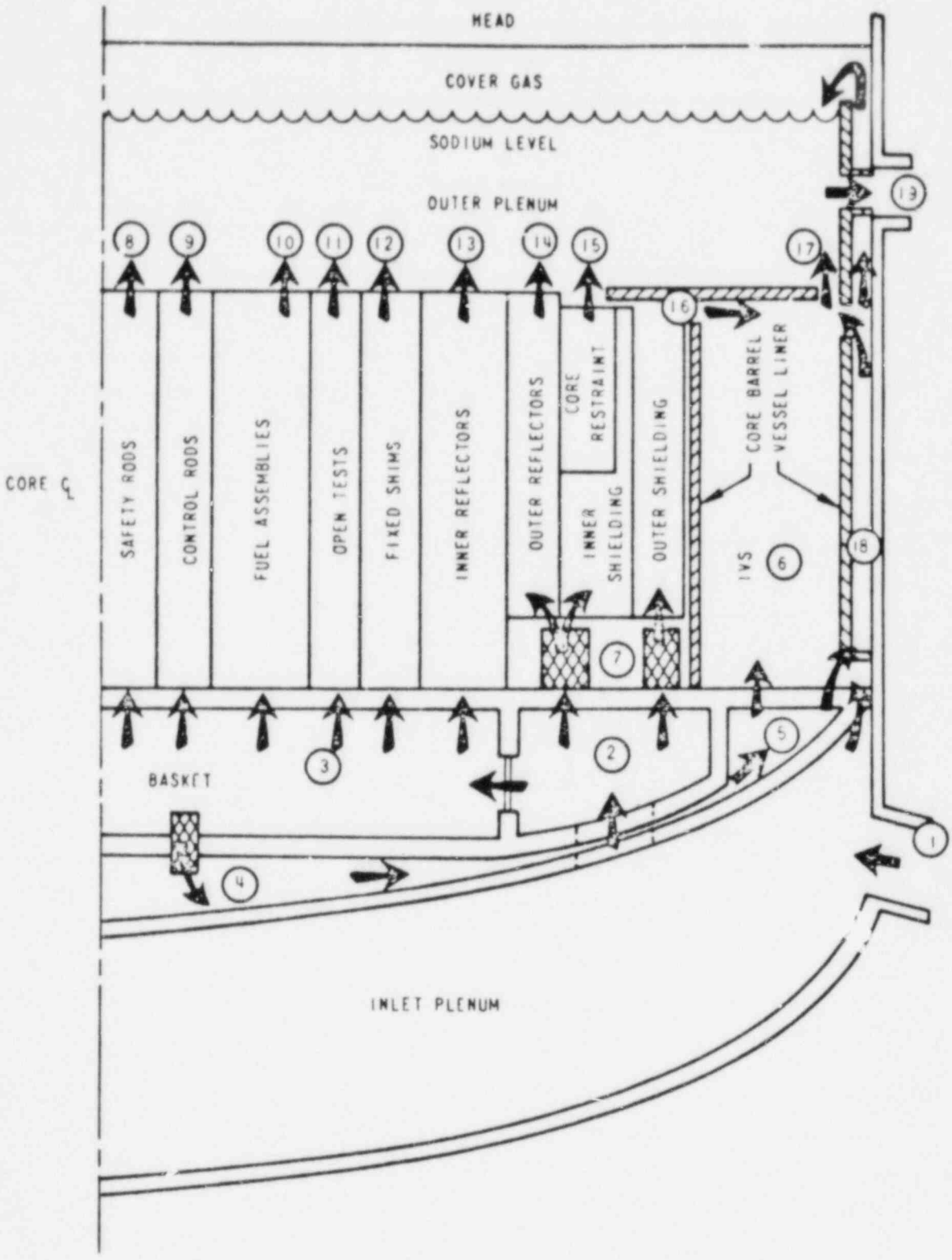

Fig. 3. Reactor Vessel Flow Distribution

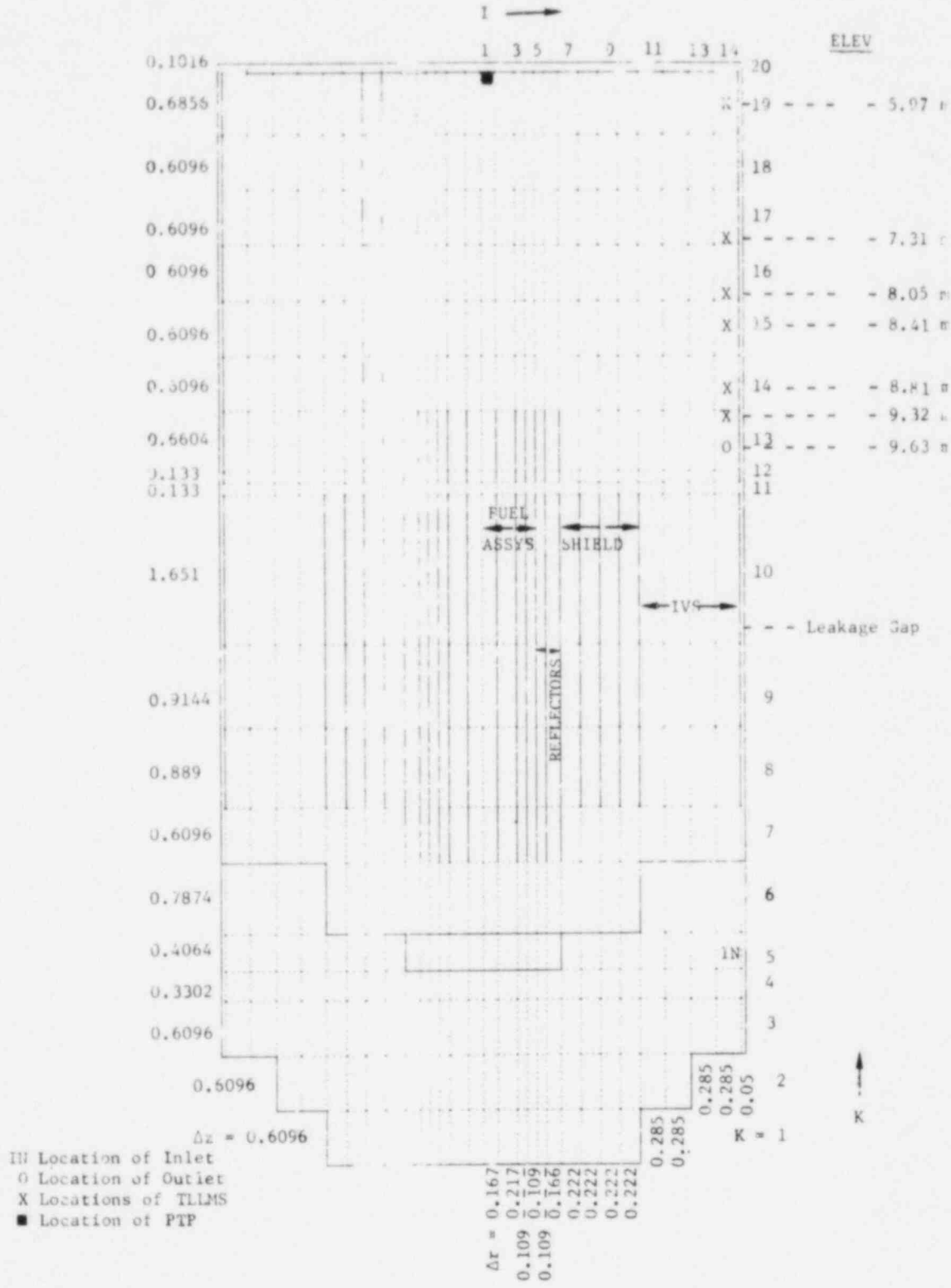

Fig. 4a. Finite-difference Grid in R-Z Plane

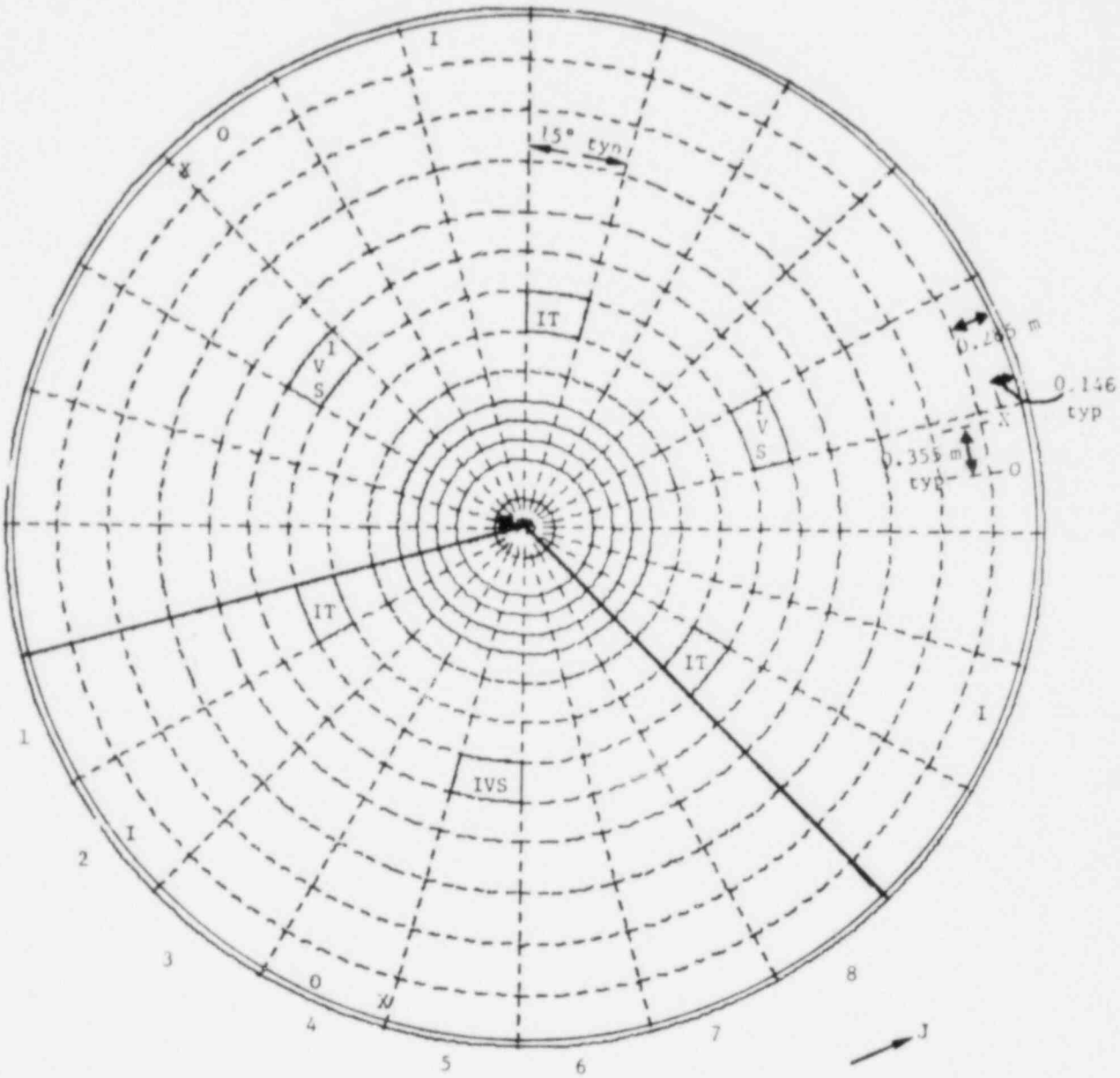

O Locations of Outlets

I Locations of Inlets

X Locations of TLLMs

■ Location of PTP (above fuel assembly 2202)

Fig. 4b. Finite-difference Grid in R-θ Plane

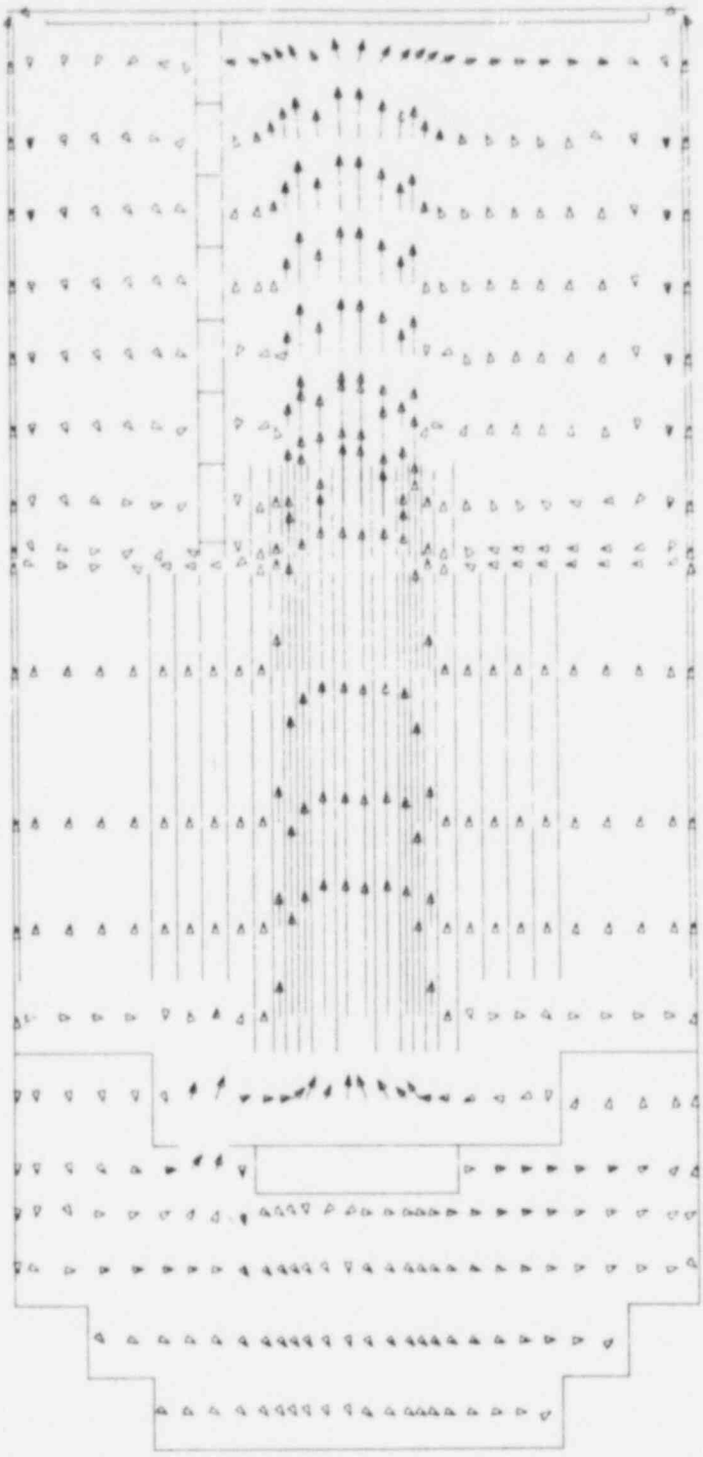

Fig. 5a. Velocity Vectors in the R-Z Plane at Steady State

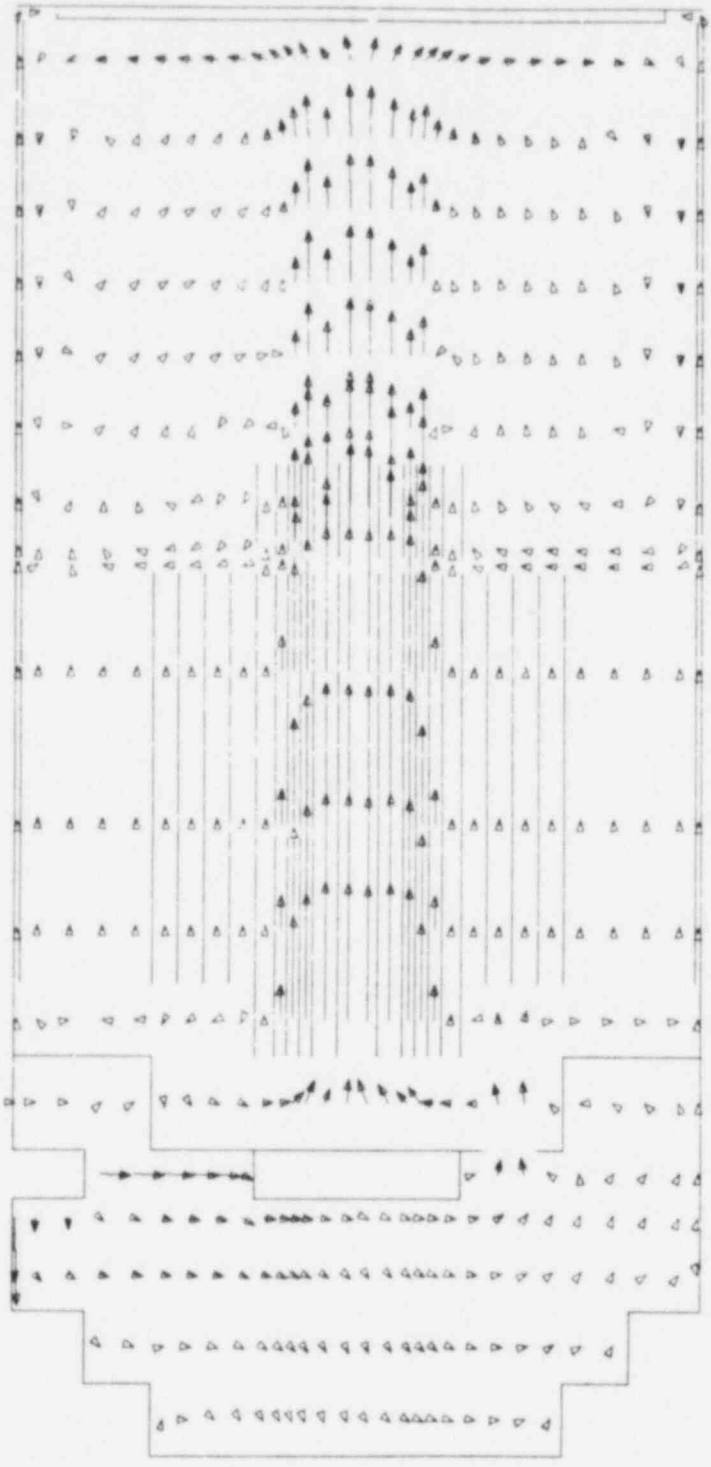

Fig. 5b. Velocity Vectors in the R-Z Plane at Steady State

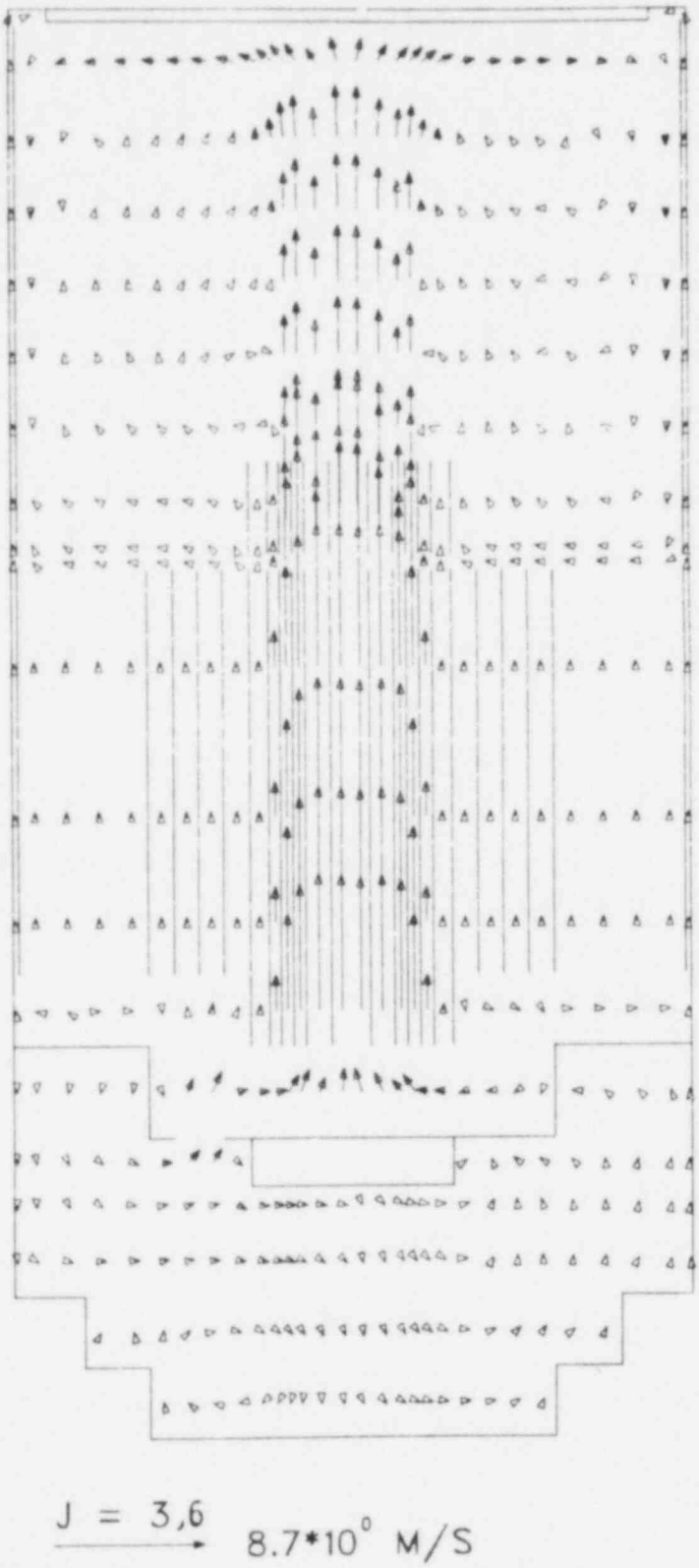

Fig. 5c. Velocity Vectors in the R-Z Plane at Steady State

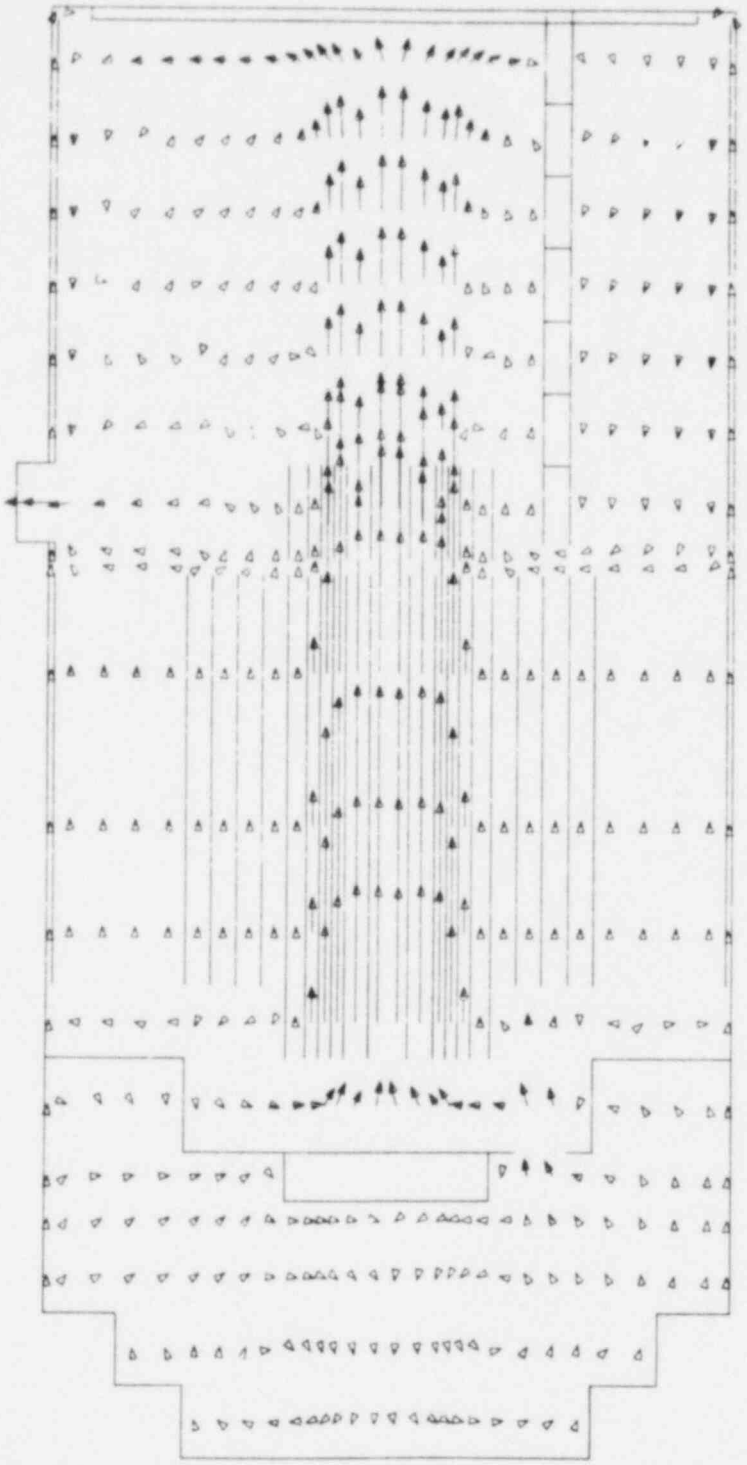

Fig. 5d. Velocity Vectors in the R-Z Plane at Steady State

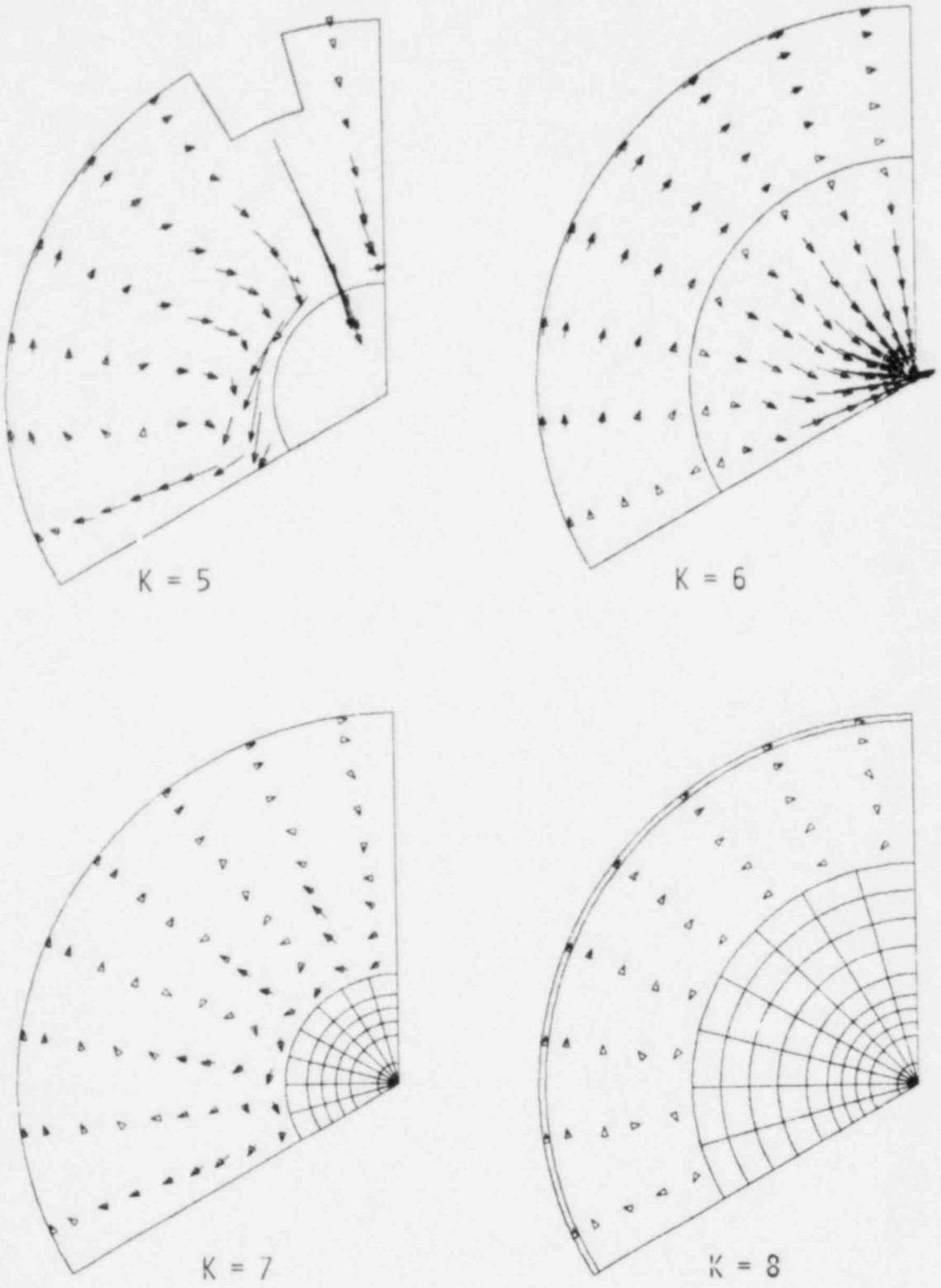

Fig. 6a. Velocity Vectors in R-θ Plane at Steady State

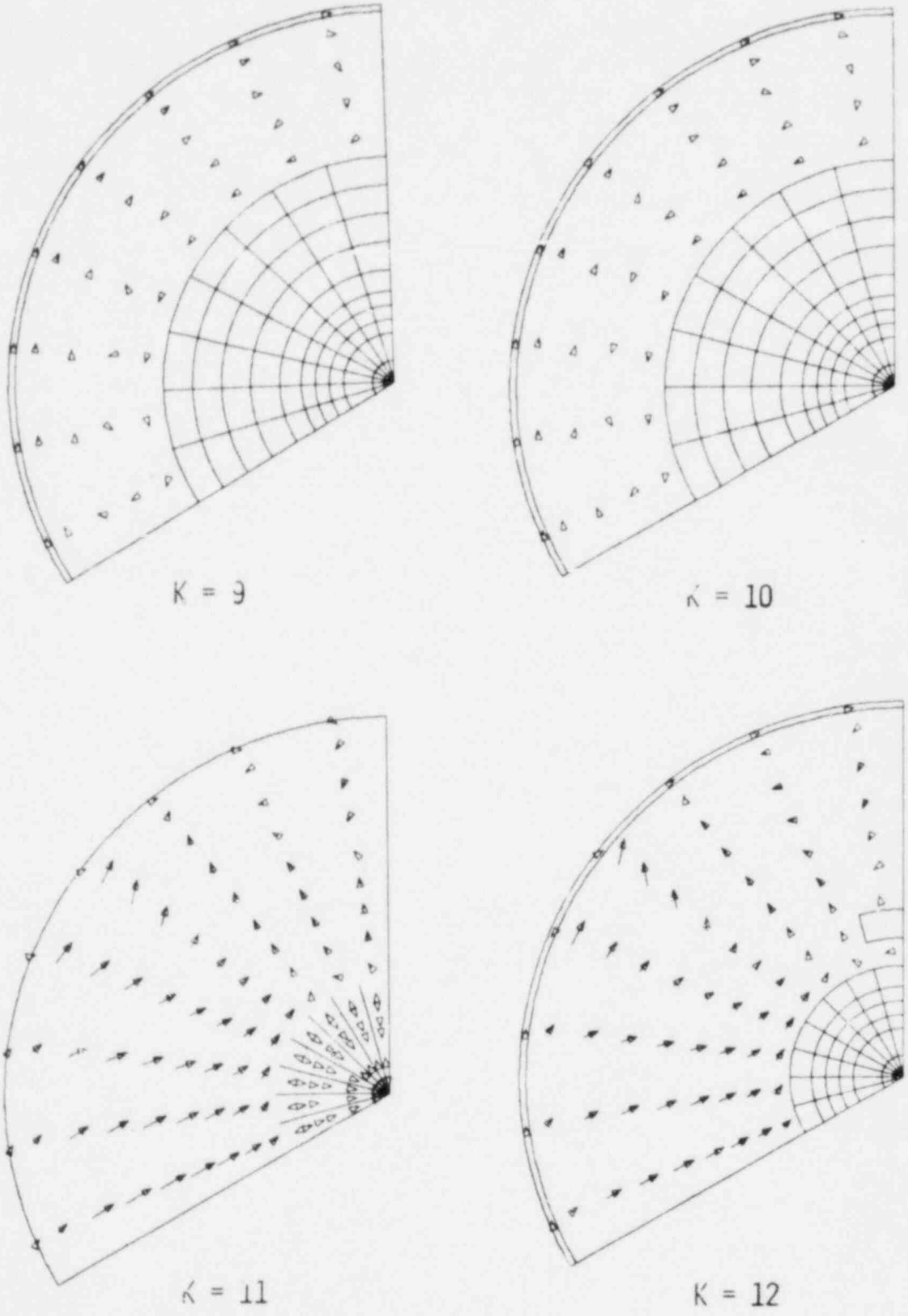

Fig. 6b. Velocity Vectors in R-θ Plane at Steady State

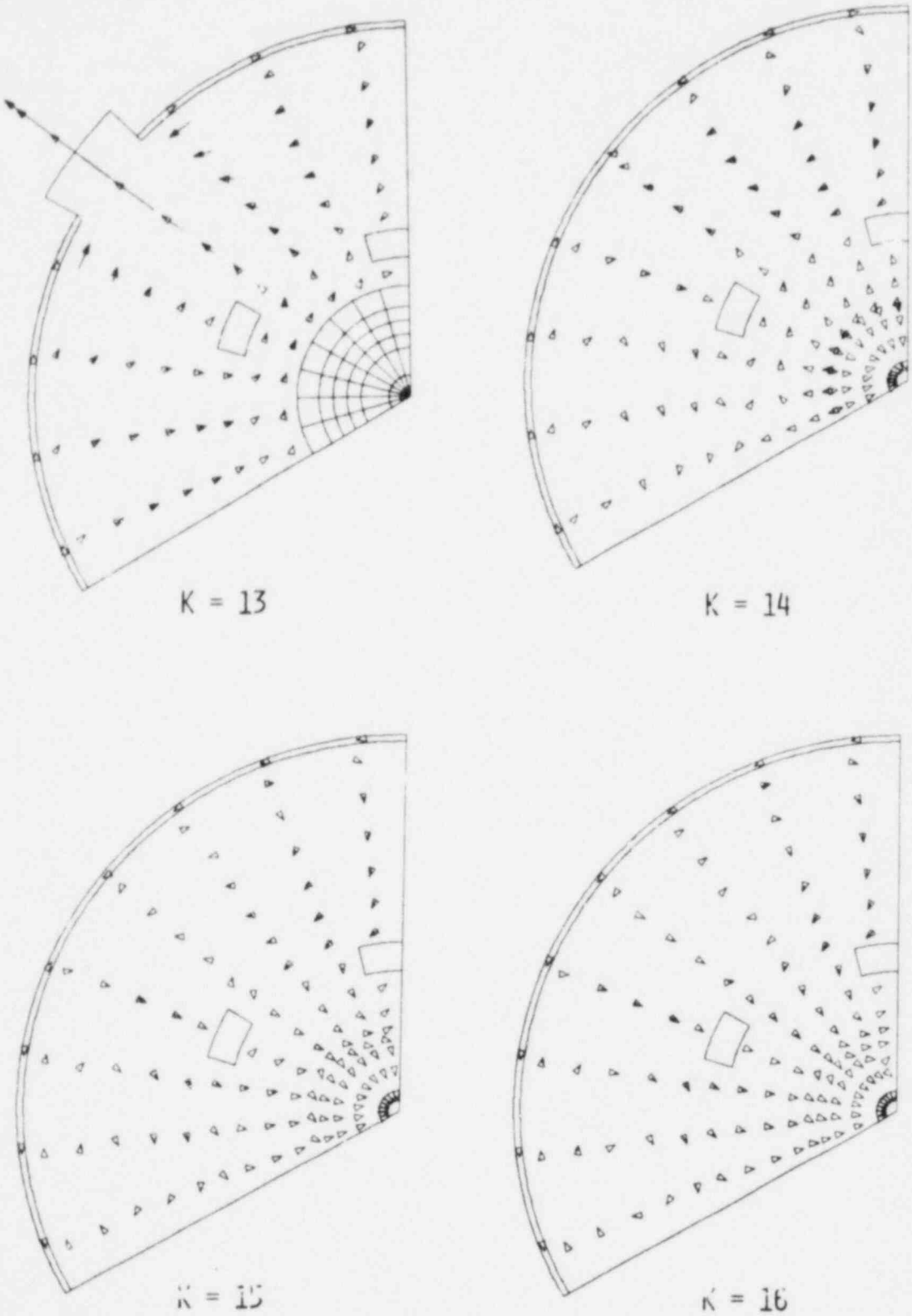

Fig. 6c. Velocity Vectors in R-θ Plane at Steady State

K = 17

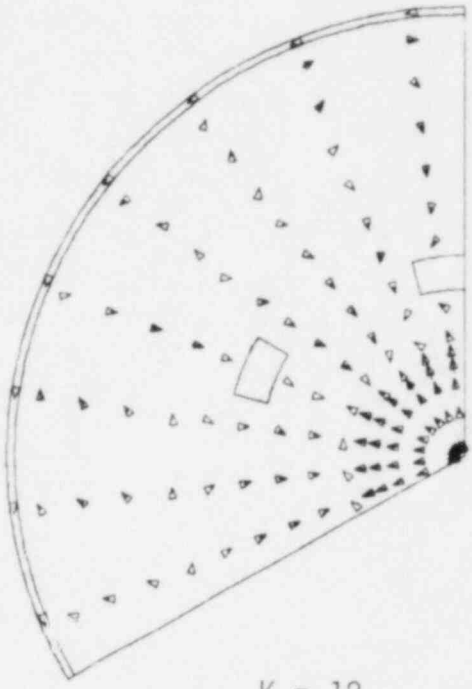

K = 13

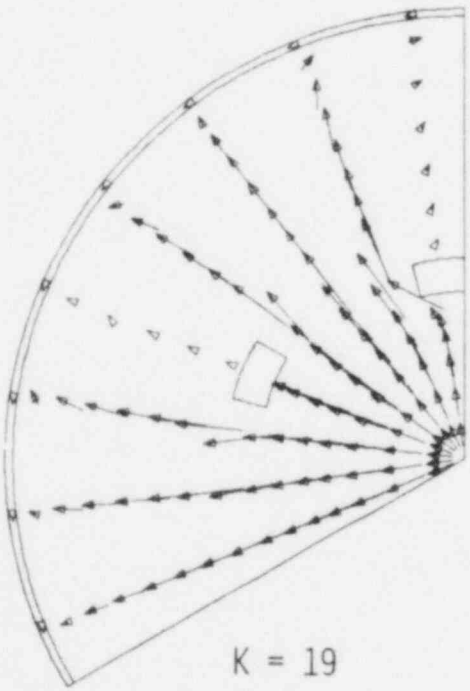

K = 19

Fig. 6d. Velocity Vectors in R-θ Plane at Steady State

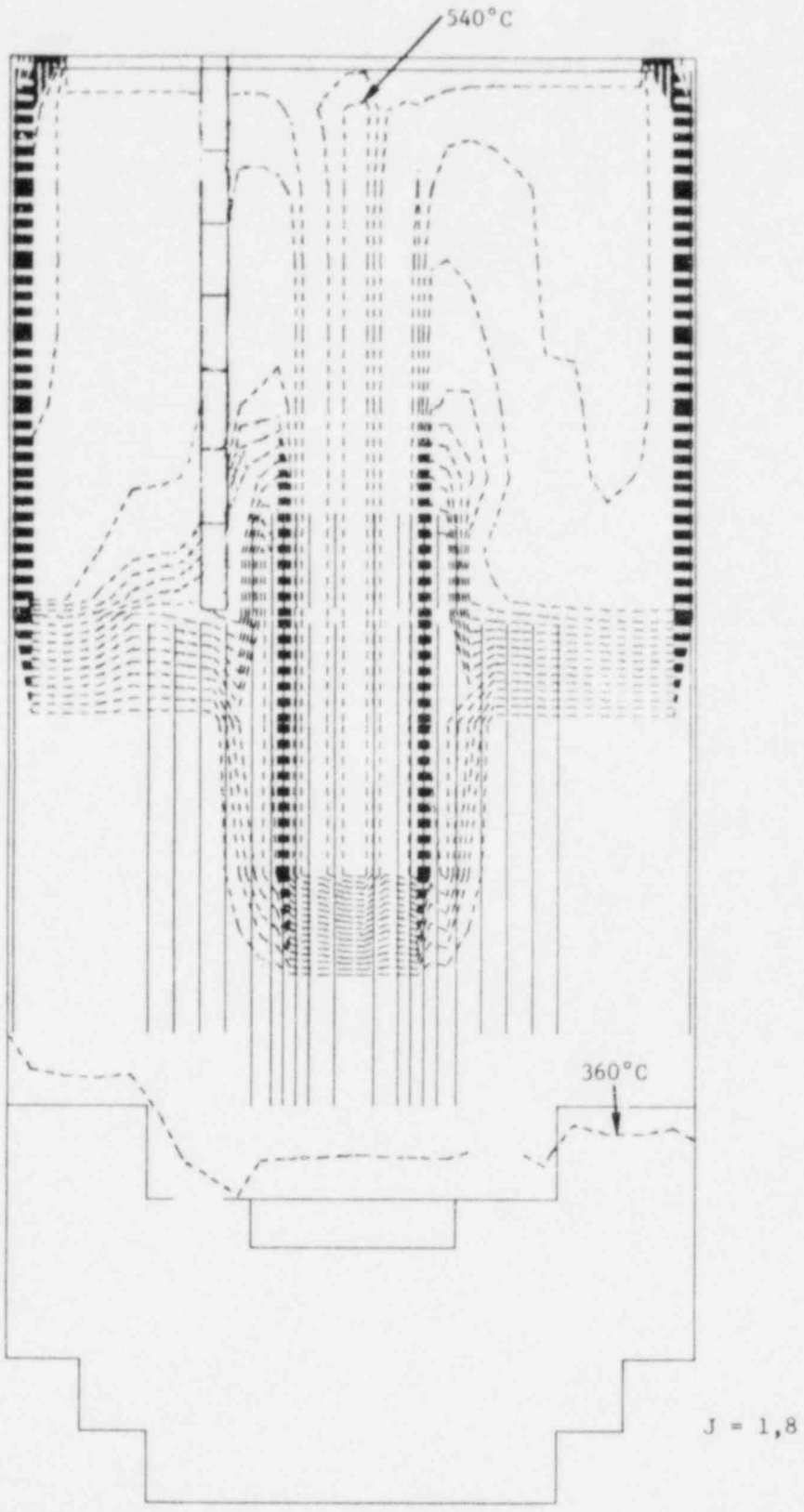

Fig. 7a. Contours of Equal Temperature at Steady State ($\Delta T = 10°C$)

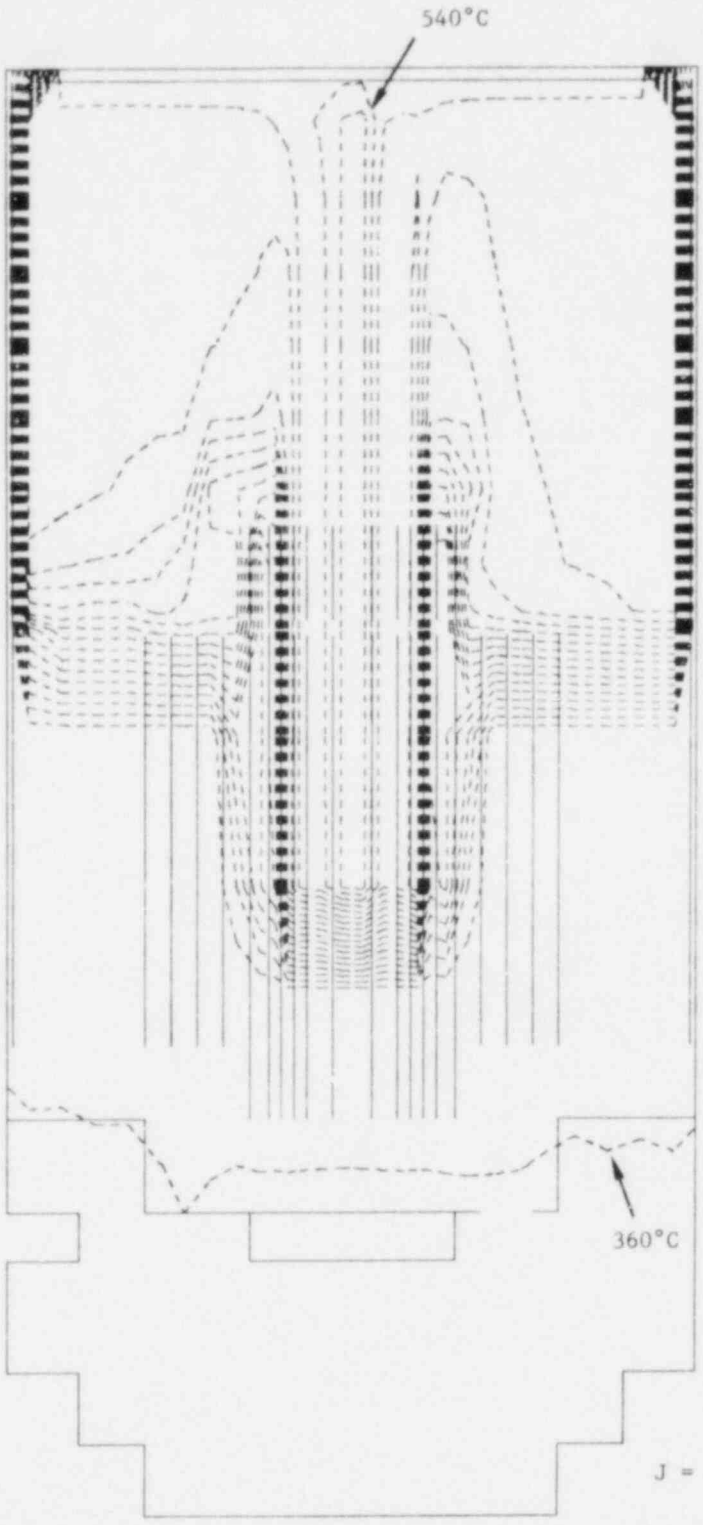

Fig. 7b. Contours of Equal Temperature at Steady State ($\Delta T = 10°C$)

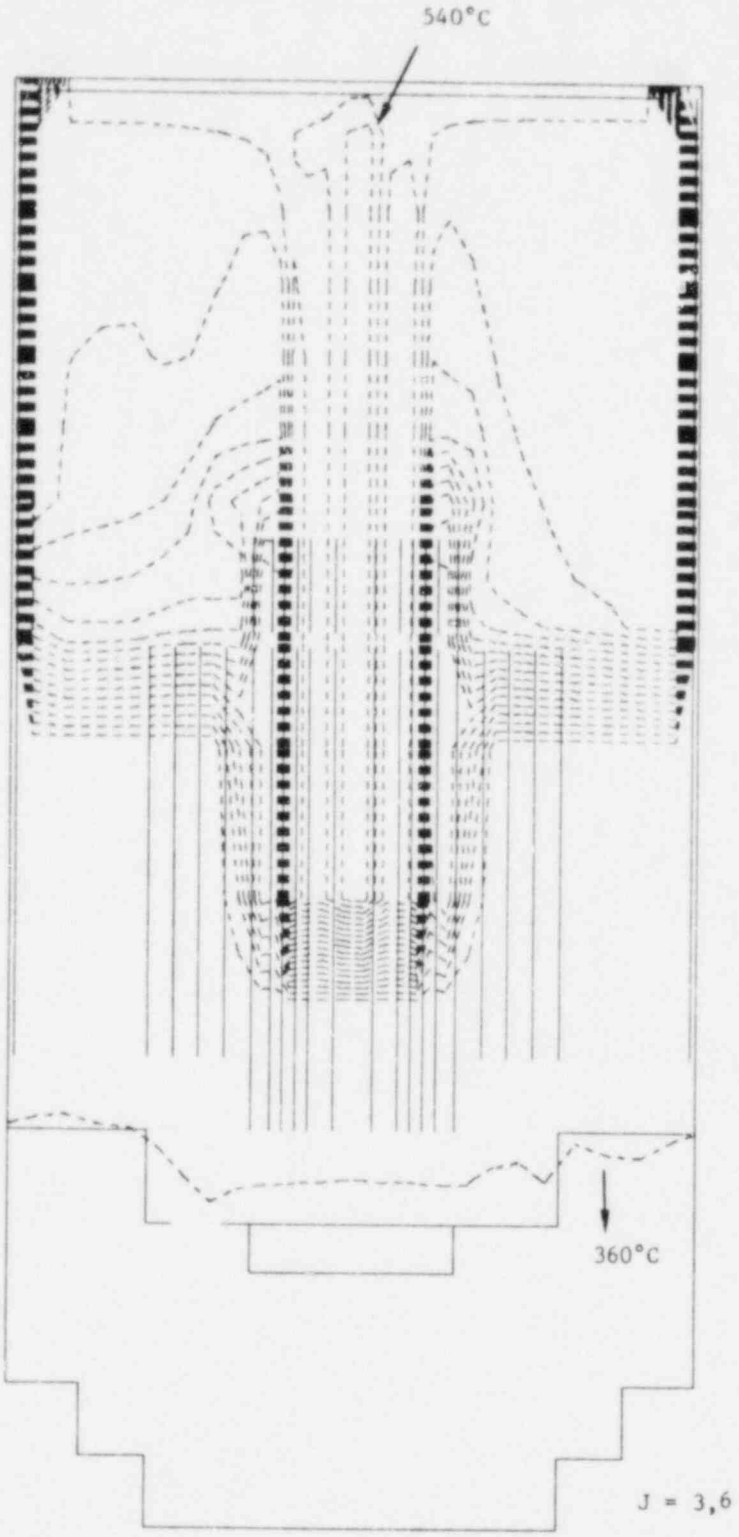

Fig. 7c. Contours of Equal Temperature at Steady State ($\Delta T = 10°C$)

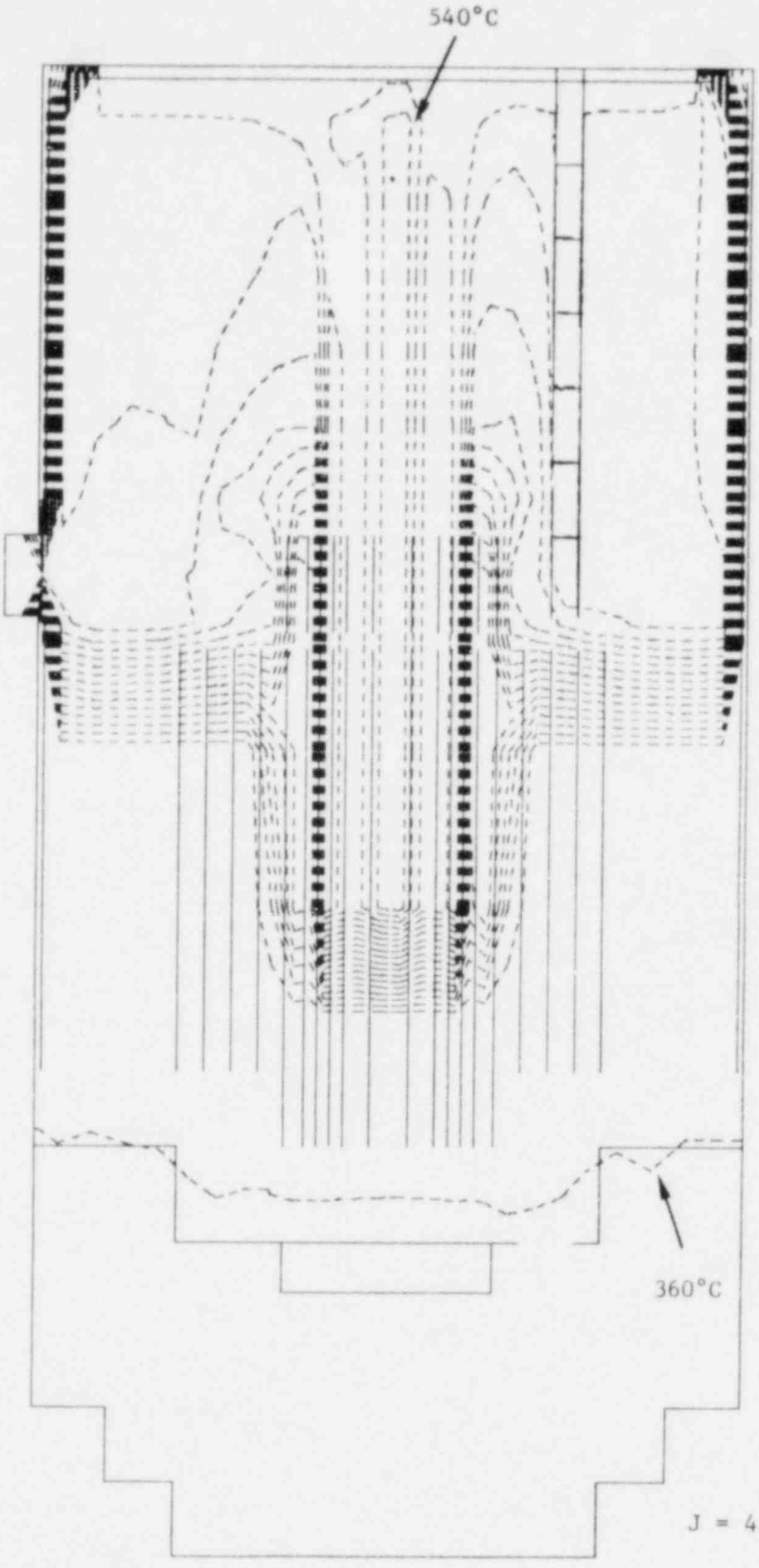

Fig. 7d. Contours of Equal Temperature at Steady State ($\Delta T = 10°C$)

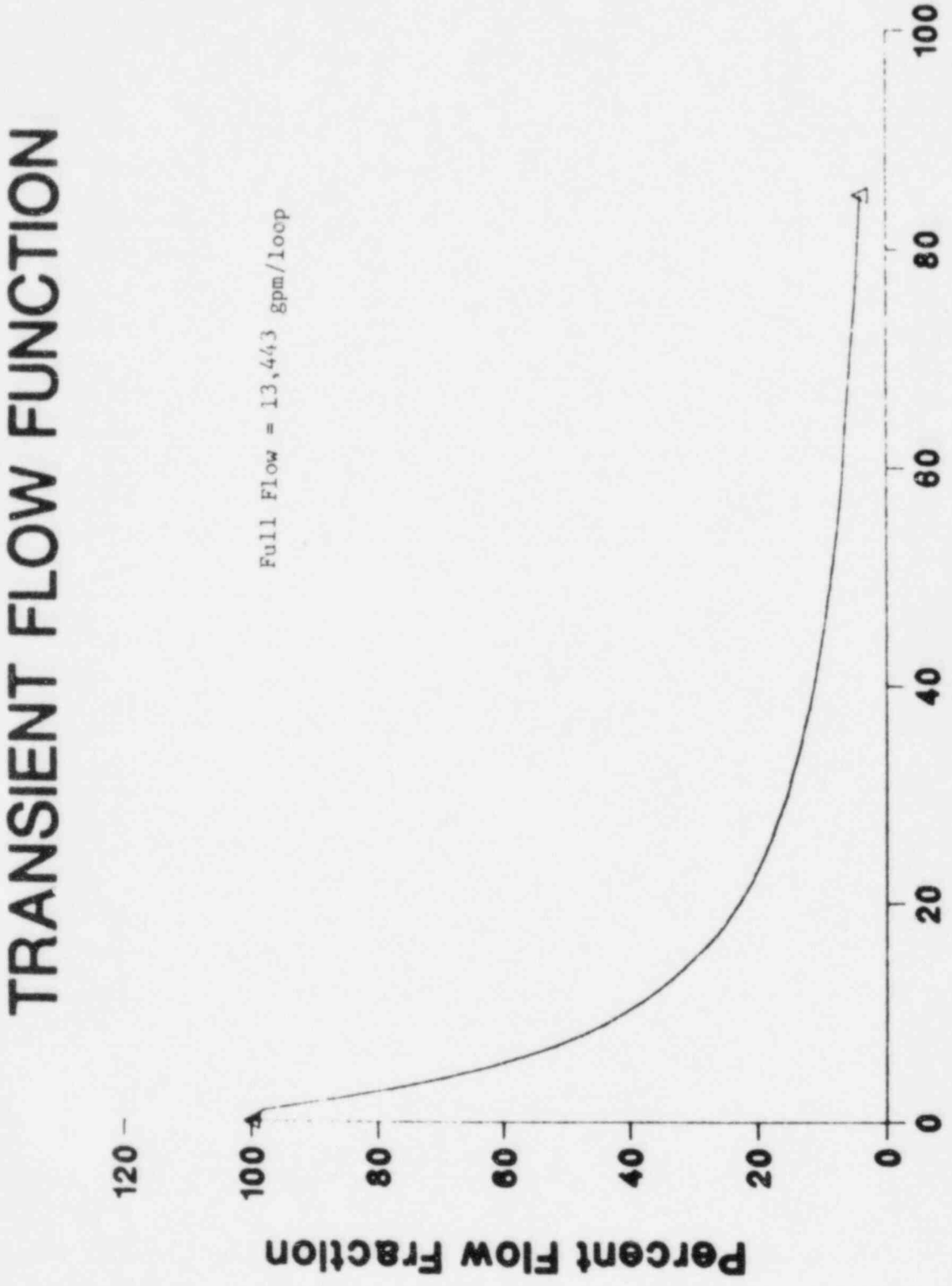

Fig. 8a. Transient Flow Function

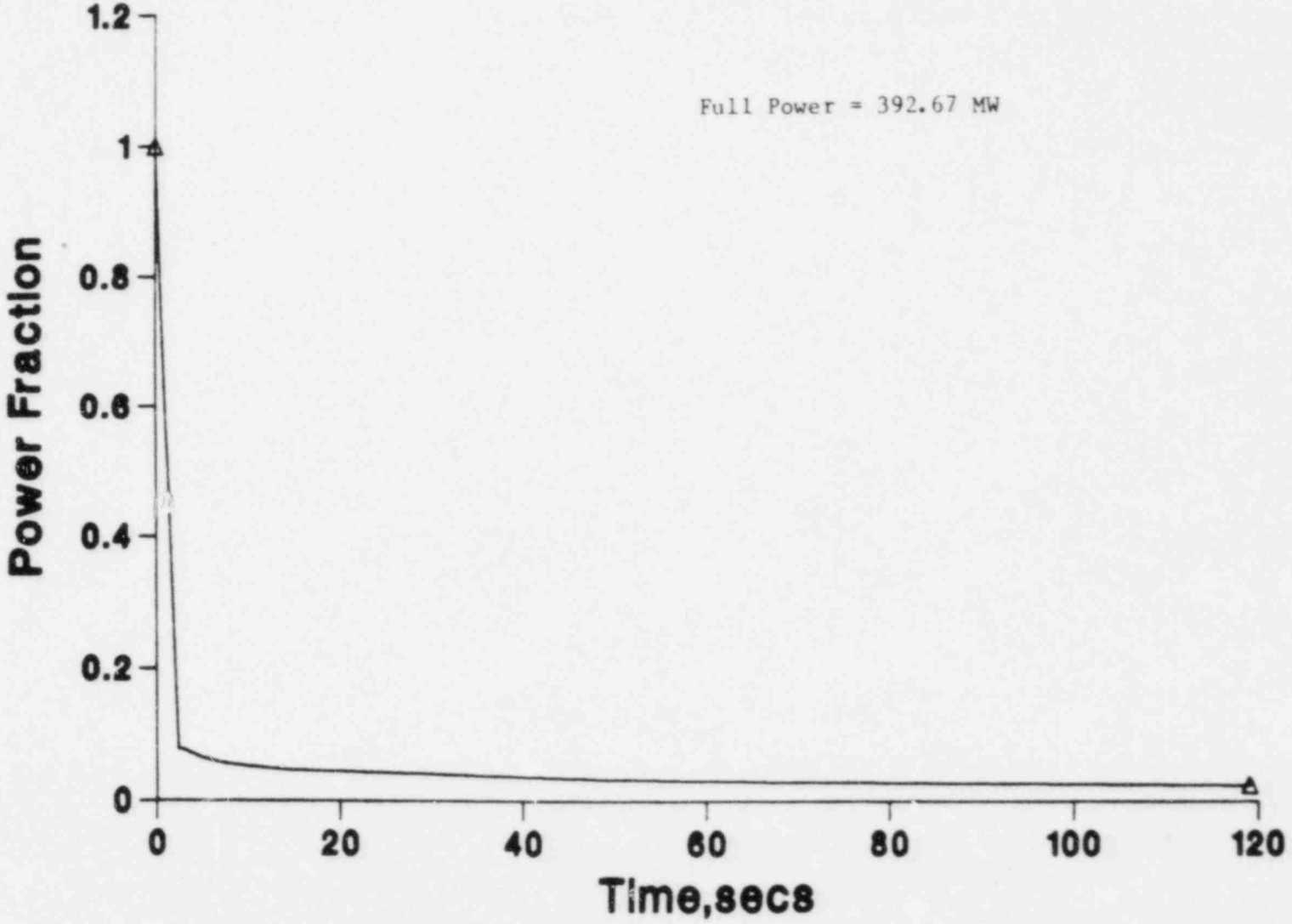

Fig. 8b. Core Power Function

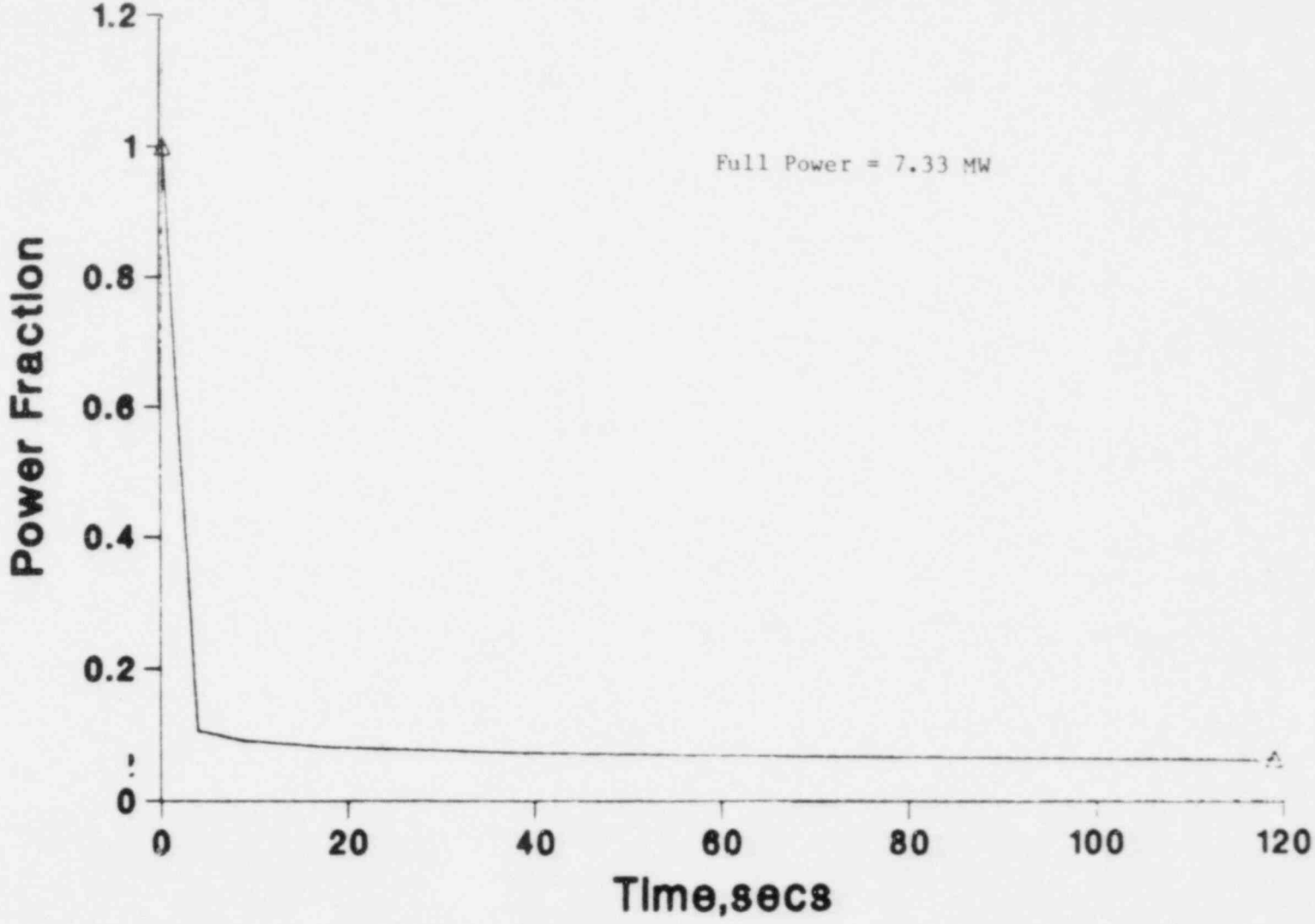

Fig. 8c. Reflector Power Function

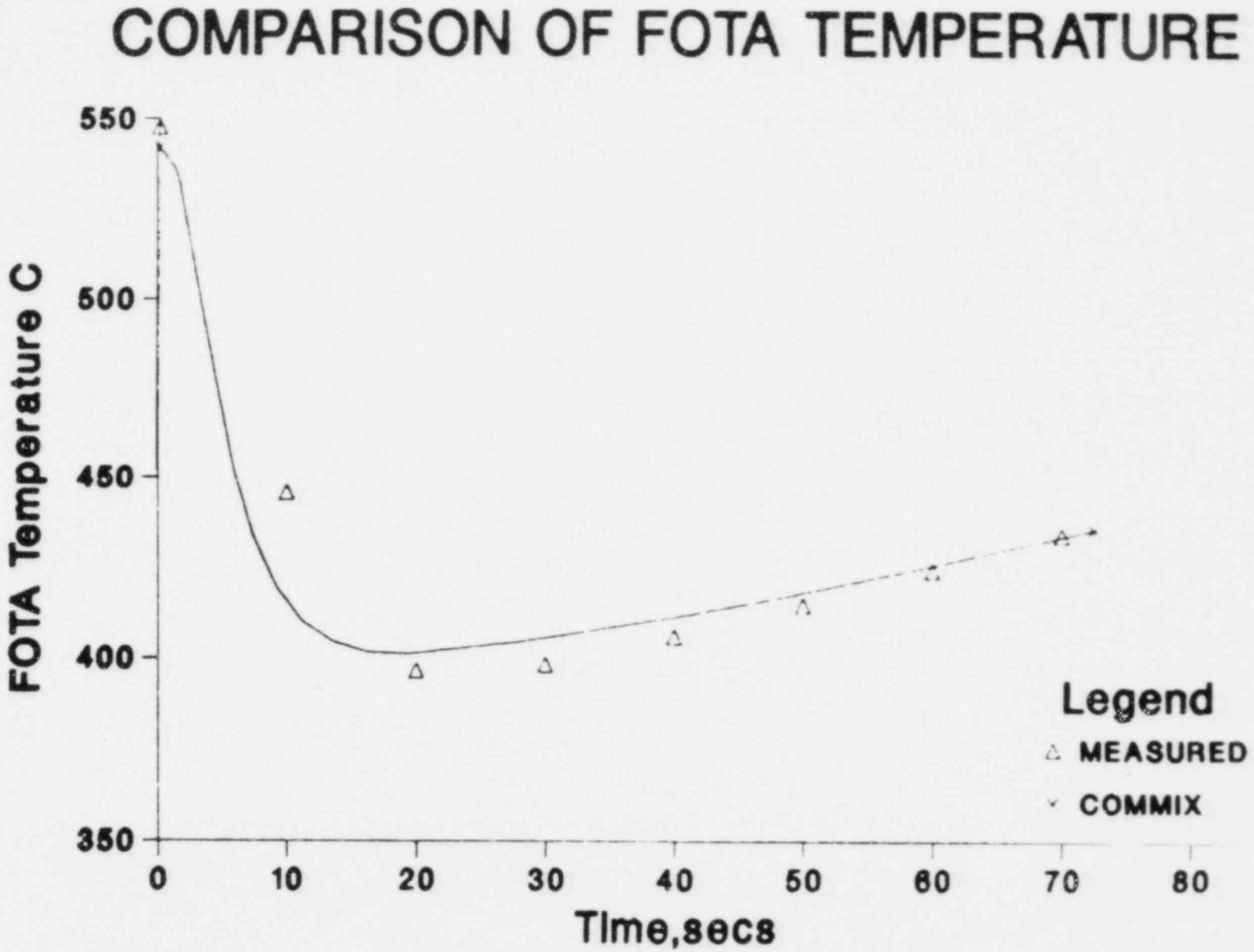

Fig. 9. Comparison of (Row 2) FOTA Exit Temperature

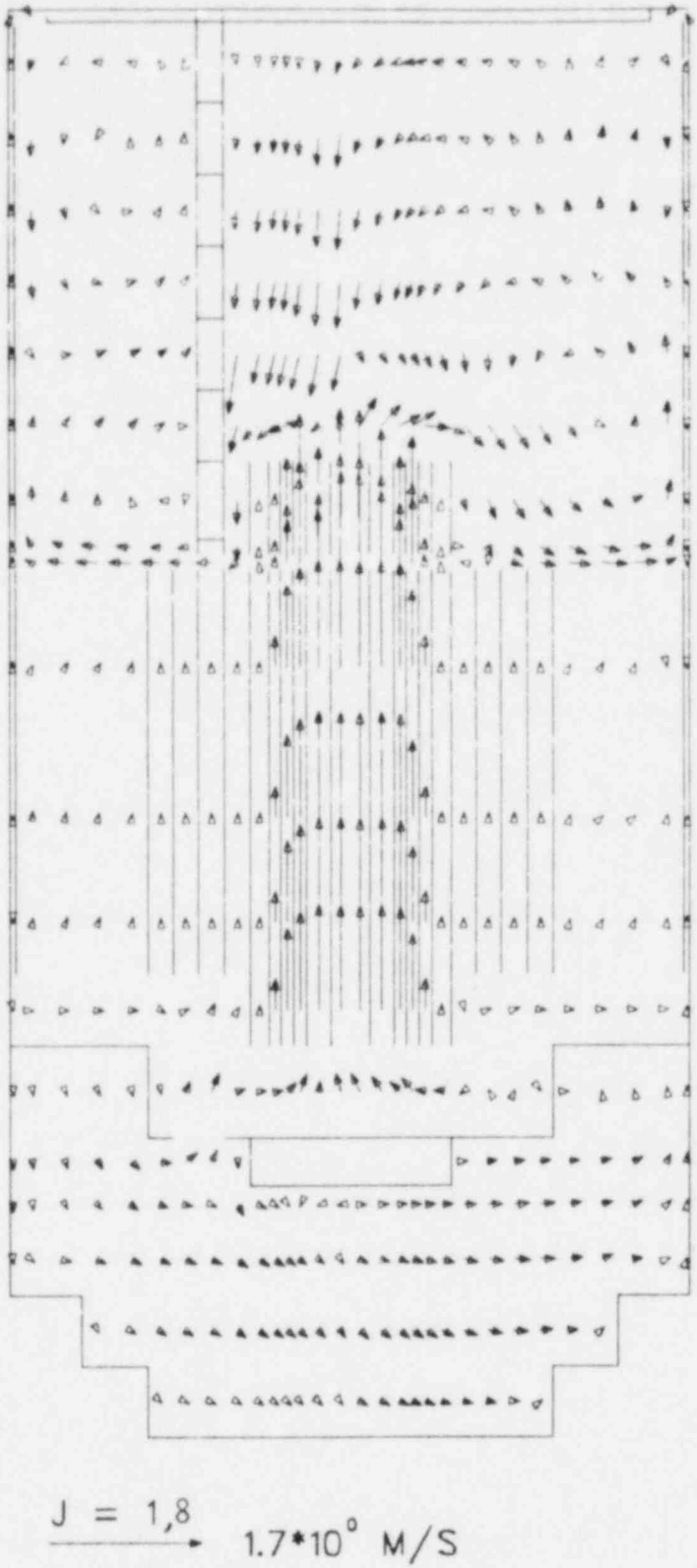

Fig. 10a. Velocity Vectors at t = 29 sec

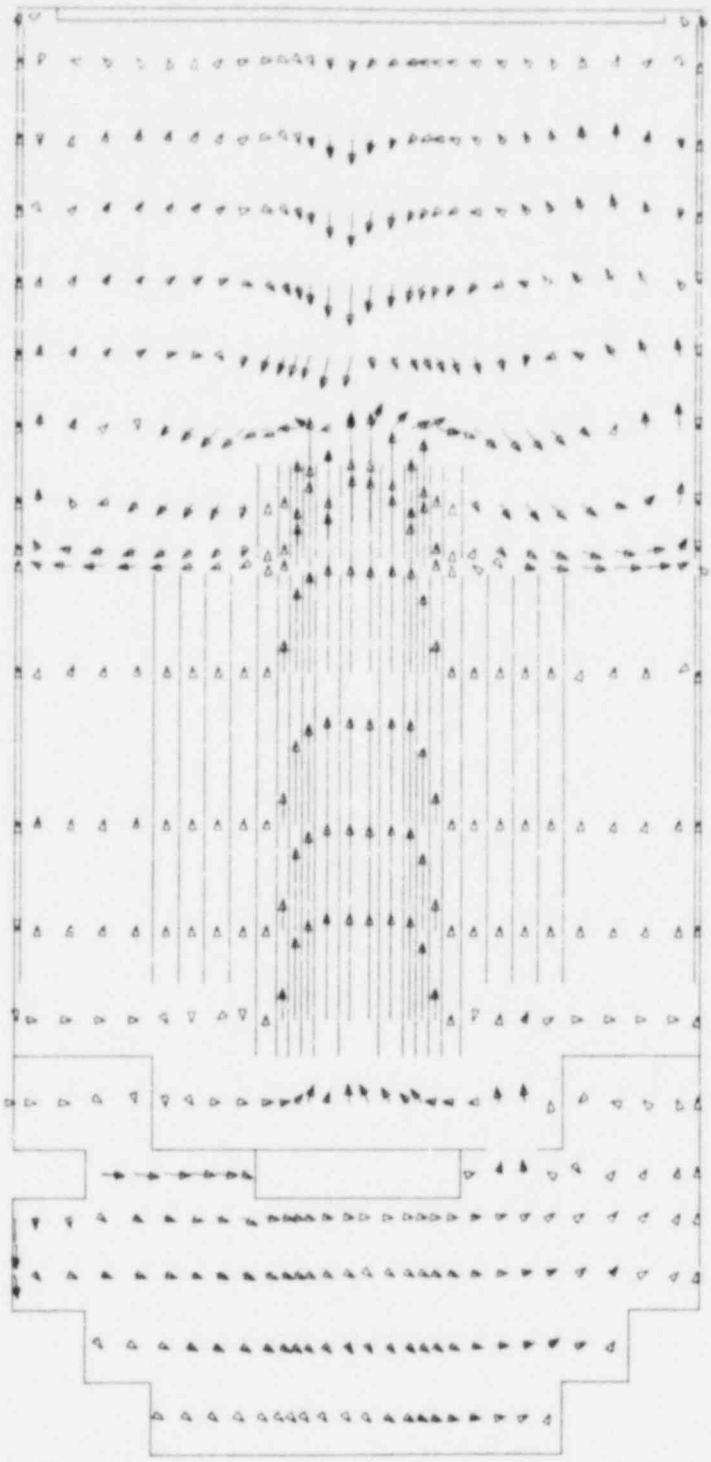

Fig. 1Cb. Velocity Vectors at t = 29 sec

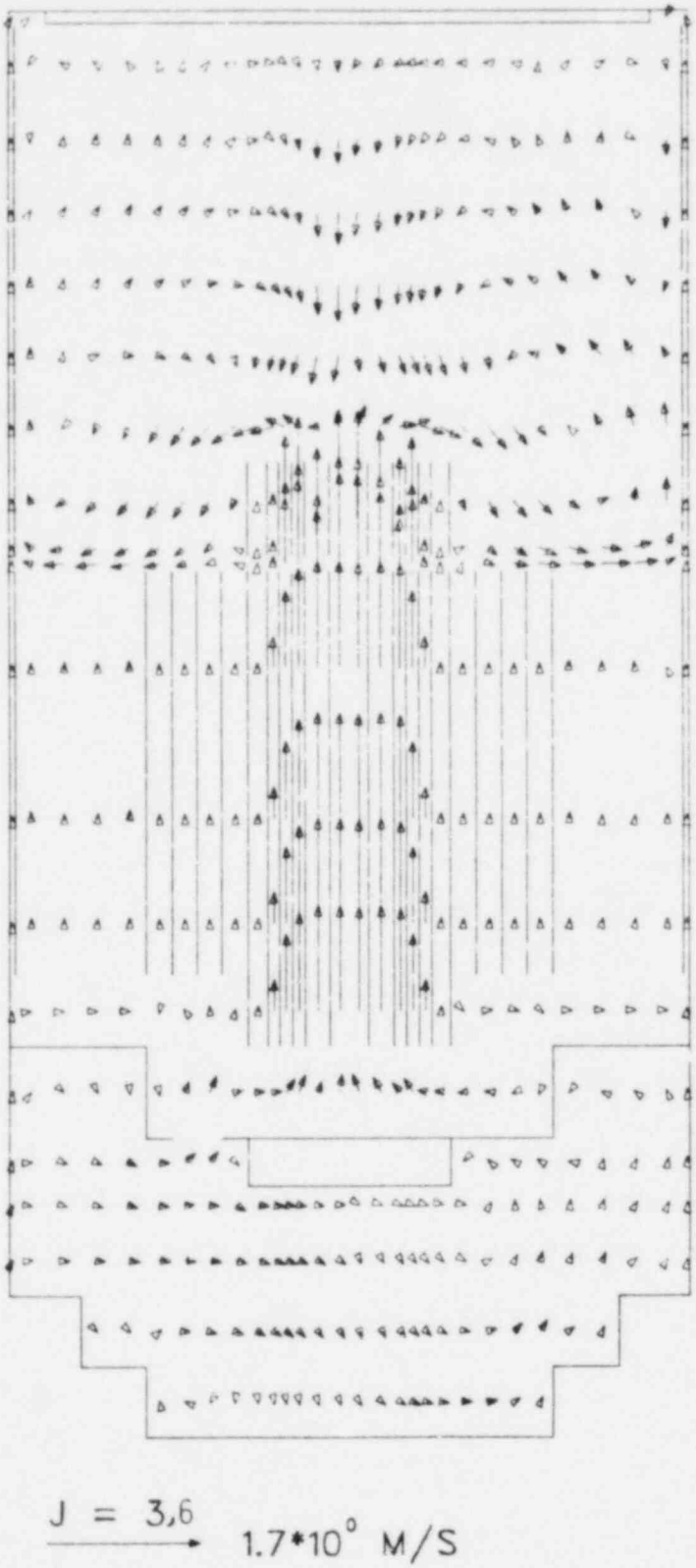

Fig. 10c. Velocity Vectors at t = 29 sec

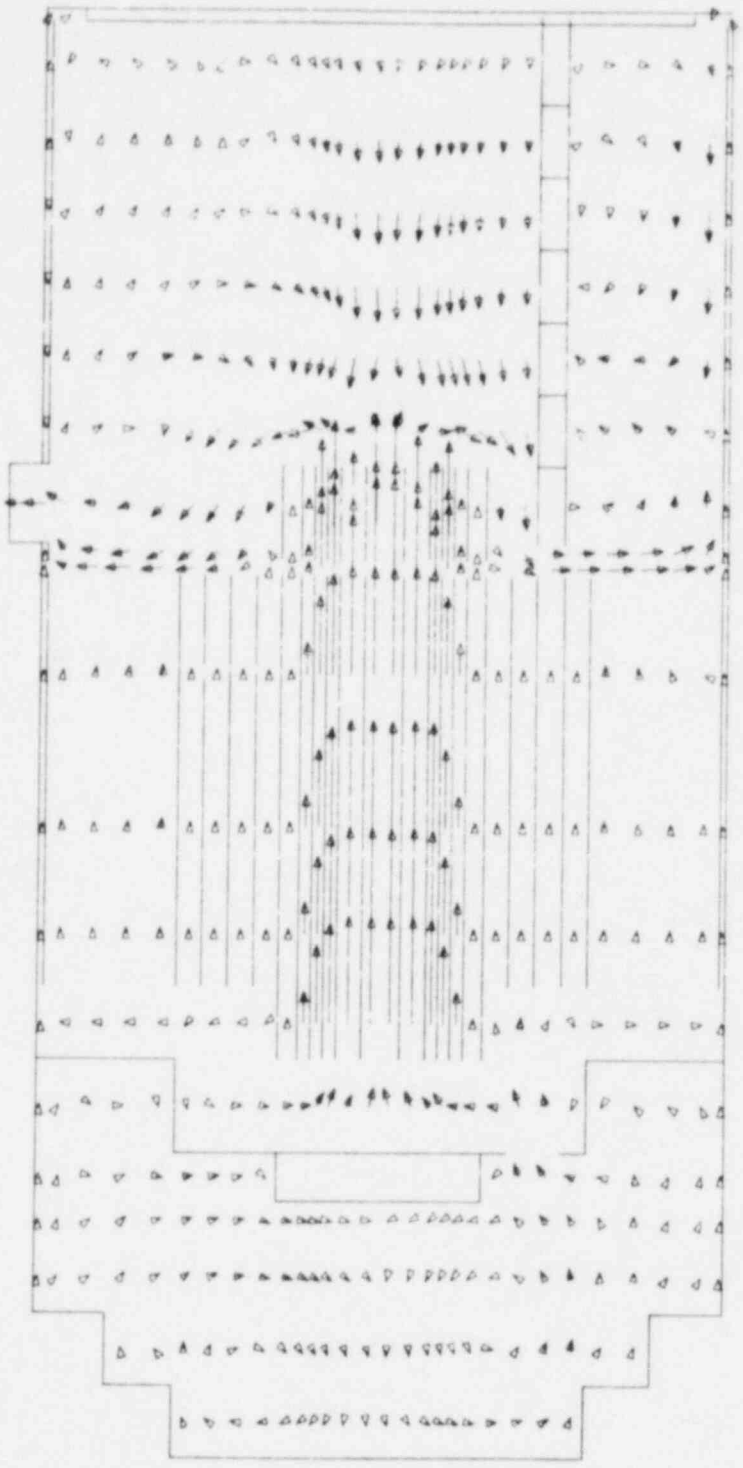

Fig. 10d. Velocity Vectors at t = 29 sec

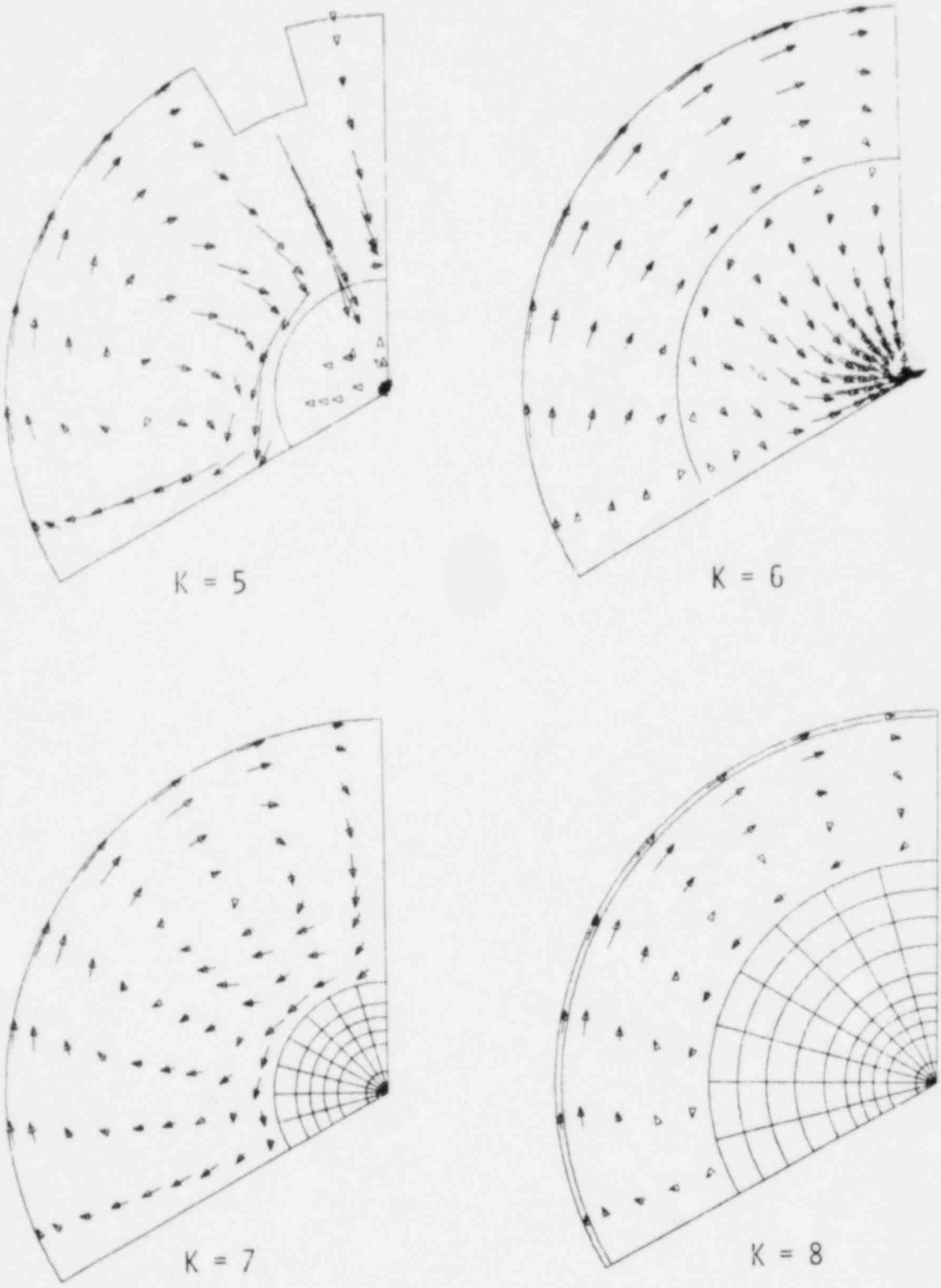

Fig. 10e. Velocity Vectors in R-Θ Plane at t = 29 sec

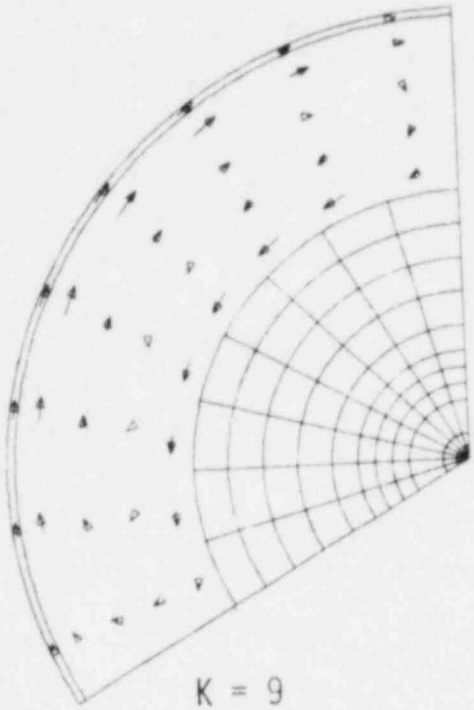

K = 9

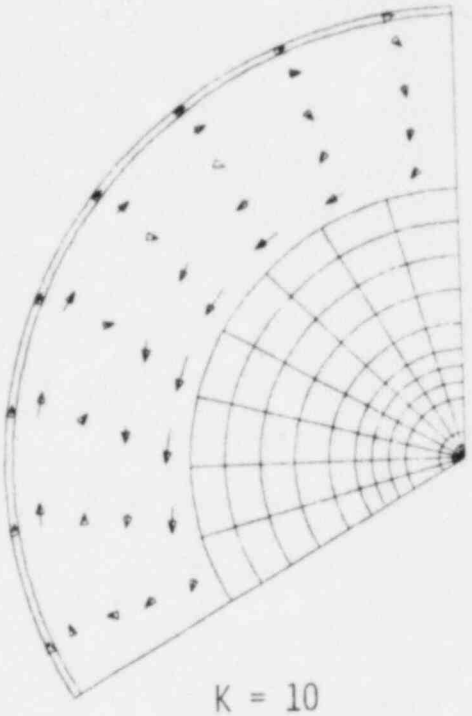

K = 10

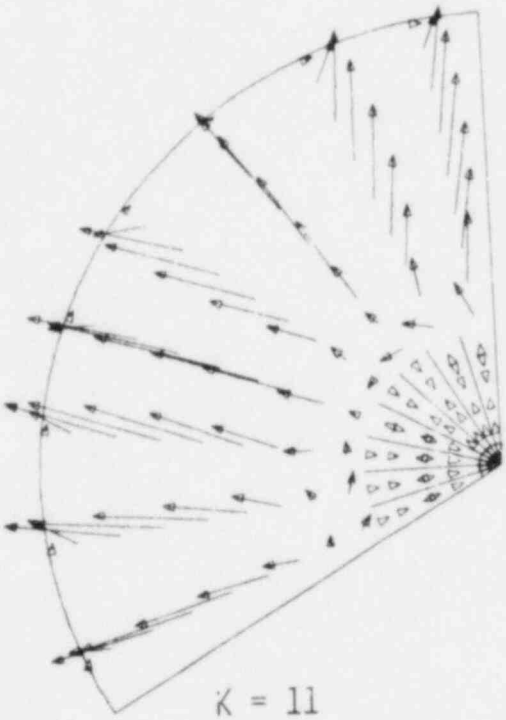

K = 11

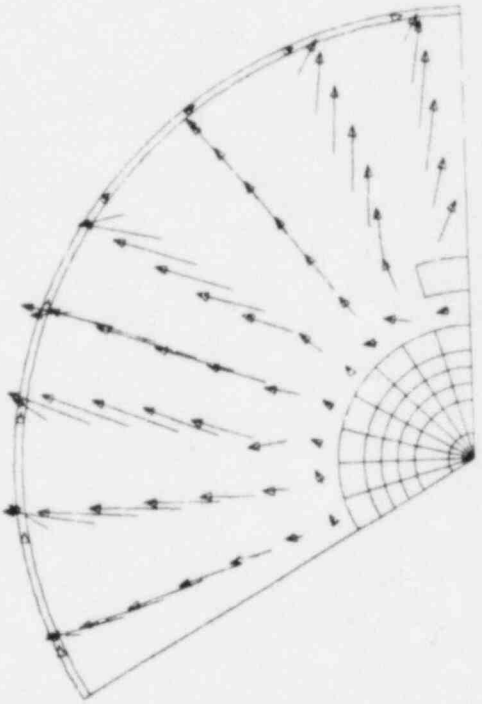

K = 12

Fig. 10f. Velocity Vectors in R-Θ Plane at t = 29 sec

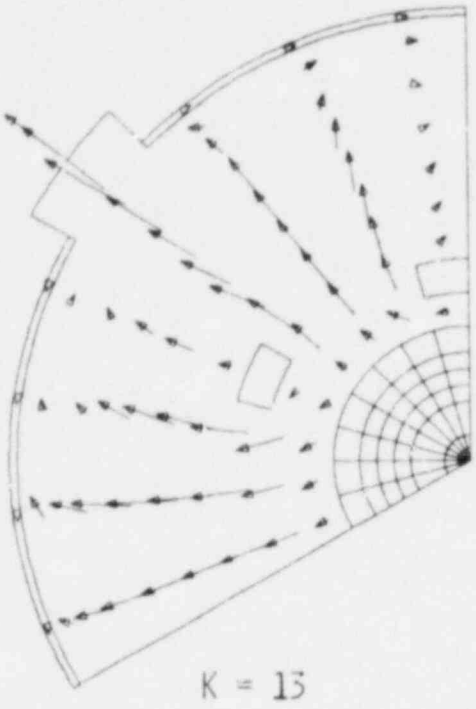

K = 13

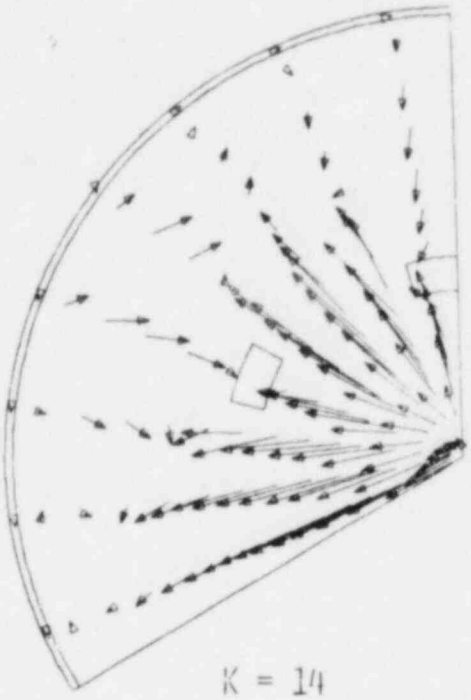

K = 14

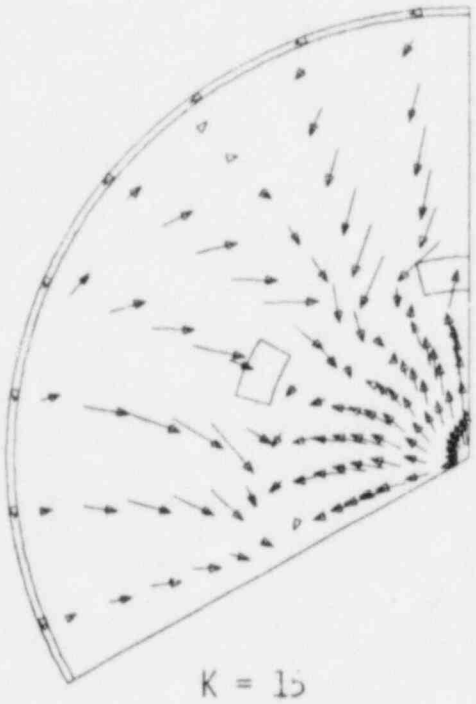

K = 15

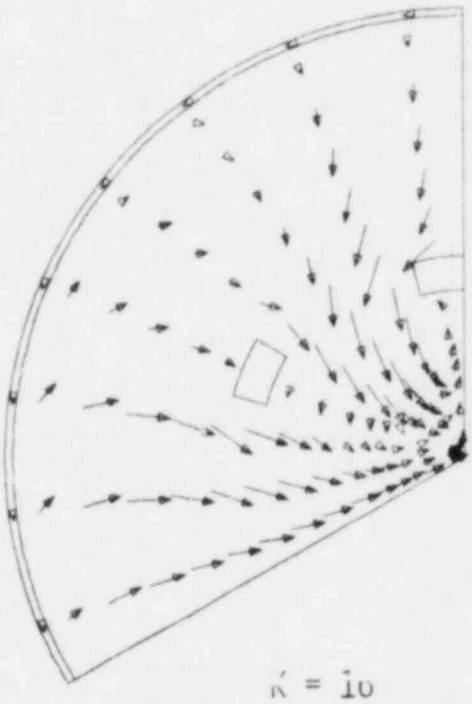

K = 16

Fig. 10g. Velocity Vectors in R-θ Plane at t = 29 sec

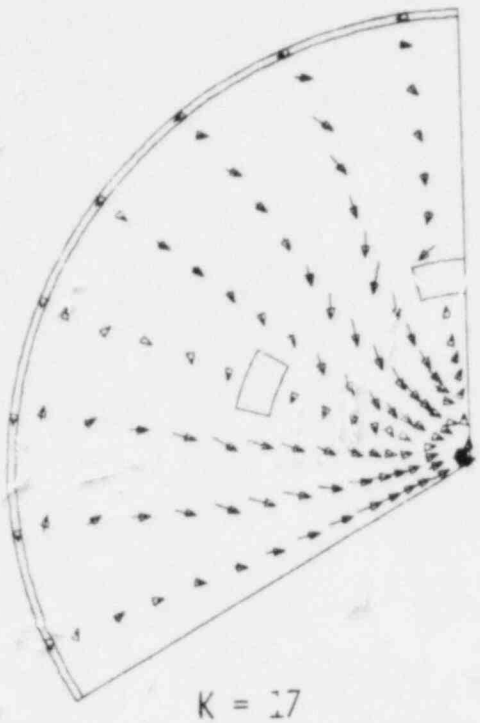

K = 17

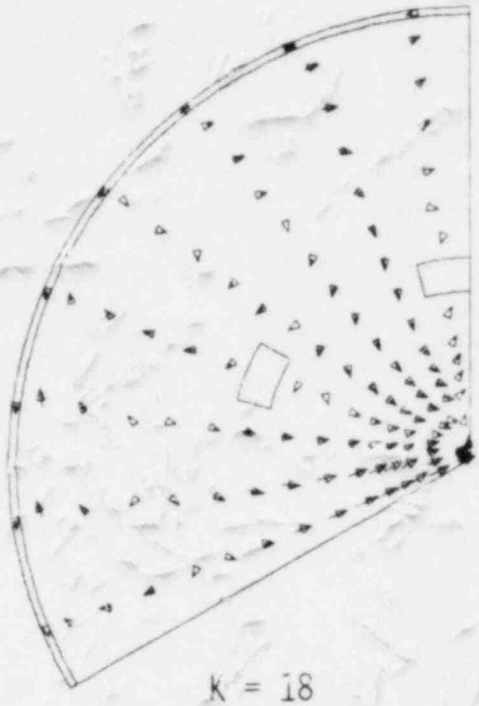

K = 18

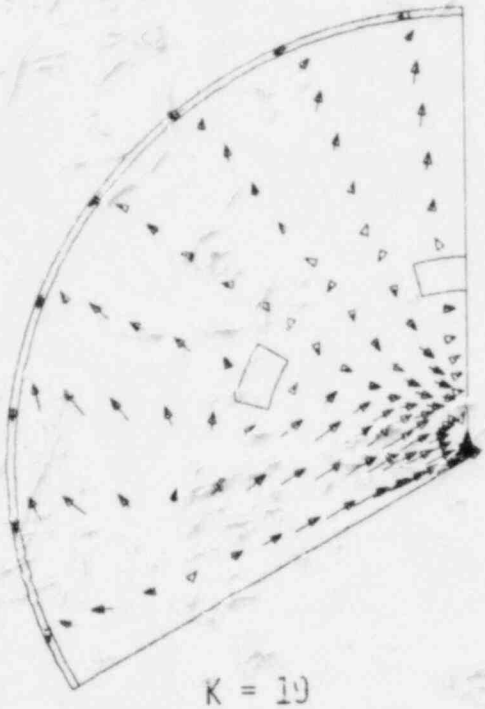

K = 19

Fig. 19h. Velocity Vectors in R-θ Plane at t = 29 sec

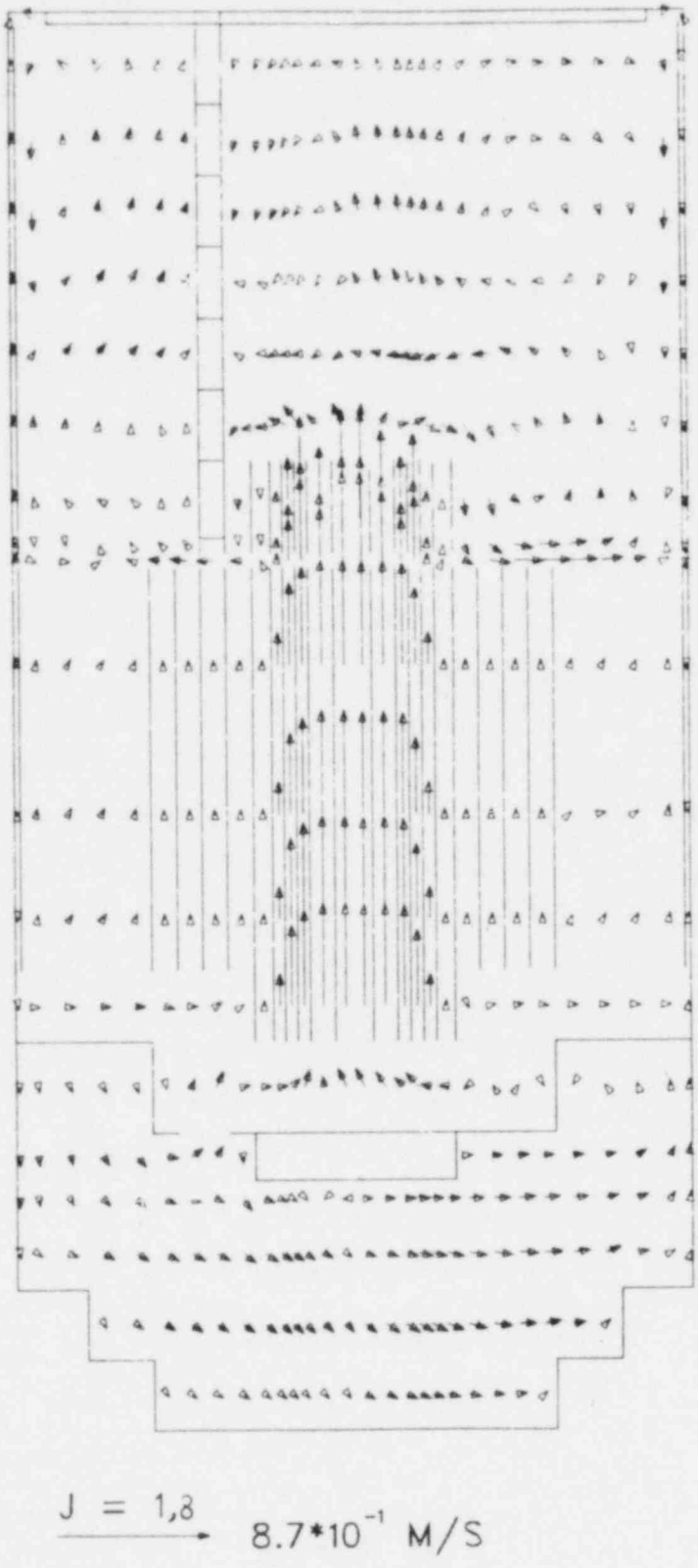

Fig. 11a. Velocity Vectors in R-Z Plane at t = 53 sec

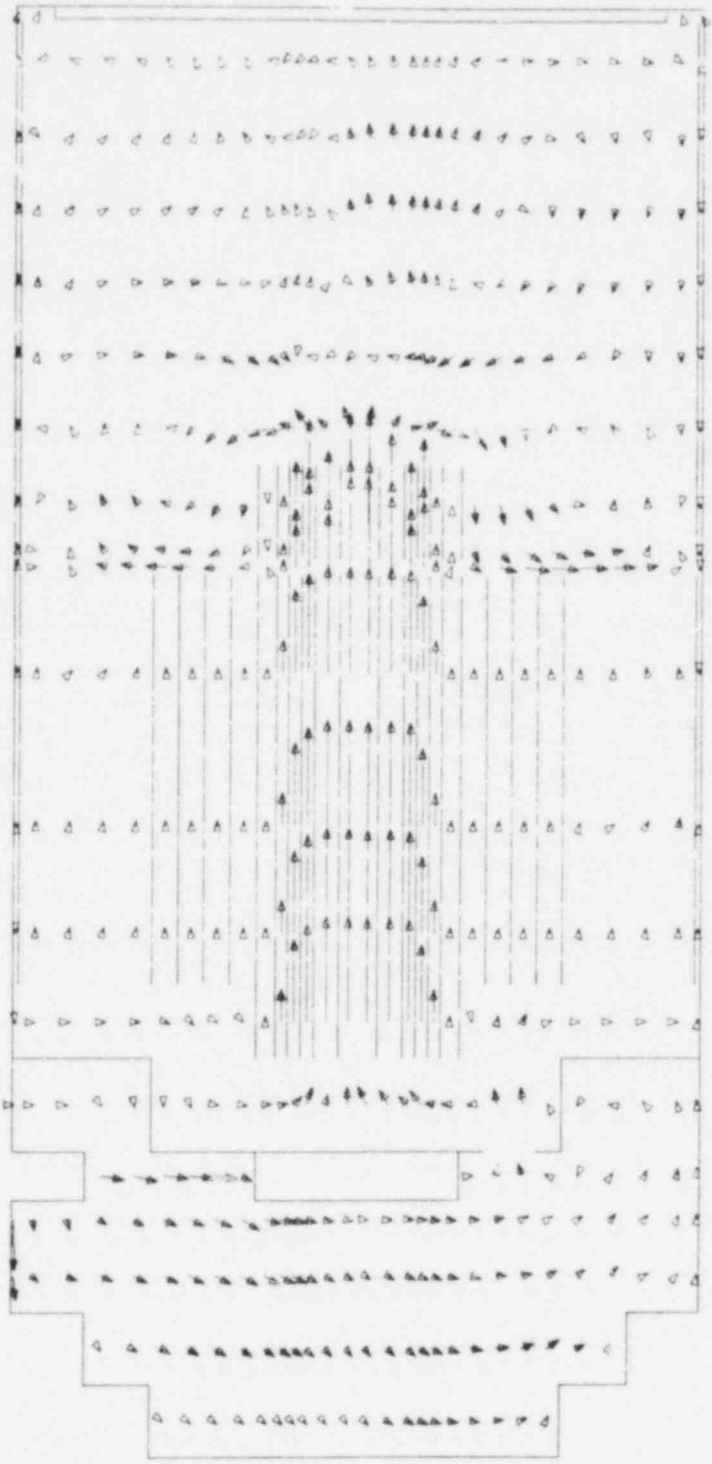

Fig. 11b. Velocity Vectors in R-Z Plane at t = 53 sec

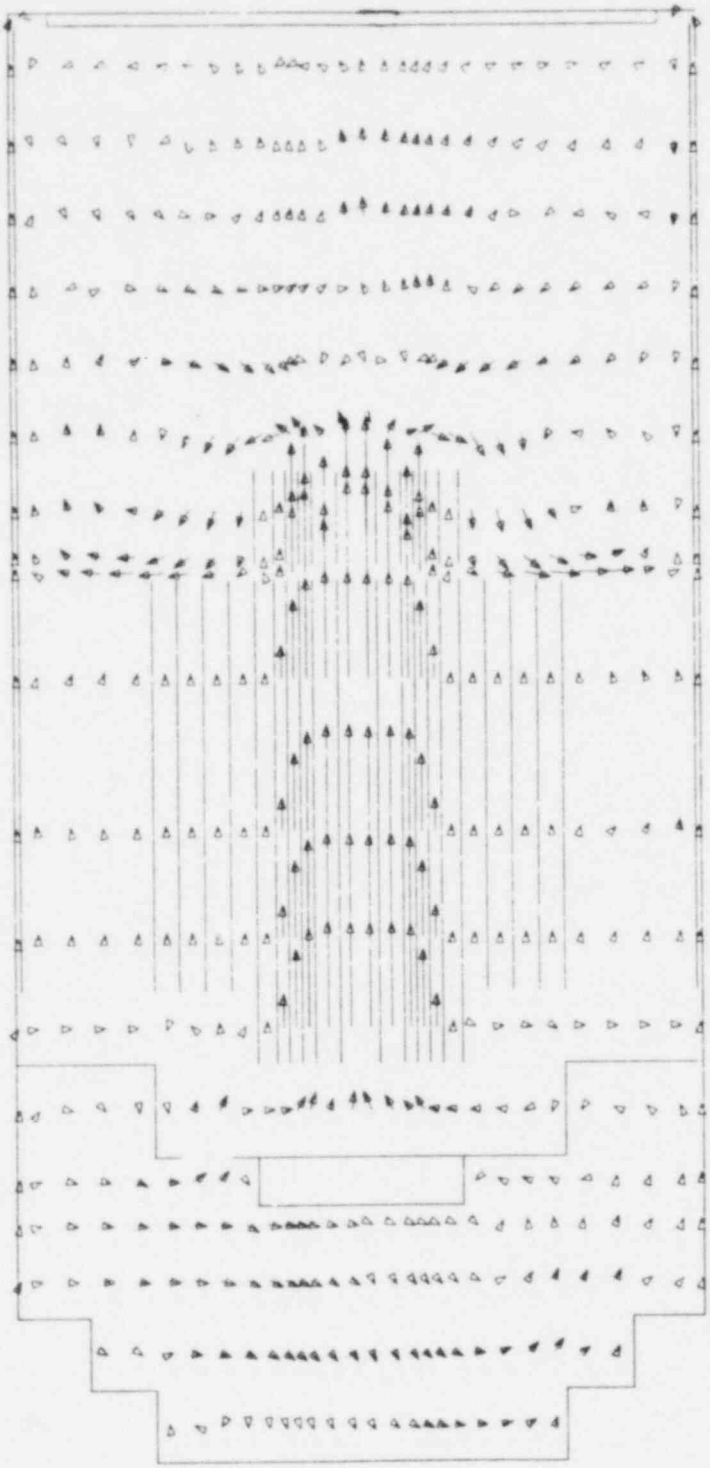

Fig. 11c. Velocity Vectors in R-Z Plane at t = 53 sec

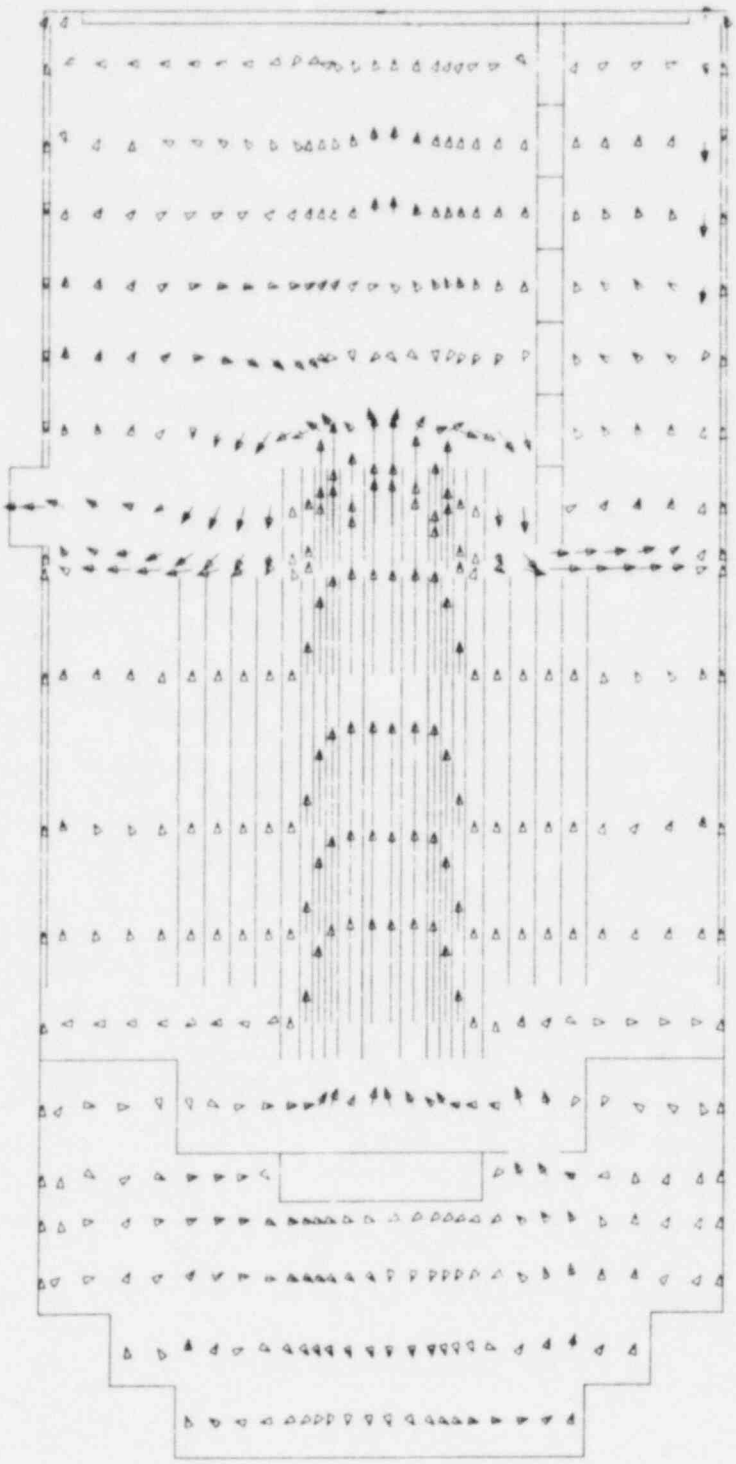

Fig. 11d. Velocity Vectors in R-Z Plane at t = 53 sec

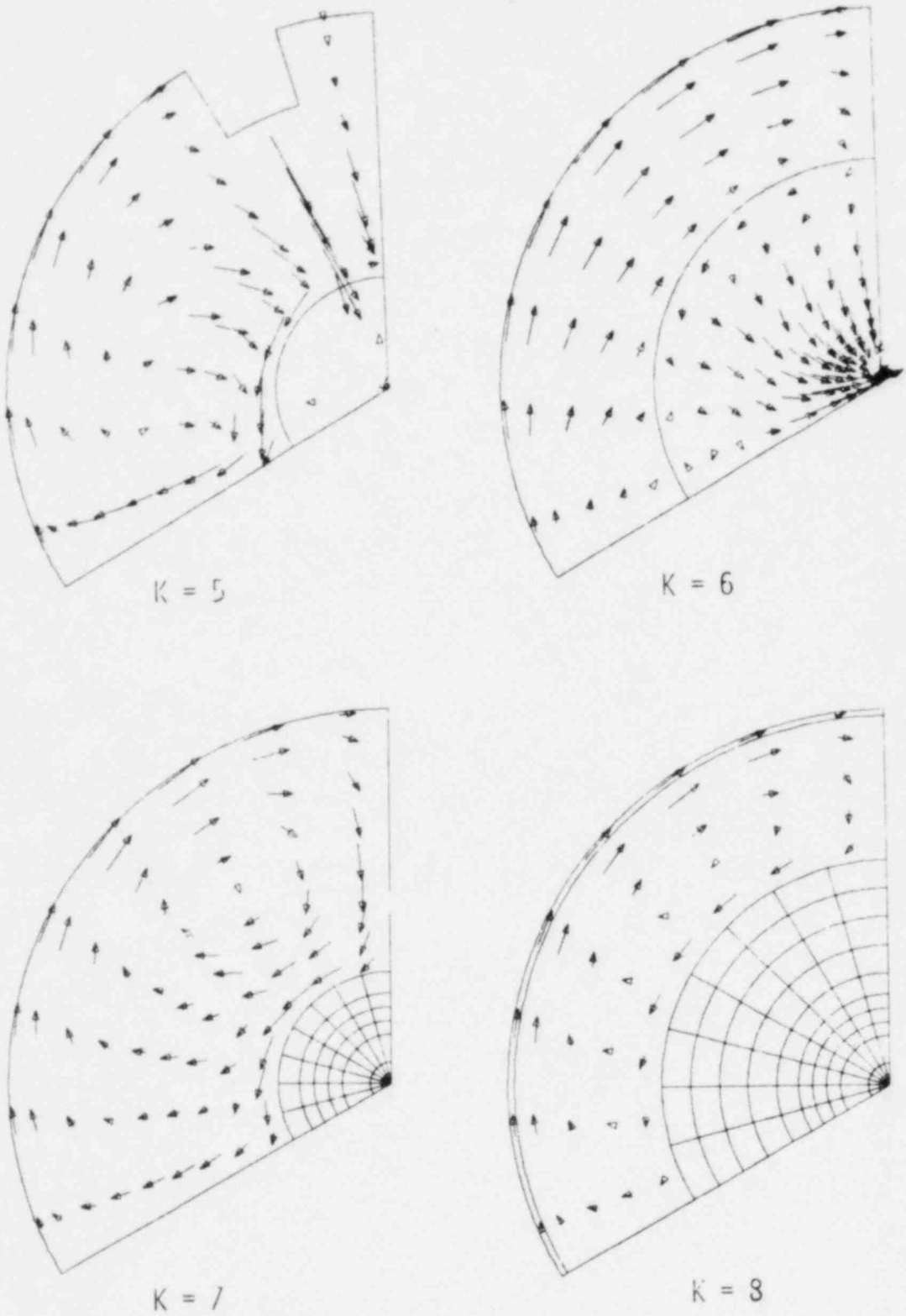

Fig. 11e. Velocity Vectors in R-Θ Plane at t - 53 sec

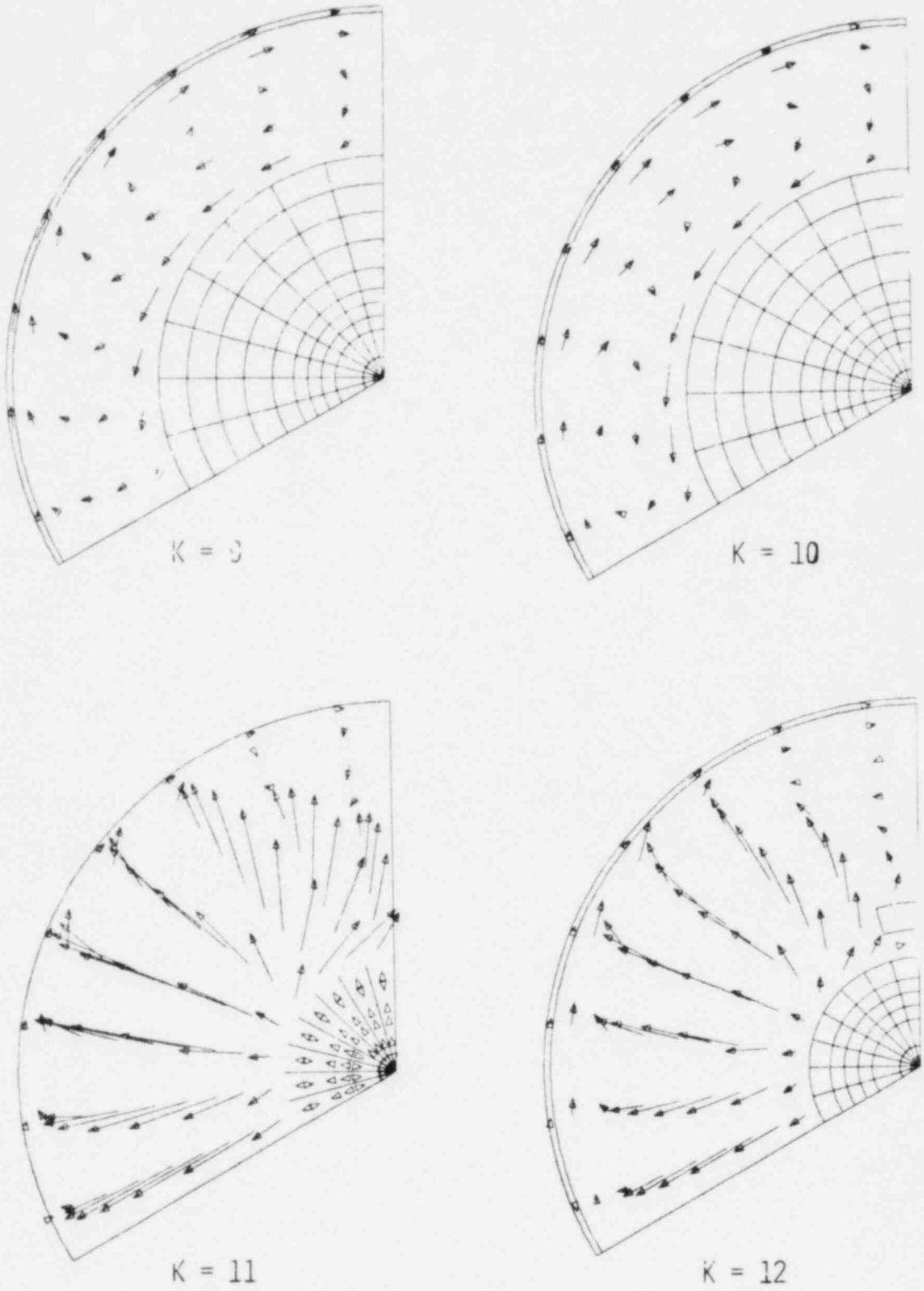

Fig. 11f. Velocity Vectors in R-Θ Plane at t = 53 sec

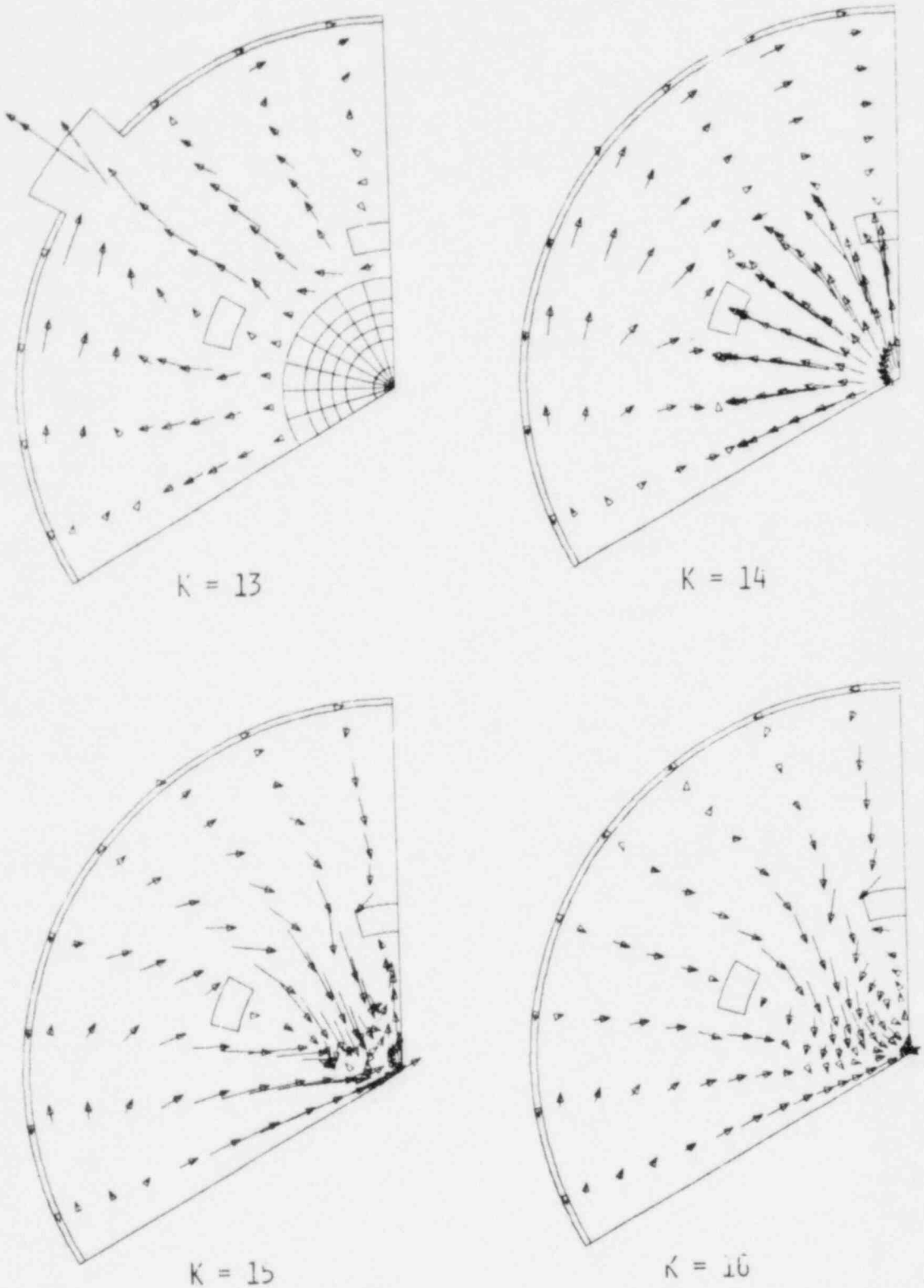

Fig. 11g. Velocity Vectors in R-θ Plane at t = 53 sec

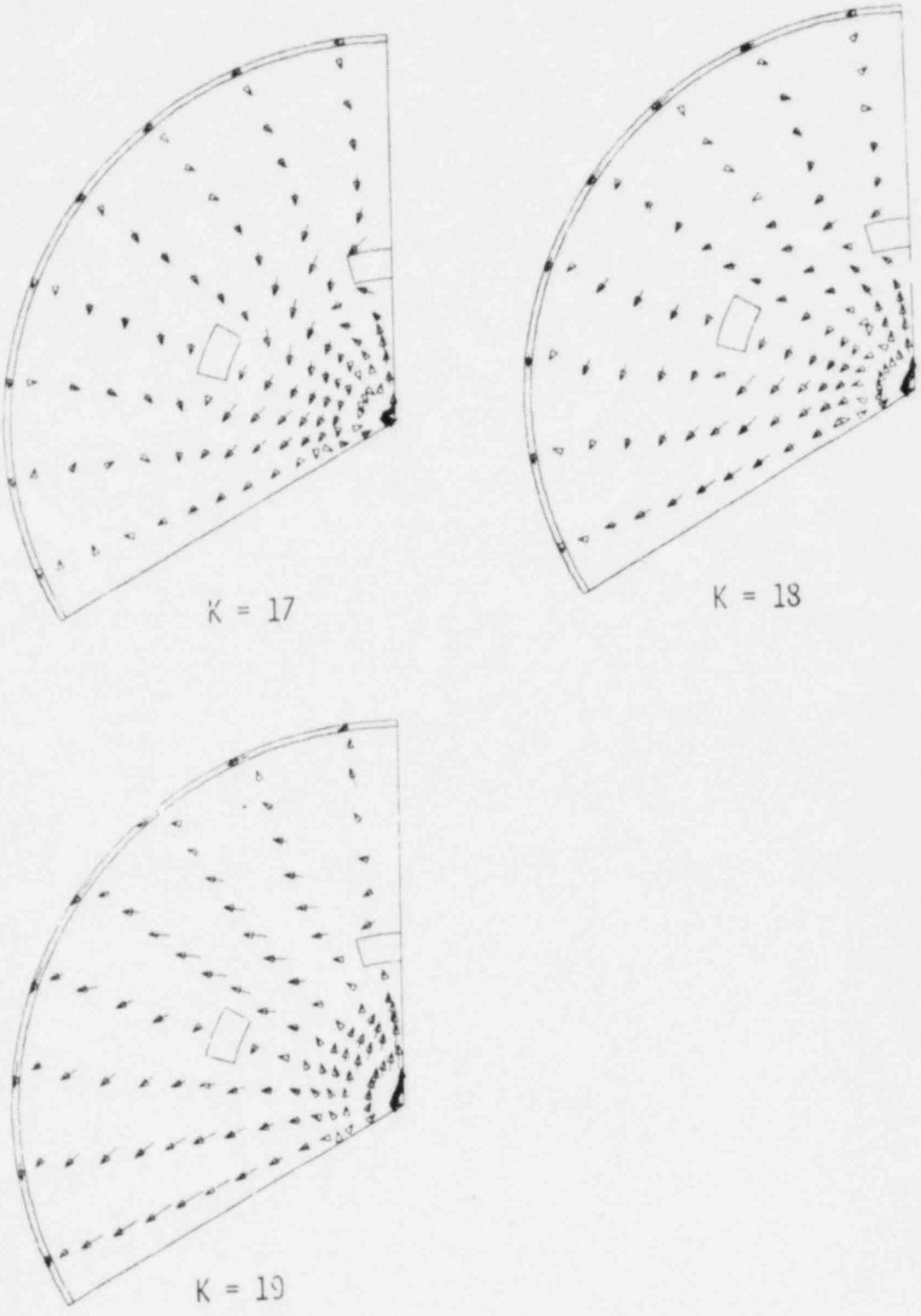

Fig. 11h. Velocity Vectors in R-θ Plane at t = 53 sec

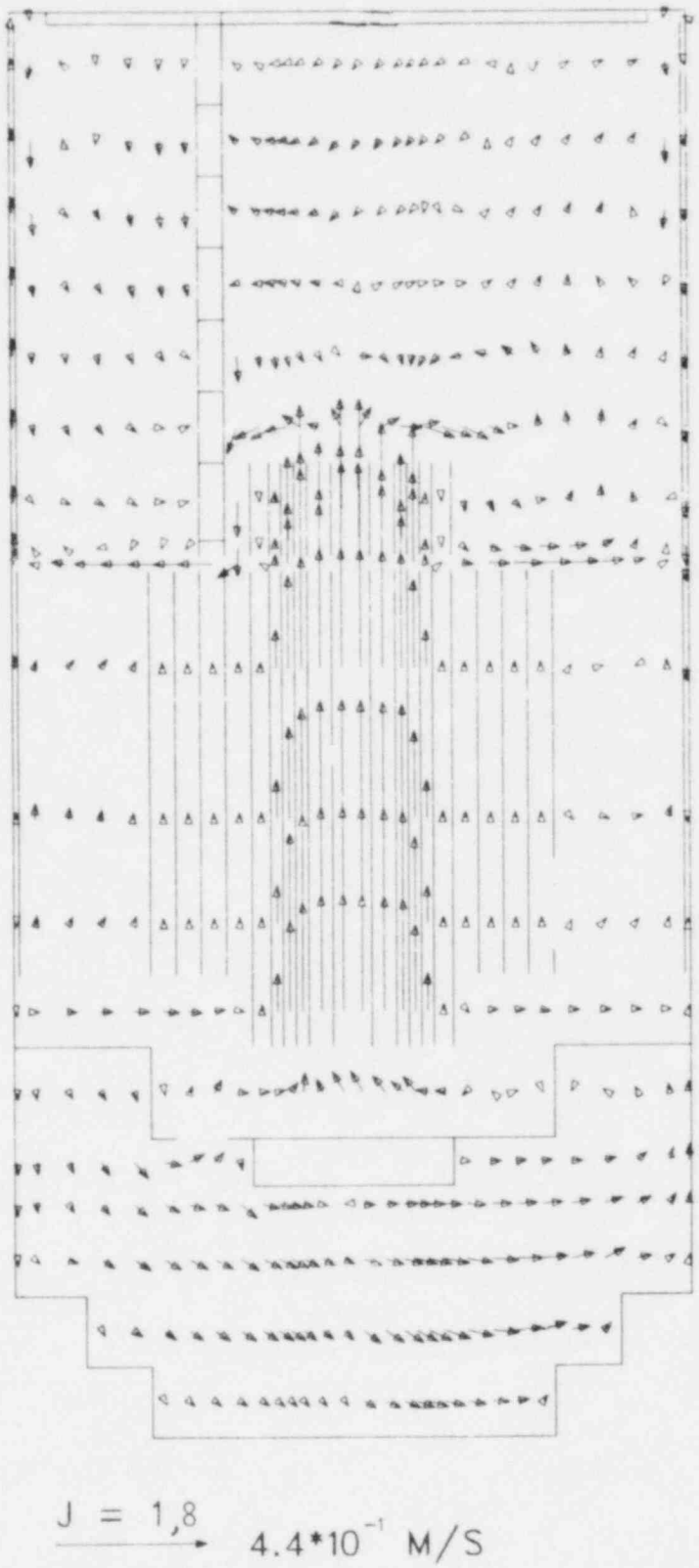

Fig. 12a. Velocity Vectors in R-Z Plane at t = 79 sec

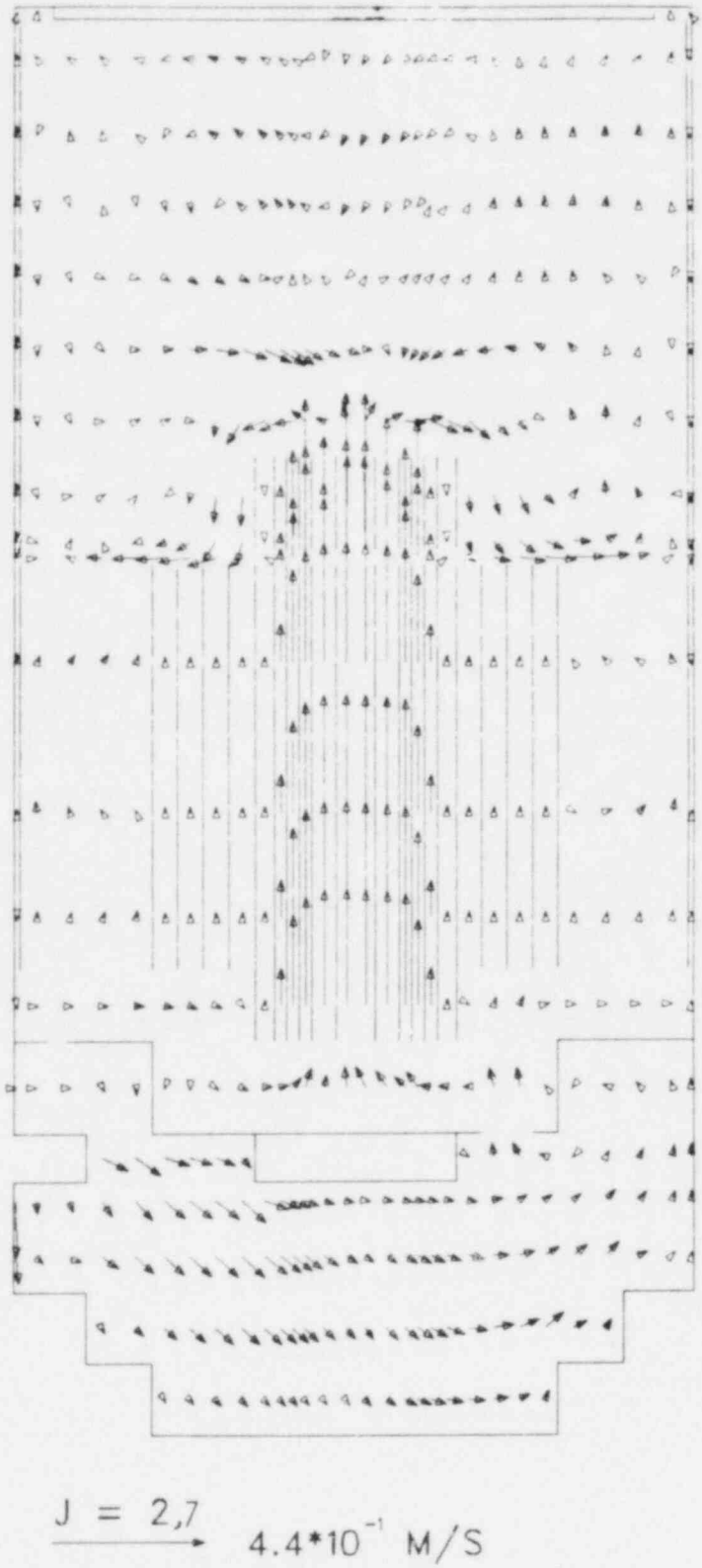

Fig. 12b. Velocity Vectors in R-Z Plane at t = 79 sec

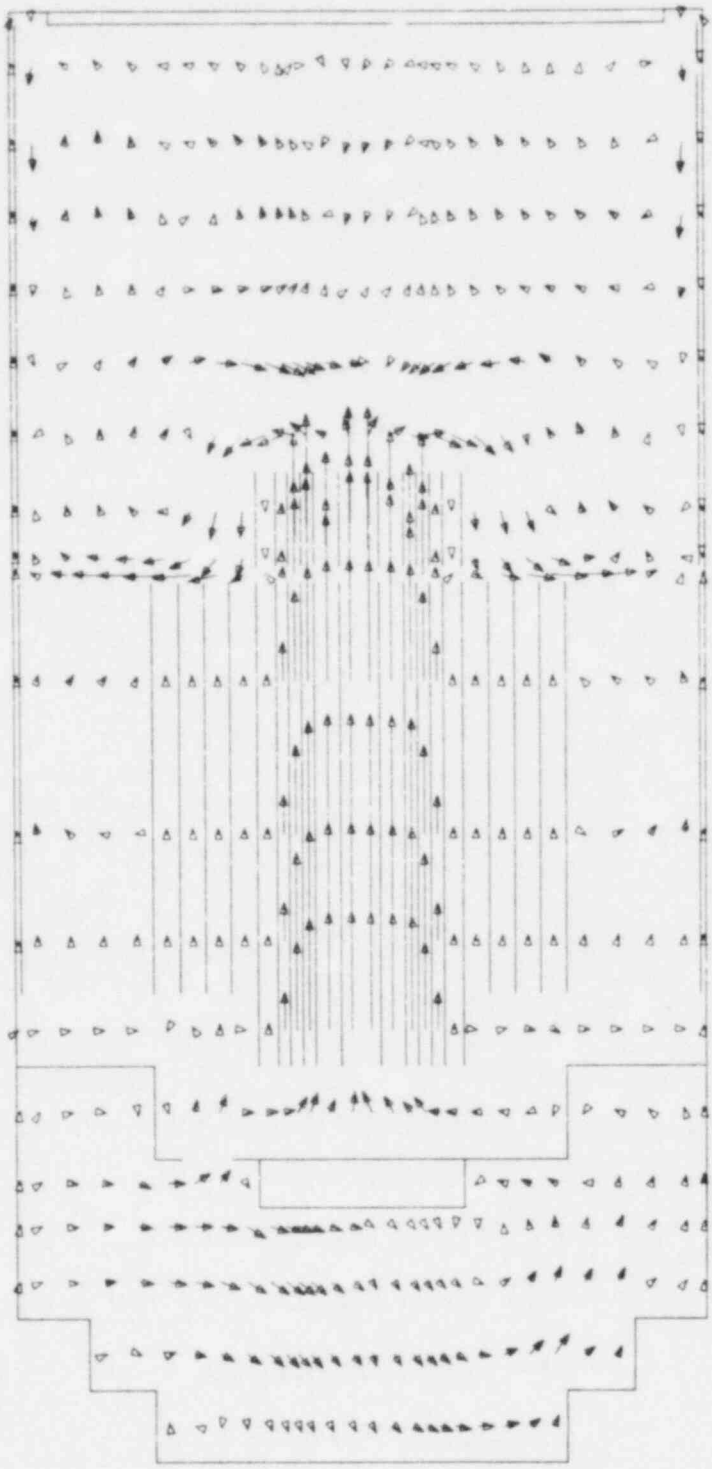

Fig. 12c. Velocity Vectors in R-Z Plane at t = 79 sec

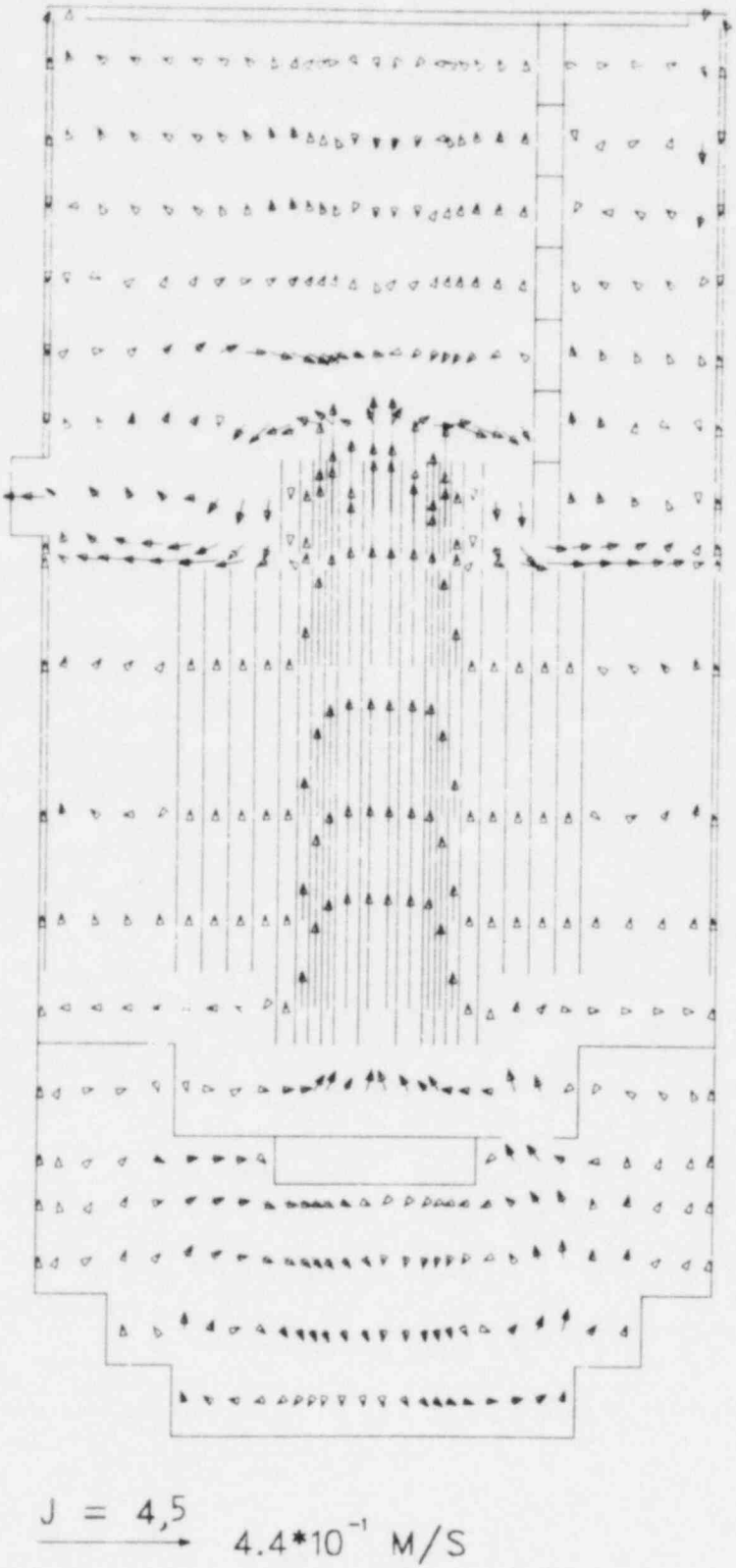

Fig. 12d. Velocity Vectors in R-Z Plane at t = 79 sec

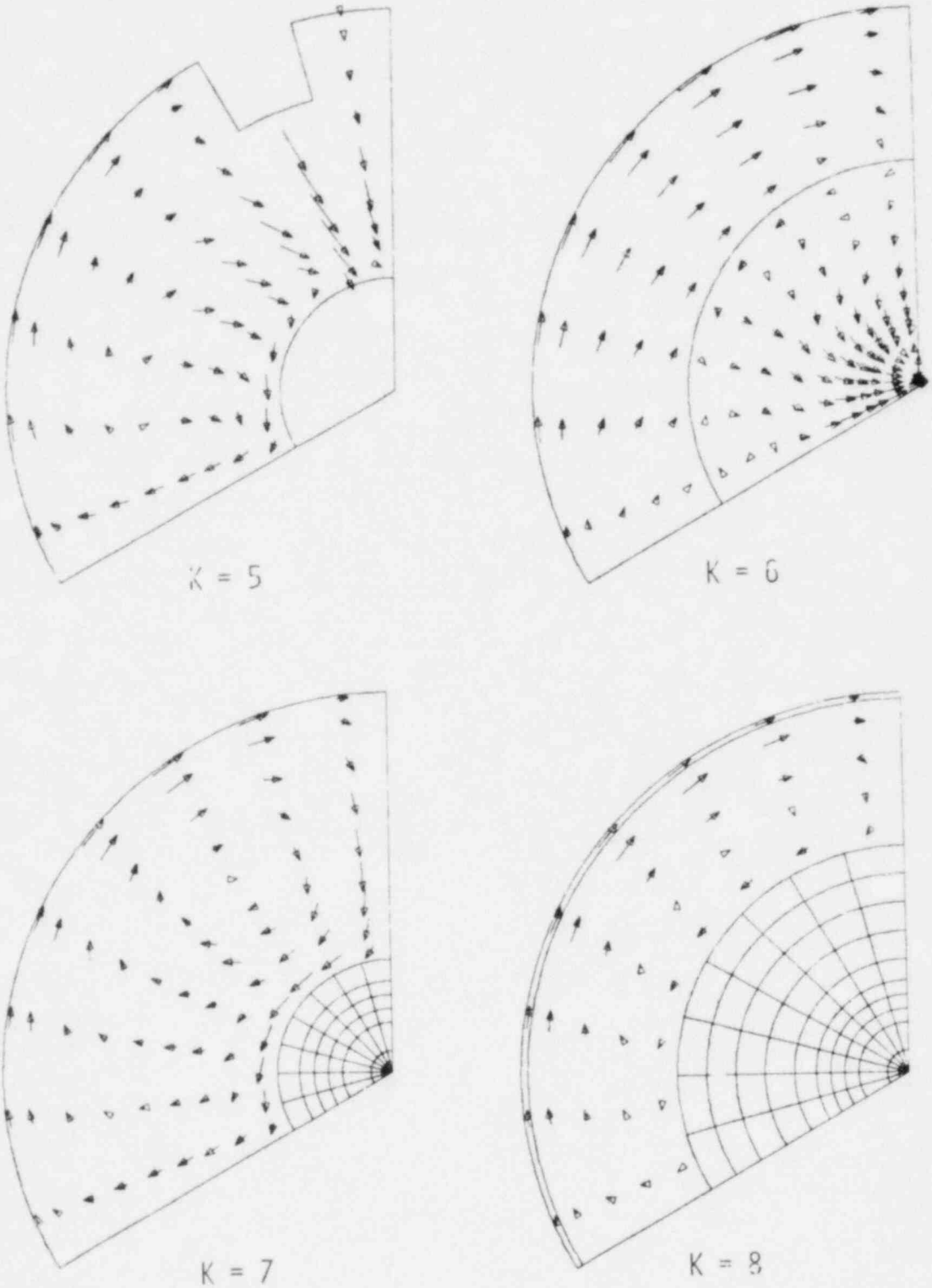

Fig. 12e. Velocity Vectors in R-Θ Plane at t = 79 sec

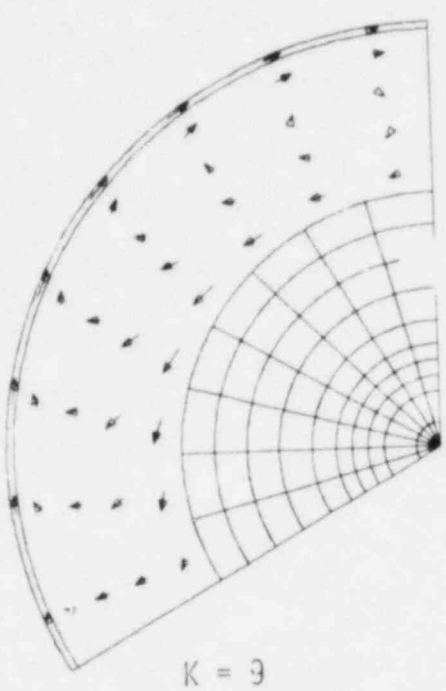

K = 9

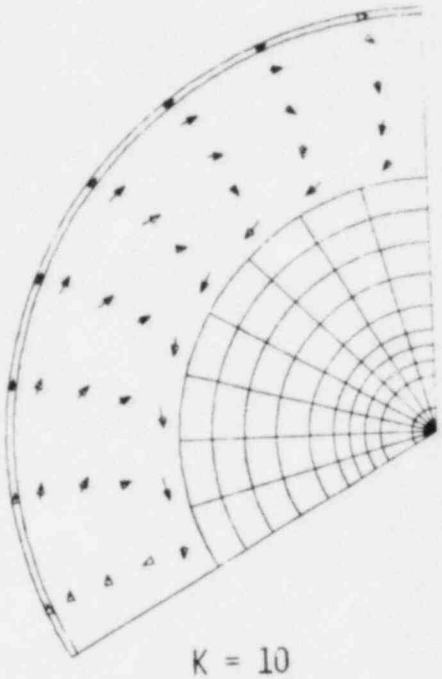

K = 10

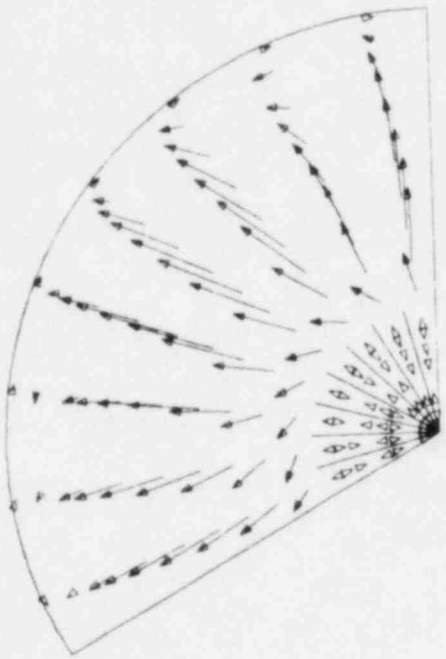

K = 11

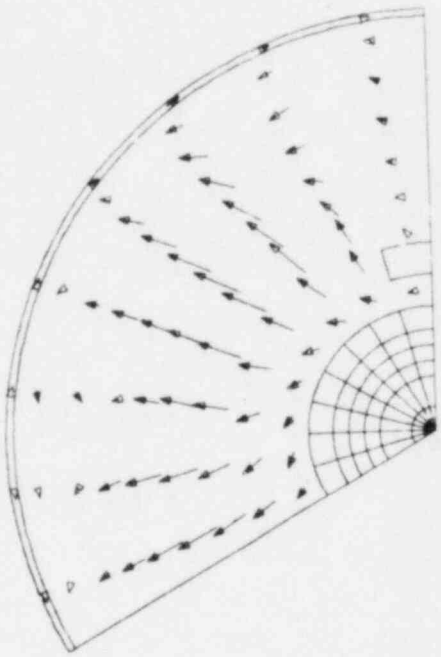

K = 12

Fig. 12f. Velocity Vectors in R-θ Plane at t = 79 sec

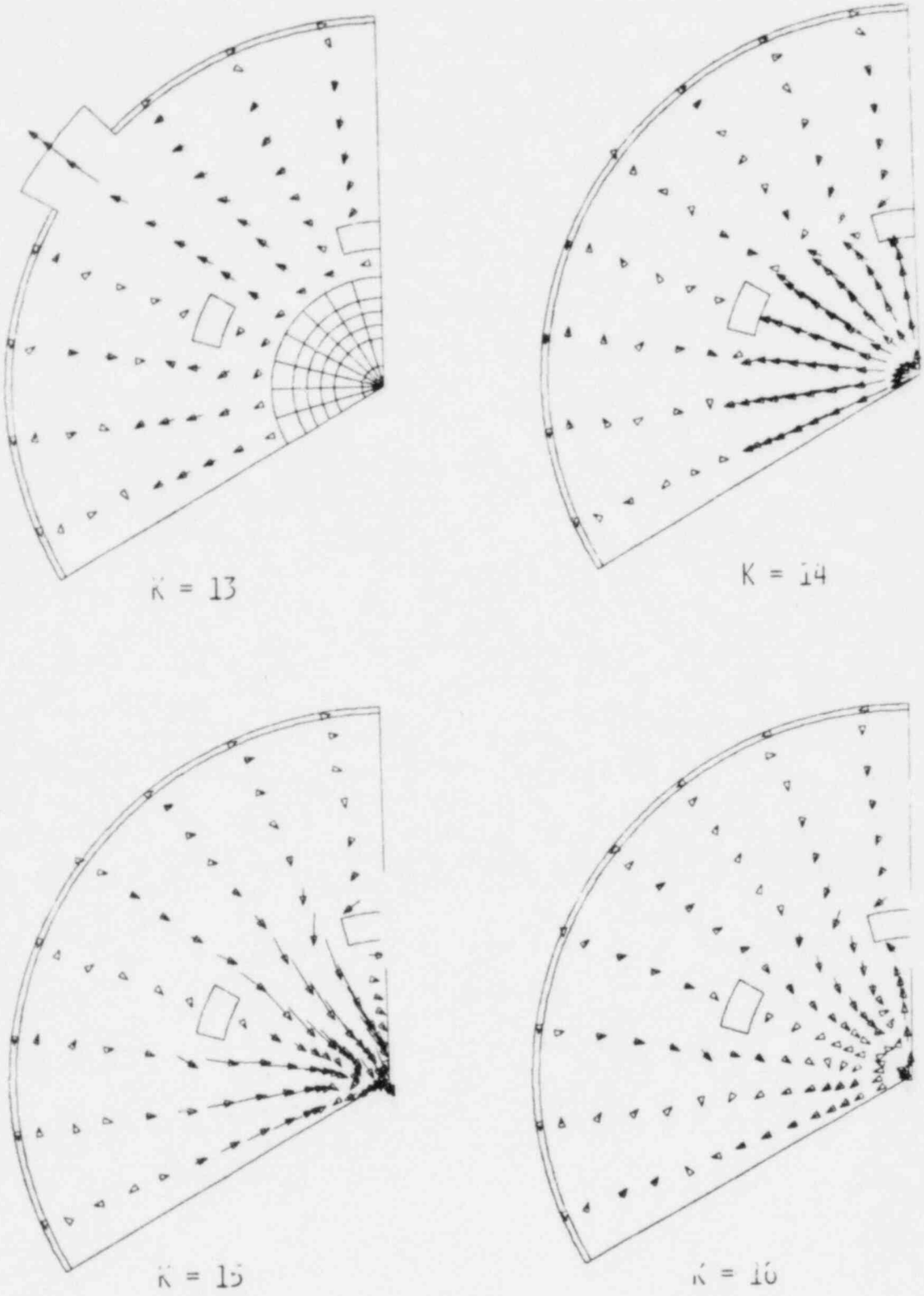

Fig. 12g. Velocity Vectors in R-θ Plane at t = 79 sec

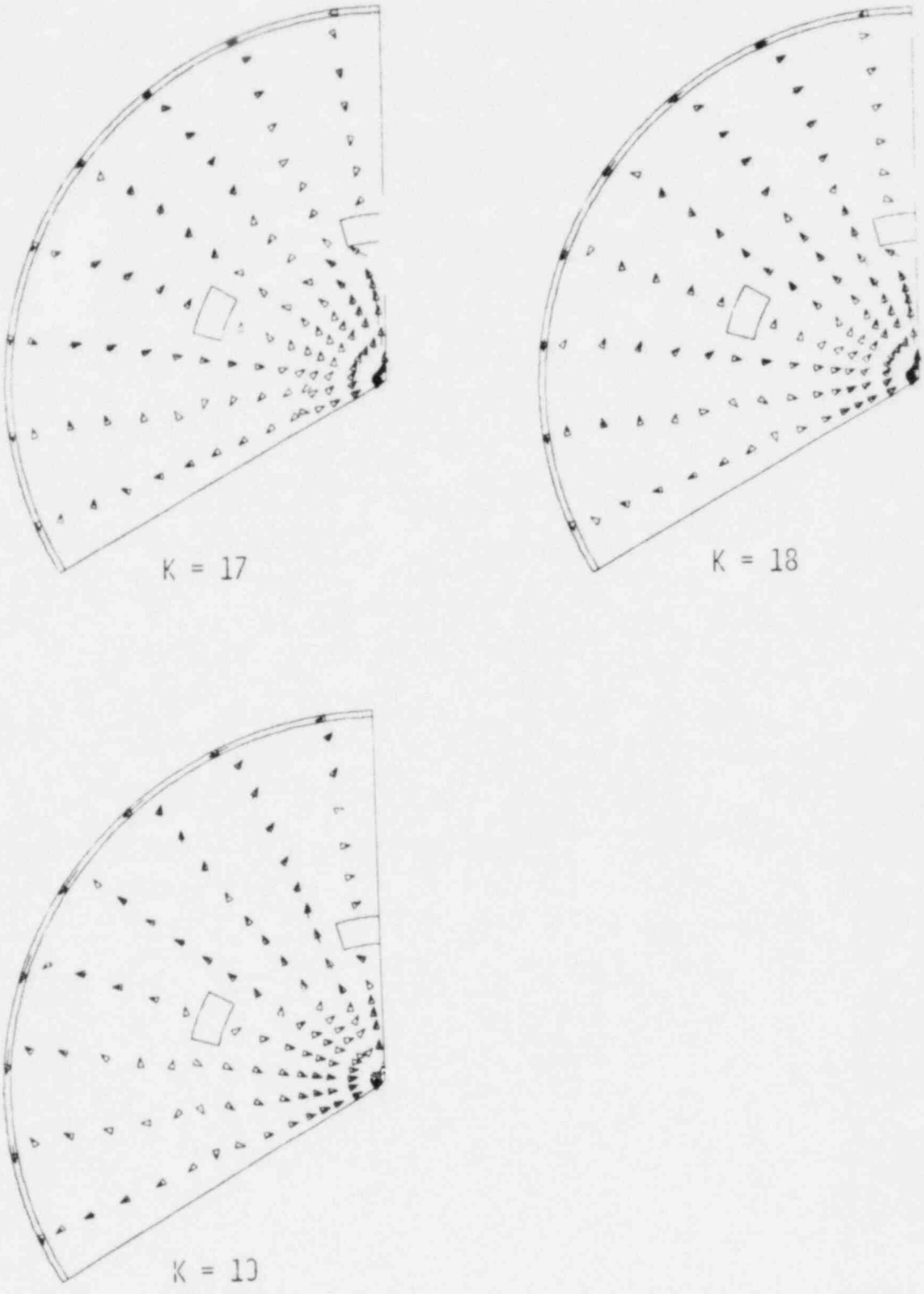

Fig. 12h. Velocity Vectors in R-θ Plane at t = 79 sec

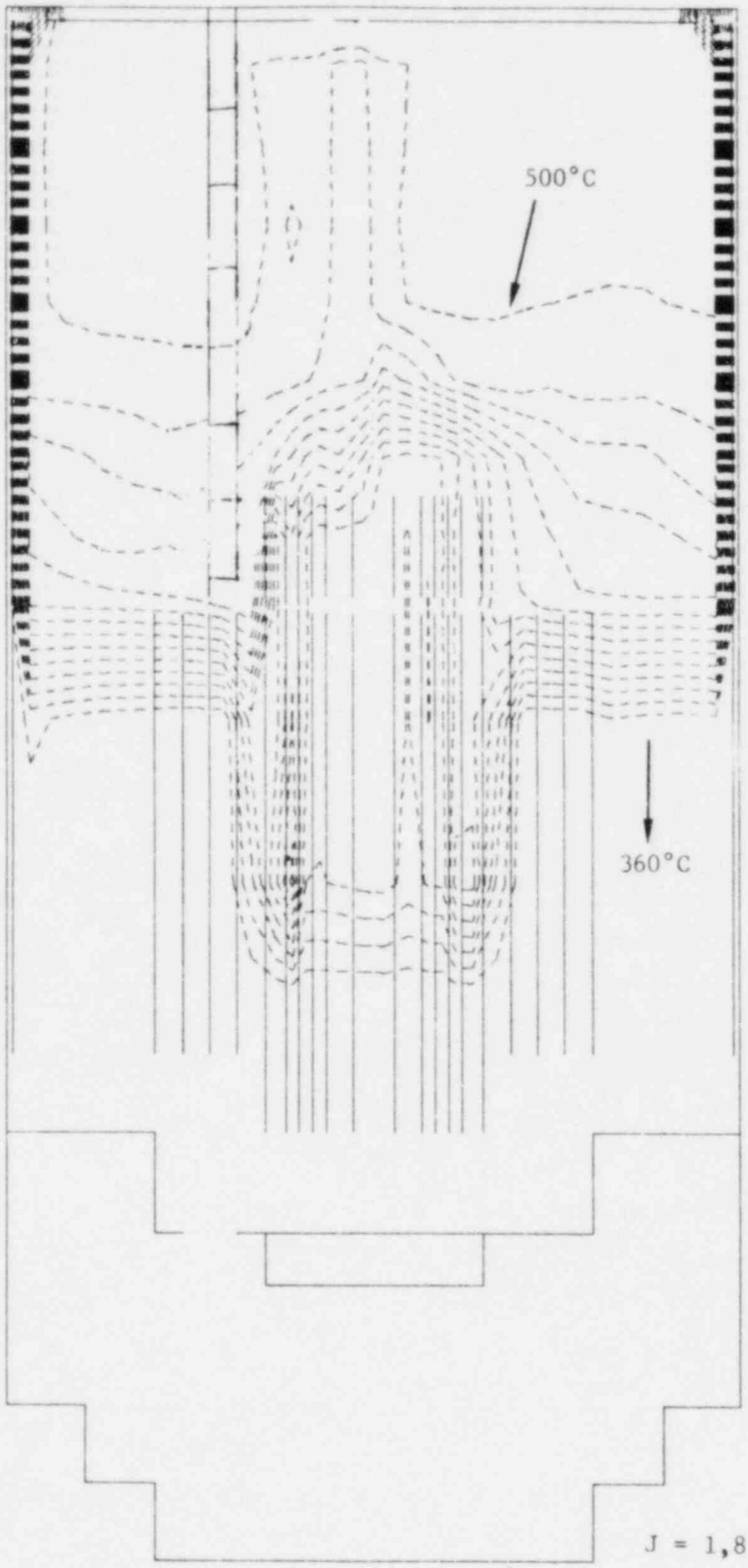

Fig. 13a. Temperature Contours at t = 29 sec
(ΔT = 10°C)

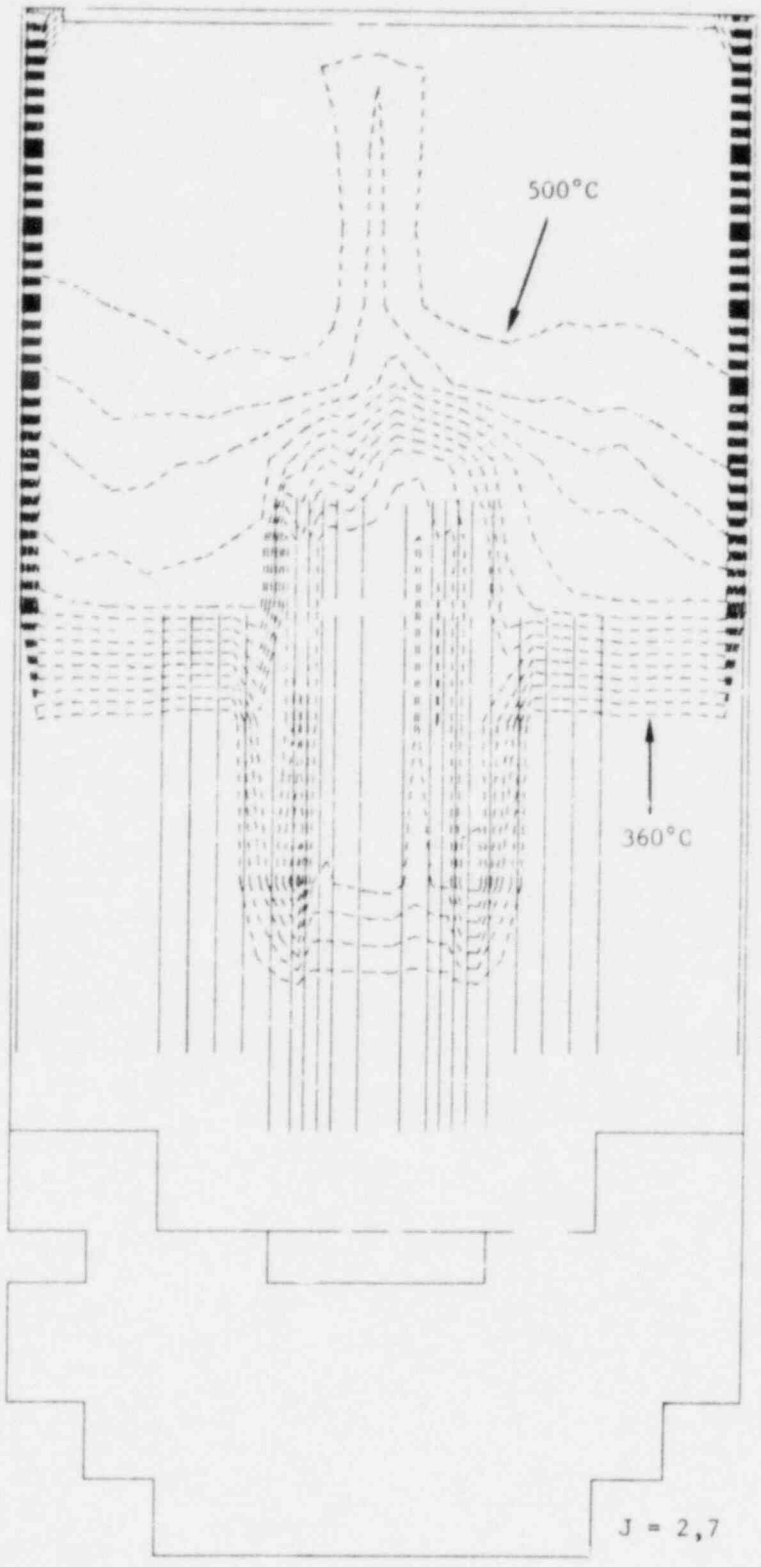

Fig. 13b. Temperature Contours at t = 29 sec
(ΔT = 10°C)

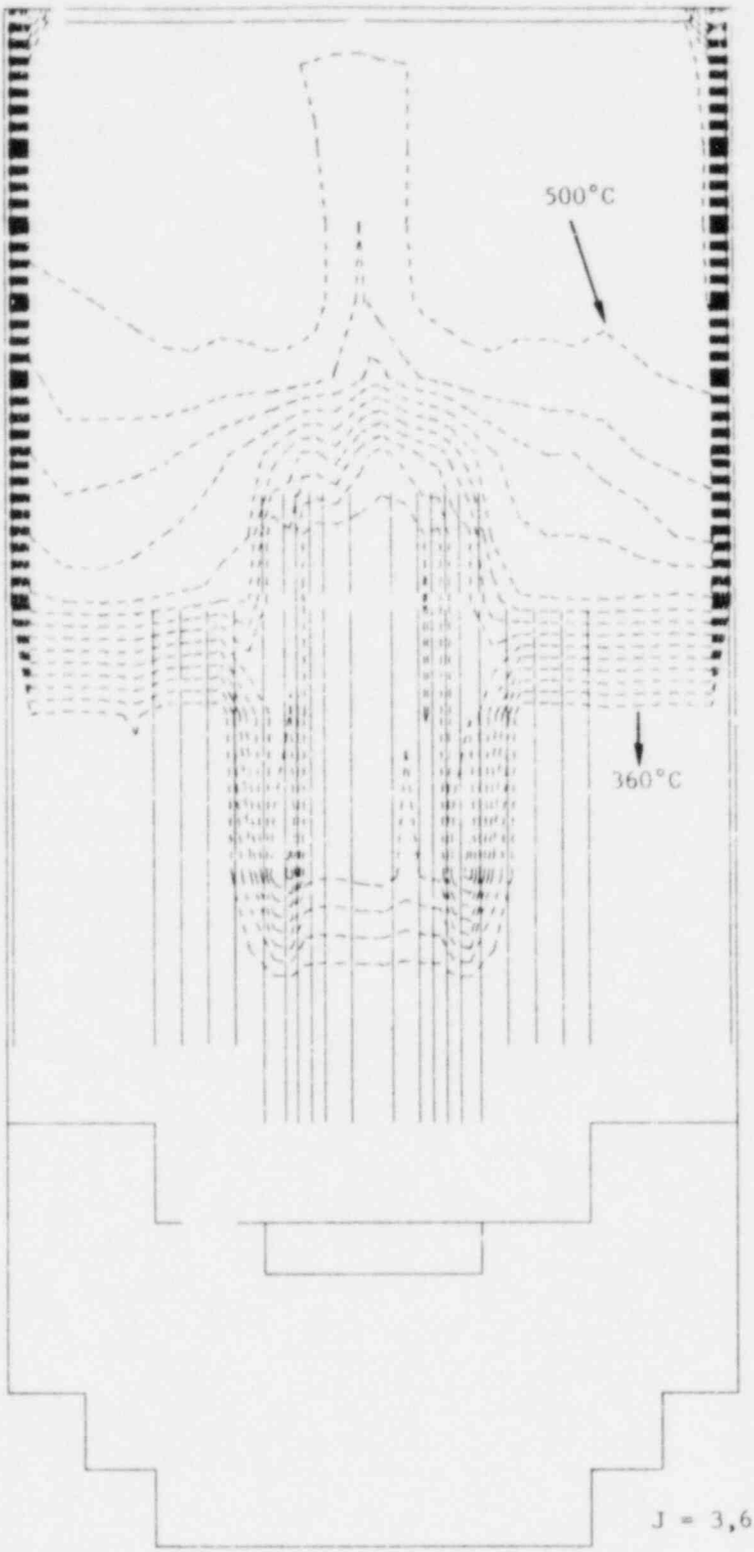

Fig. 13c. Temperature Contours at t = 29 sec
(ΔT = 10°C)

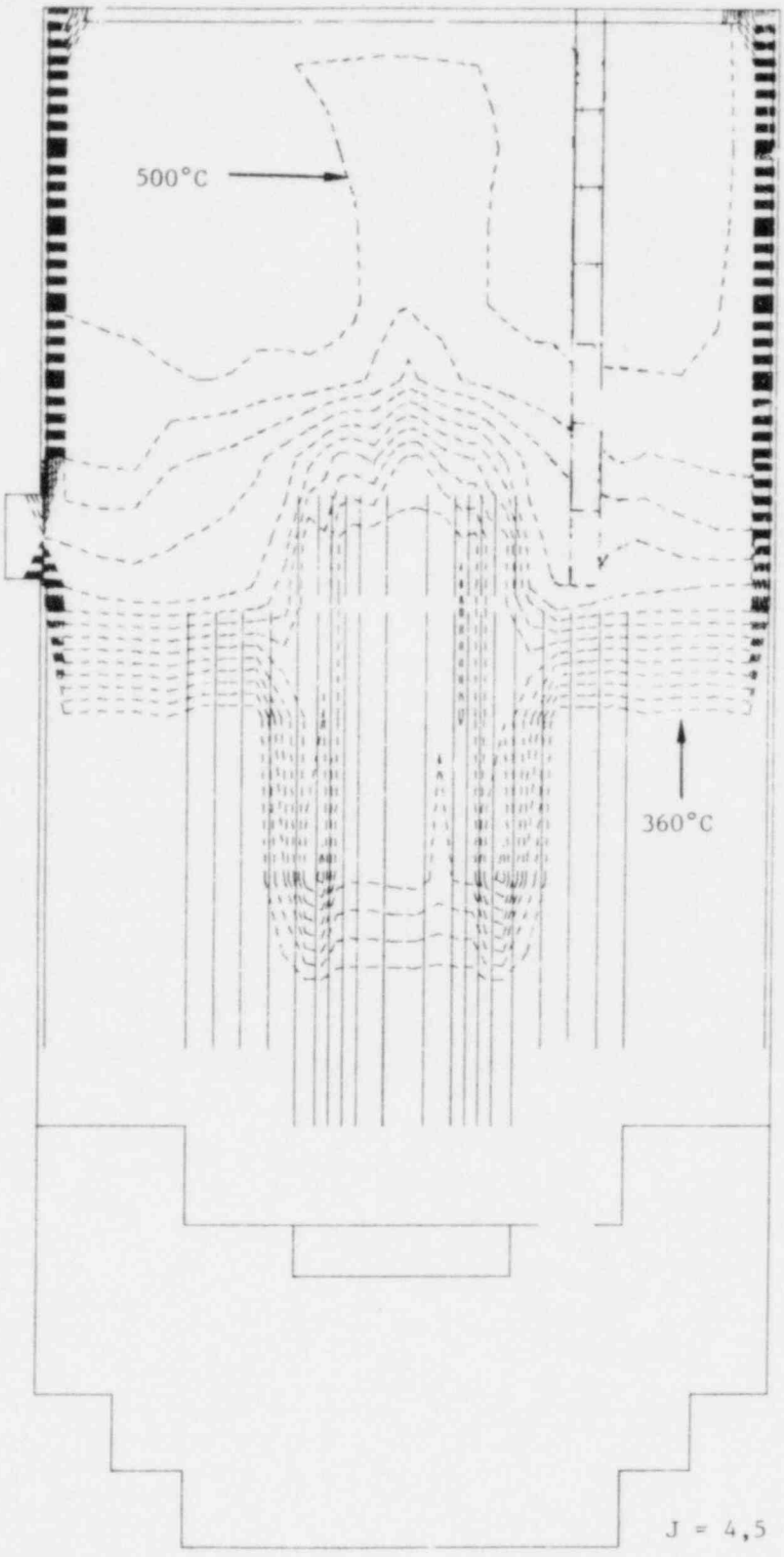

Fig. 13d. Temperature Contours at t = 29 sec
(ΔT = 10°C)

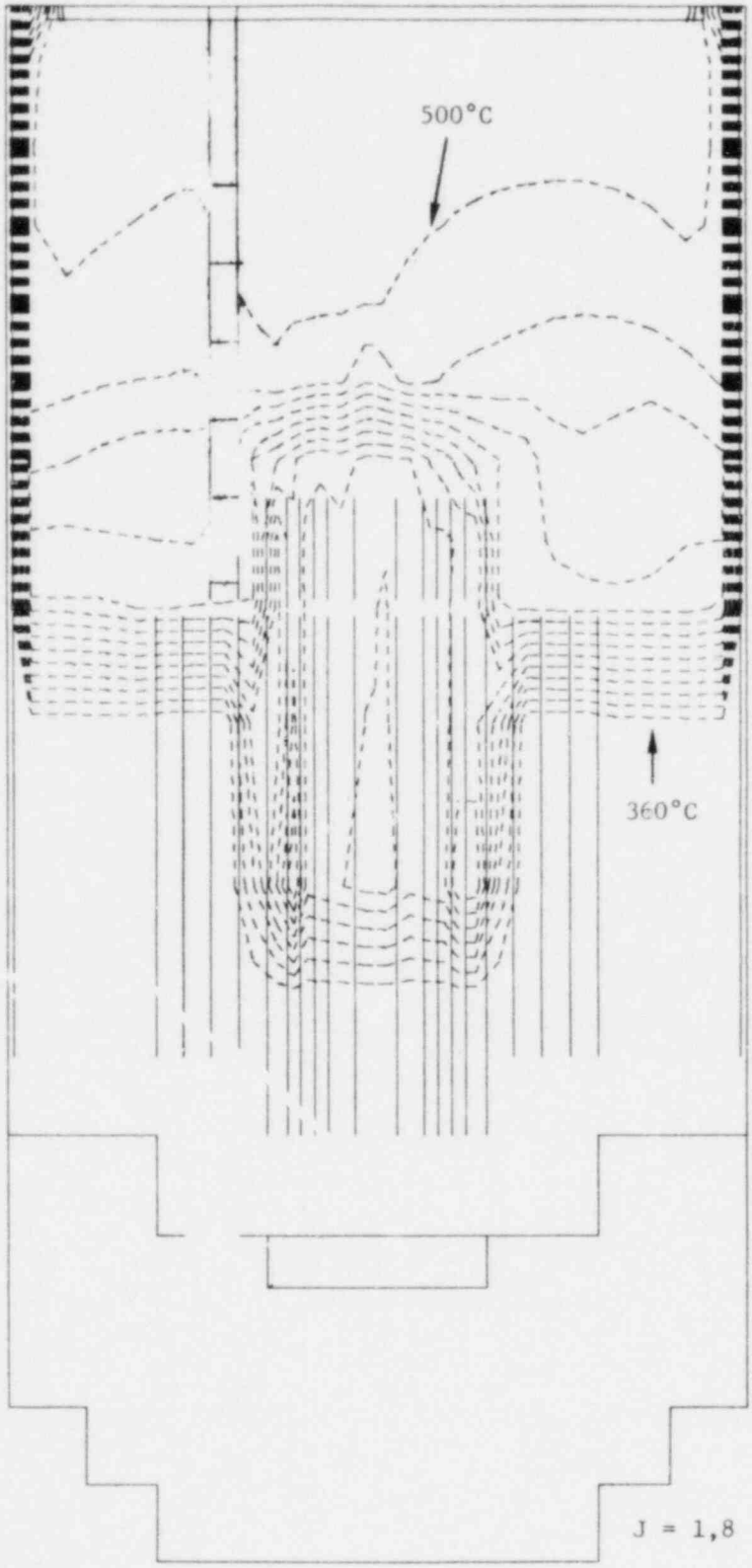

Fig. 14a. Temperature Contours at t = sec
(ΔT = 10°C)

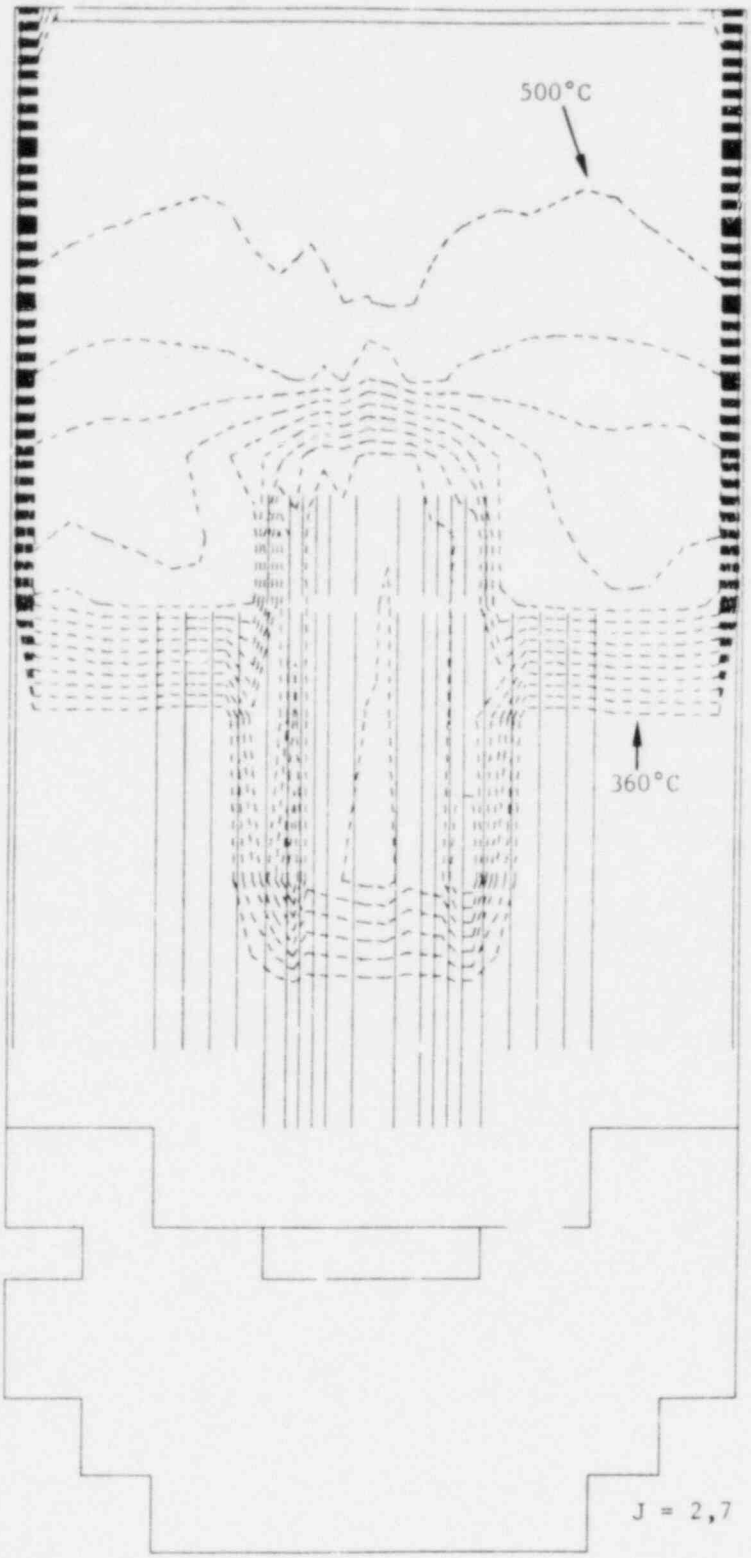

Fig. 14b. Temperature Contours at t = 53 sec
(ΔT = 10°C)

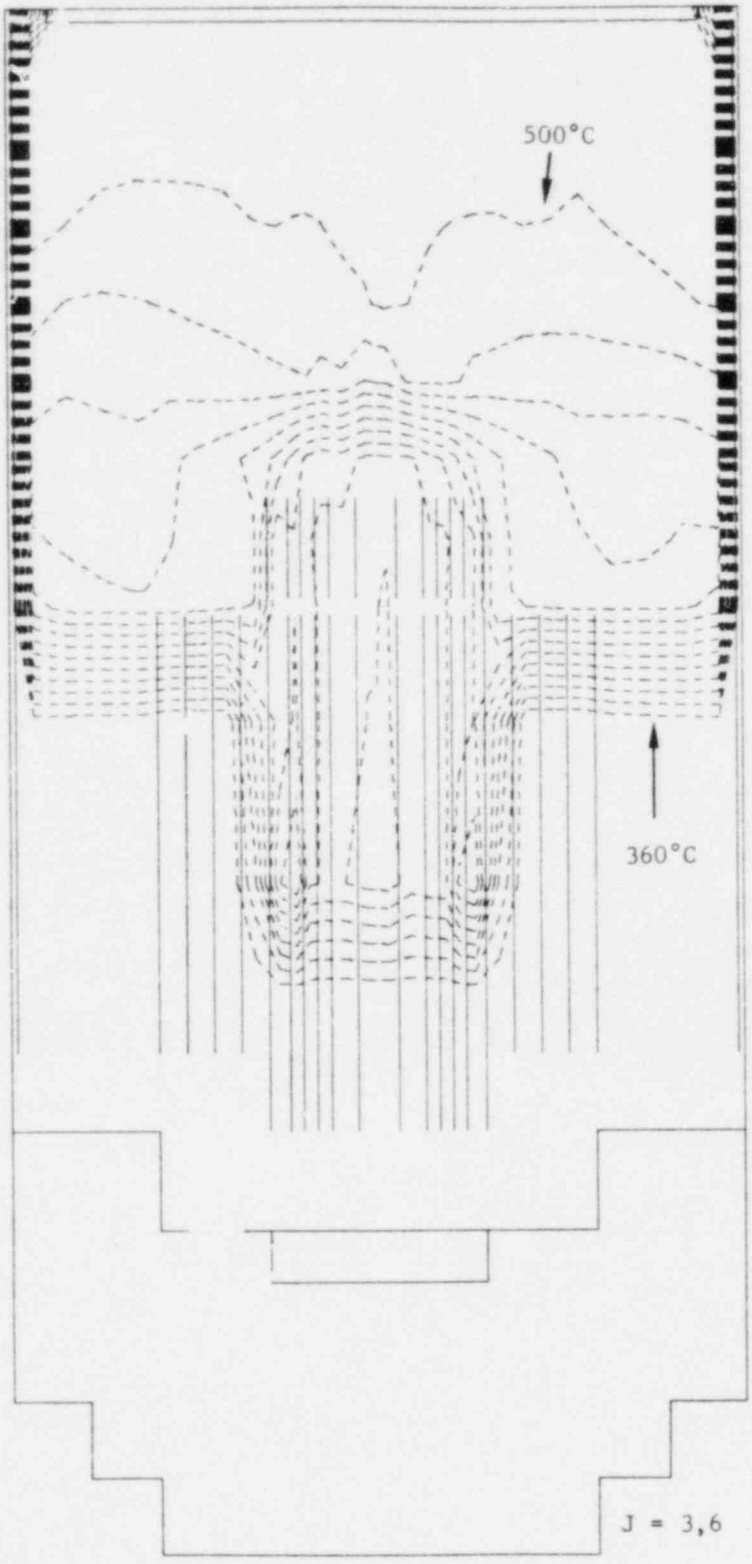

Fig. 14c. Temperature Contours at t = 53 sec
(ΔT = 10°C)

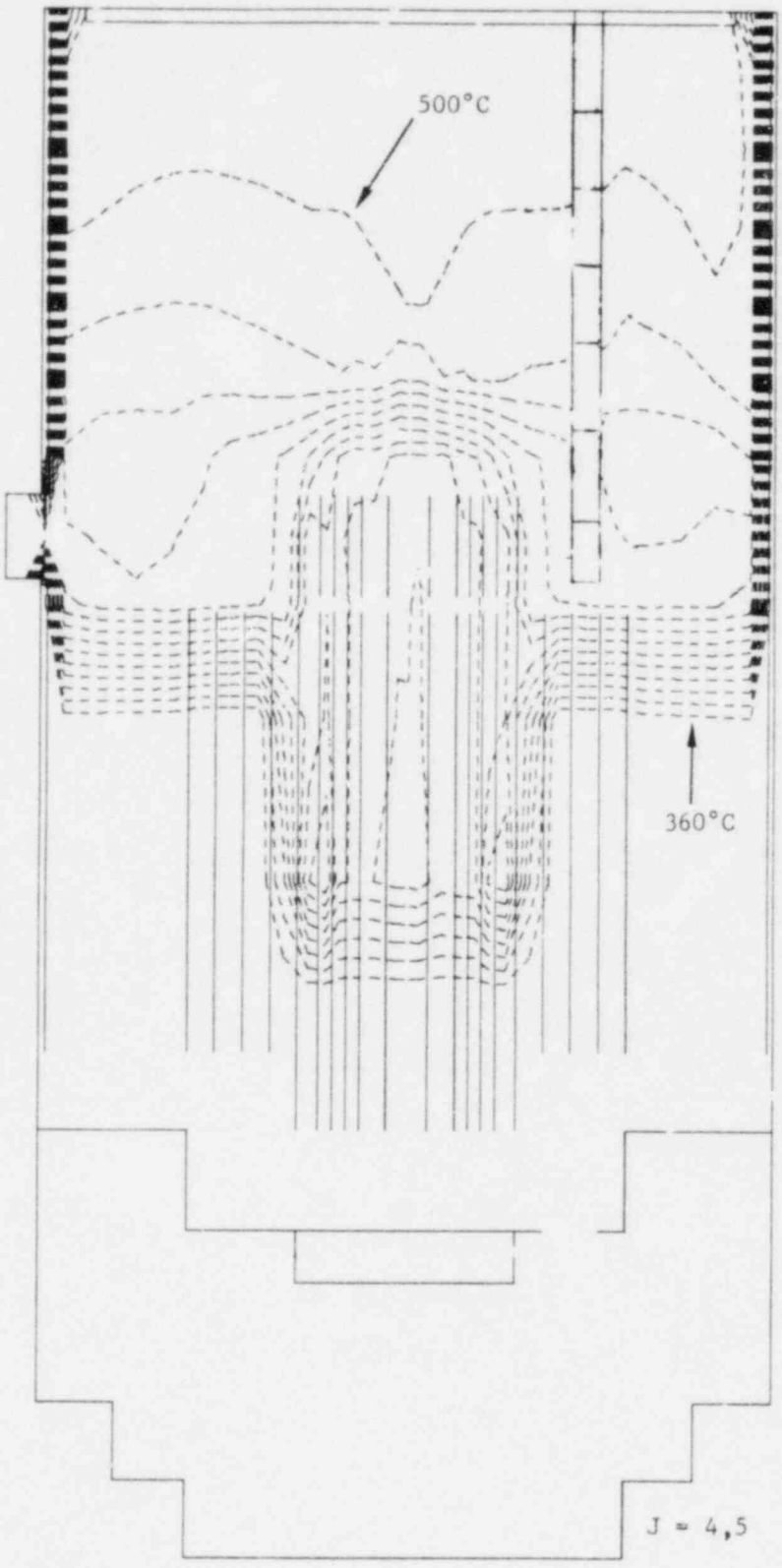

Fig. 14d. Temperature Contours at t = 53 sec
(ΔT = 10°C)

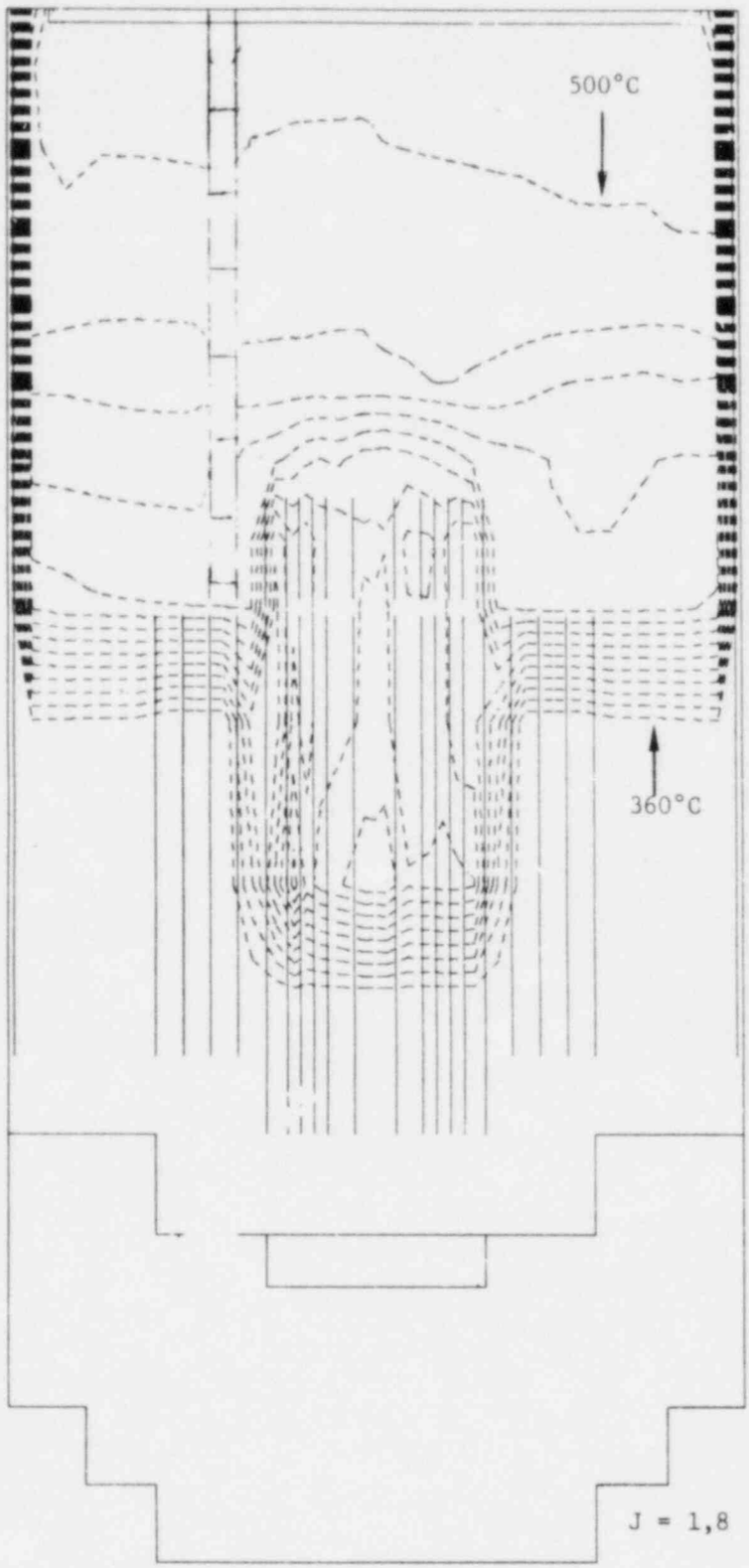

Fig. 15a. Temperature Contours at t = 79 sec
(ΔT = 10°C)

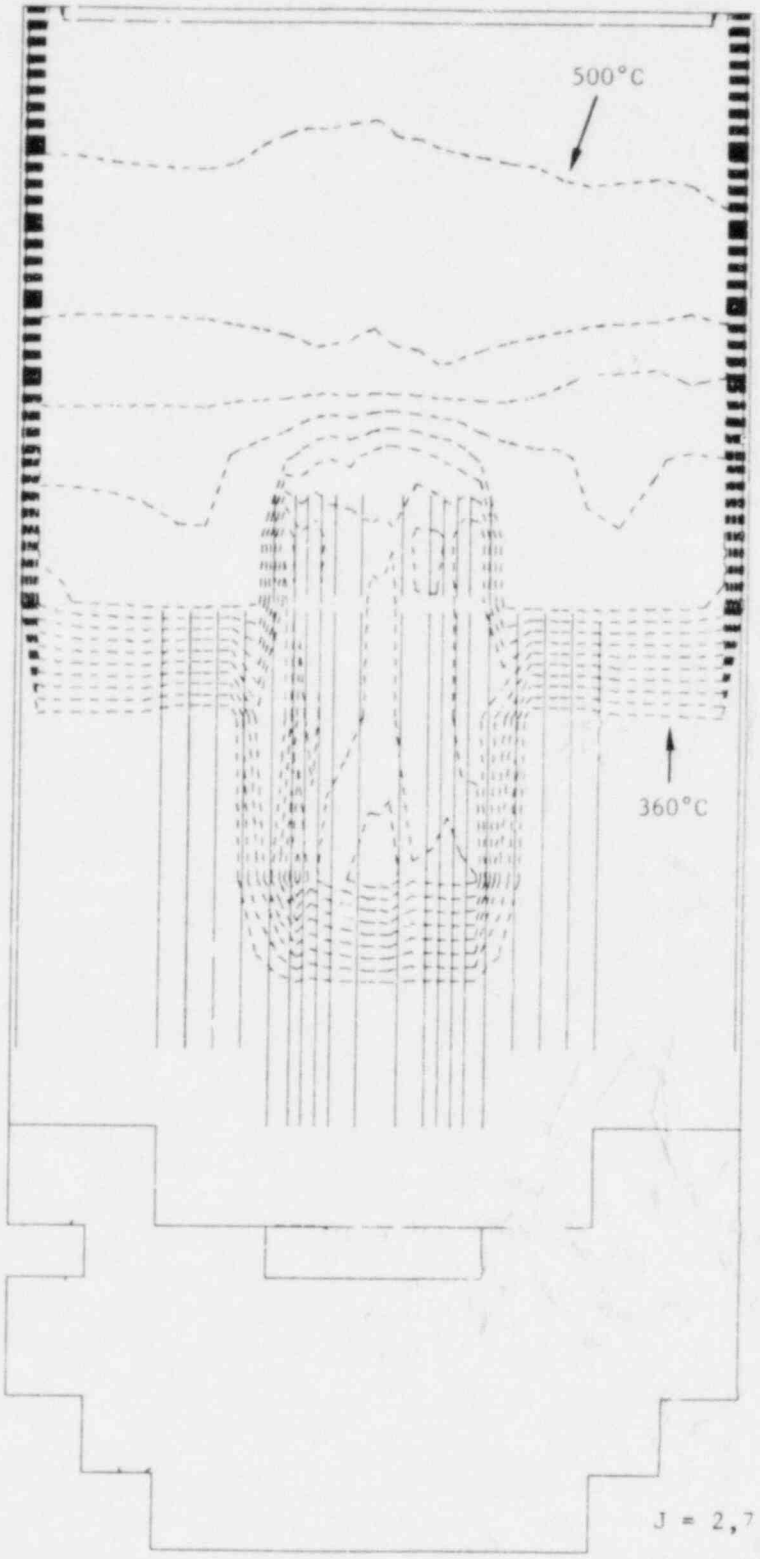

Fig. 15b. Temperature Contours at t = 79 sec
(ΔT = 10°C)

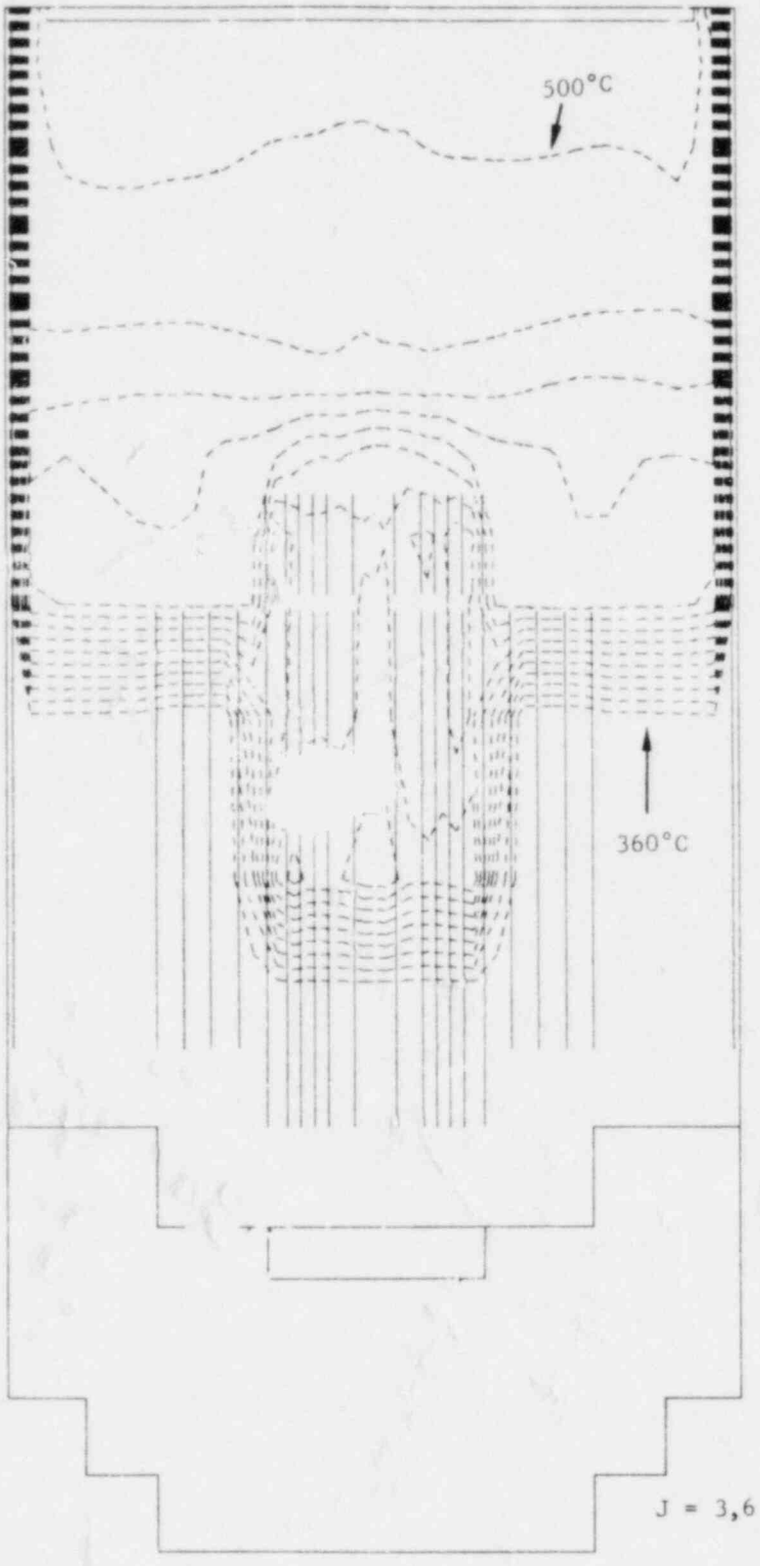

Fig. 15c. Temperature Contours at t = 79 sec
(ΔT = 10°C)

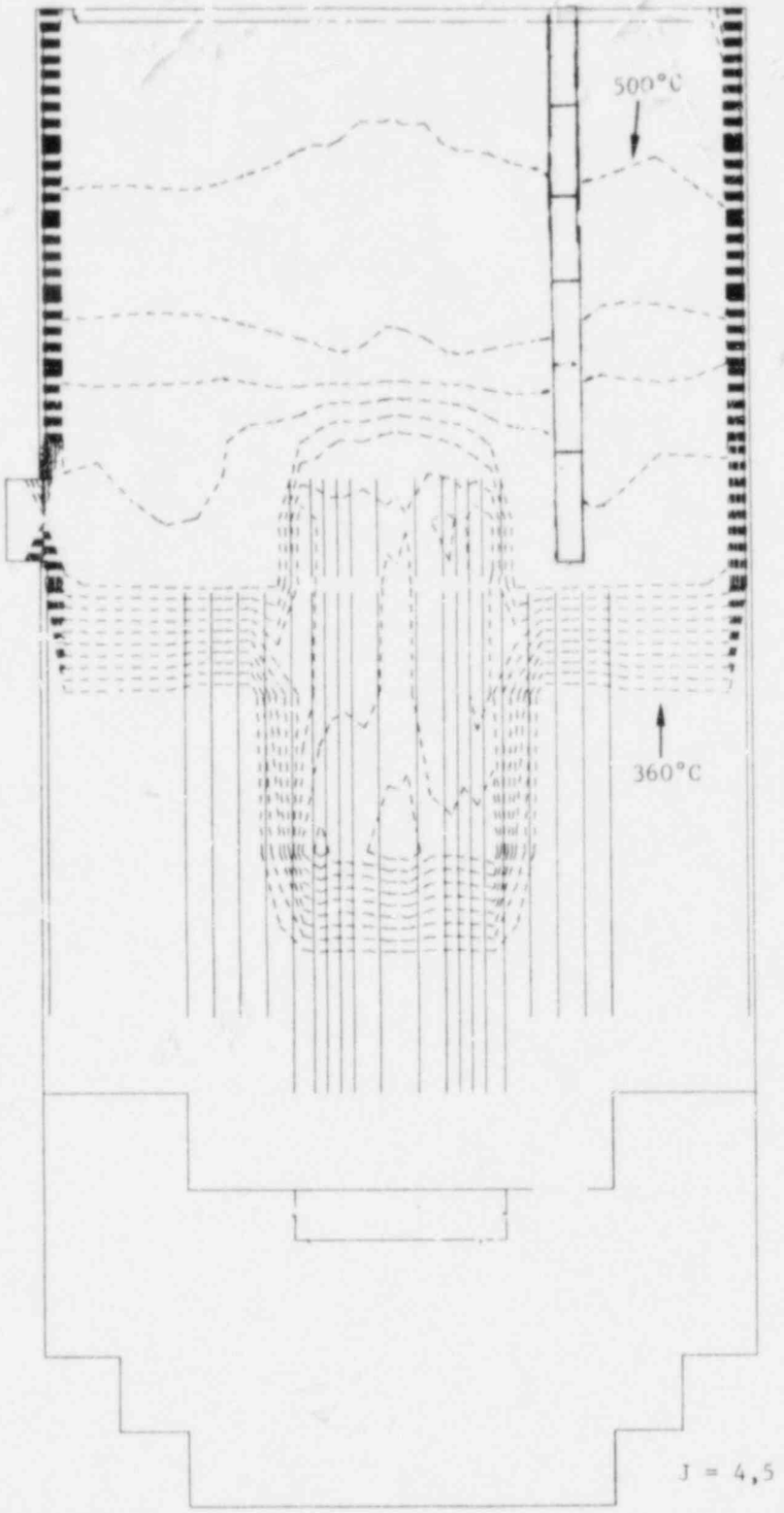

Fig. 15d. Temperature Contours at t = 79 sec
(ΔT = 10°C)

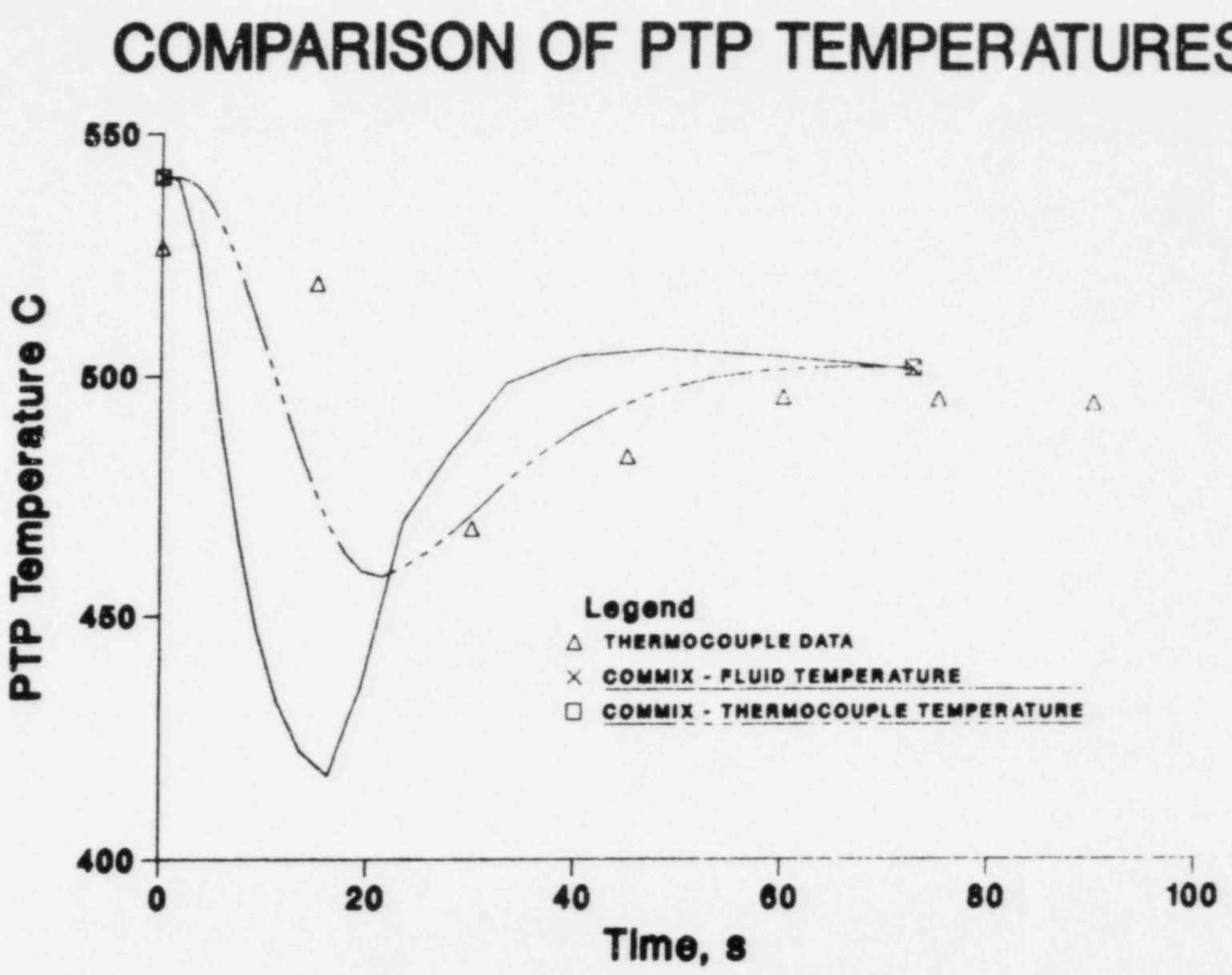

Fig. 16. Comparison of Calculated and Measured PTP Temperatures

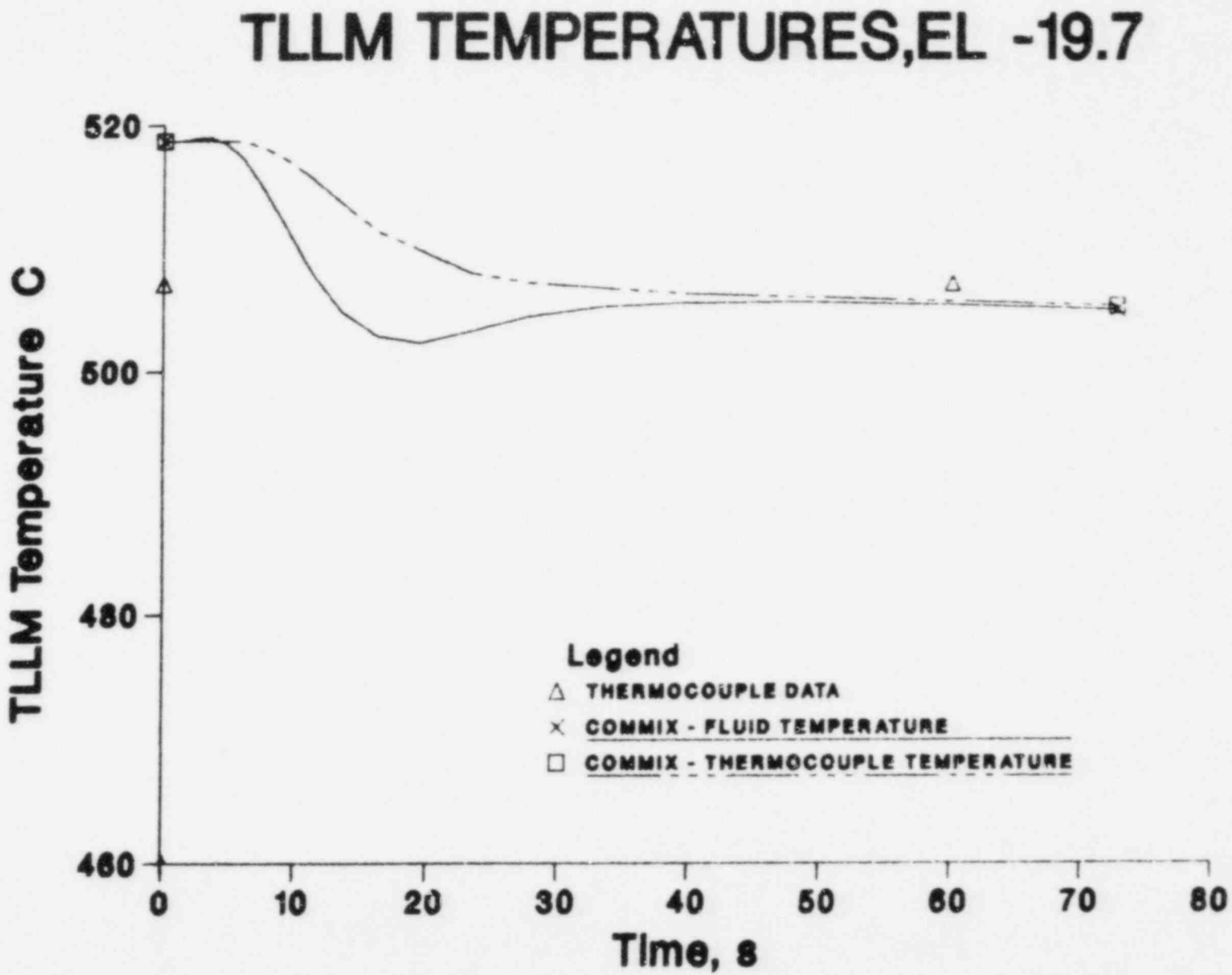

Fig. 17a. Comparison of Calculated and Measured TLLM Temperatures at Elevation -19'7" (-5.97m)

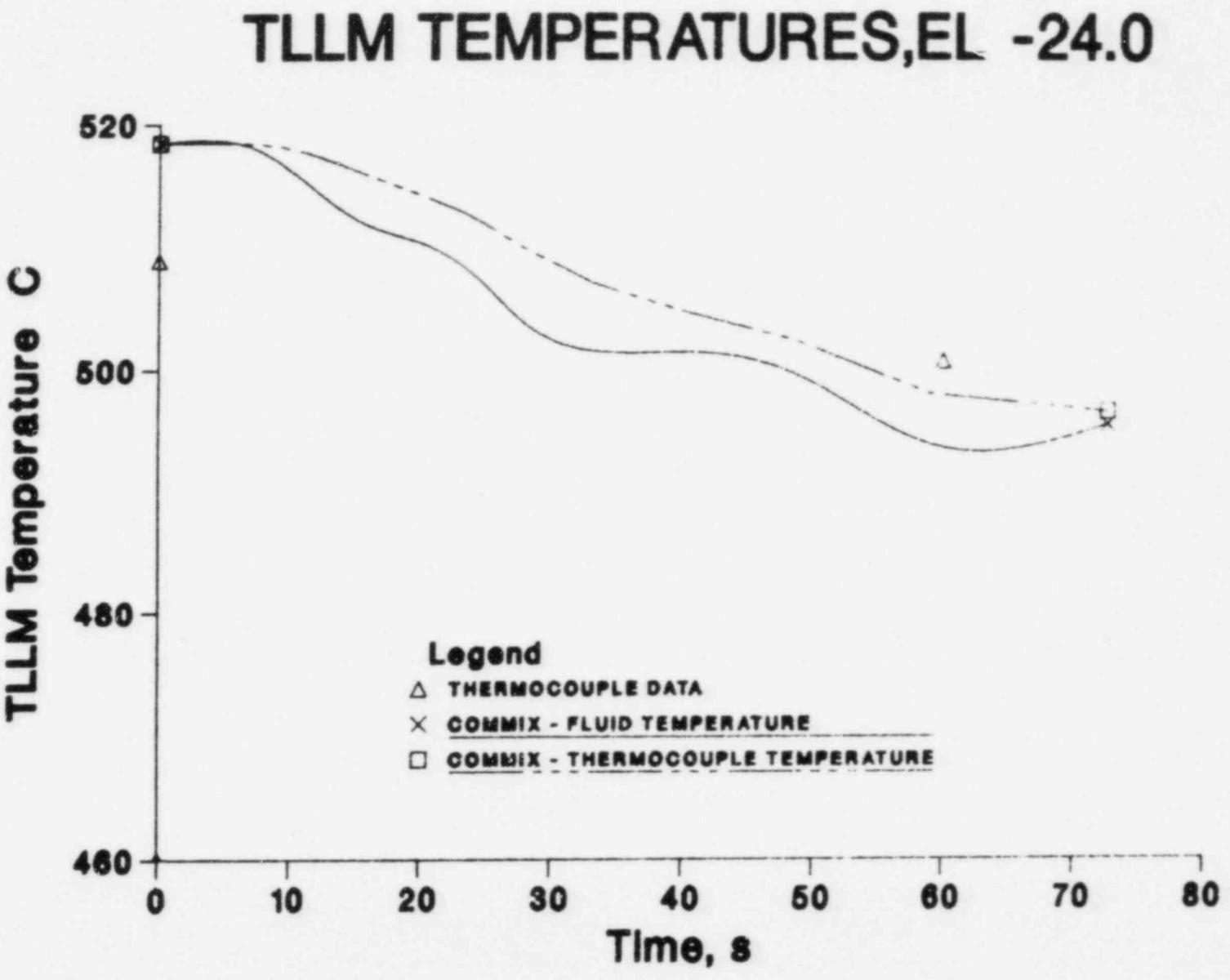

Fig. 17b. Comparison of Calculated and Measured TLLM Temperatures at Elevation -24'0" (-7.31m)

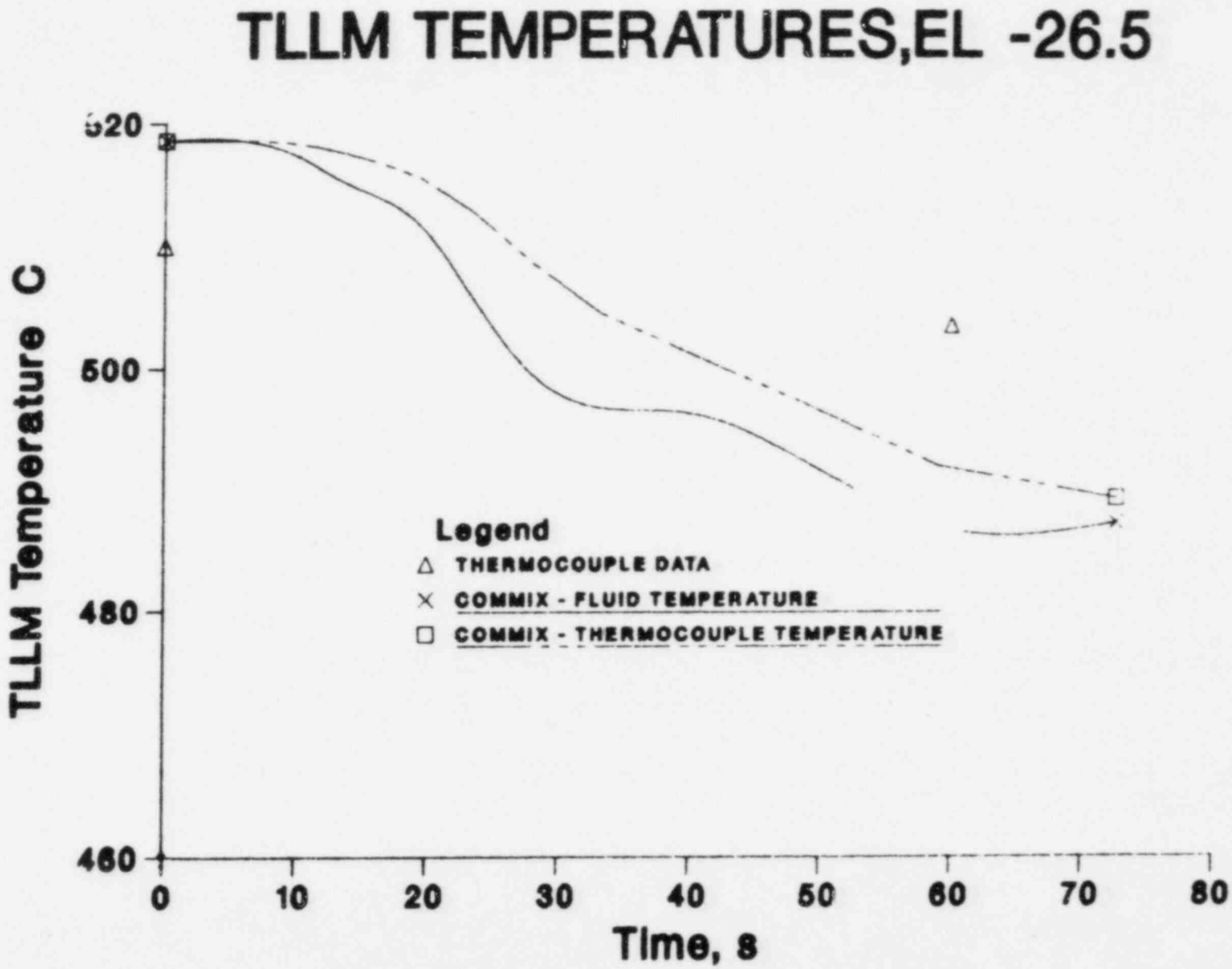

Fig. 17c. Comparison of Calculated and Measured TLLM Temperatures at Elevation -26'5" (-8.05m)

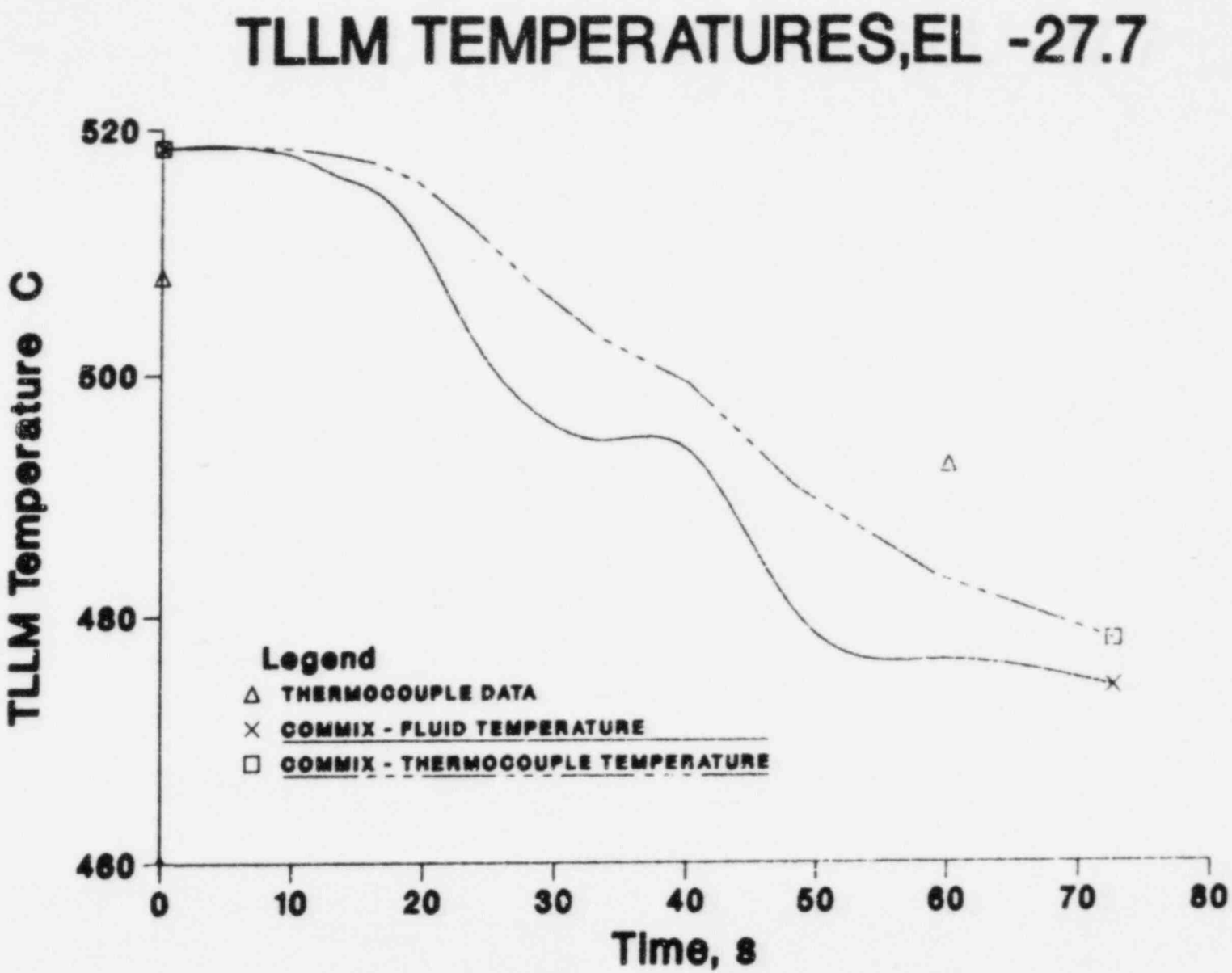

Fig. 17d. Comparison of Calculated and Measured TLLM Temperatures at Elevation -27'7" (-8.41m)

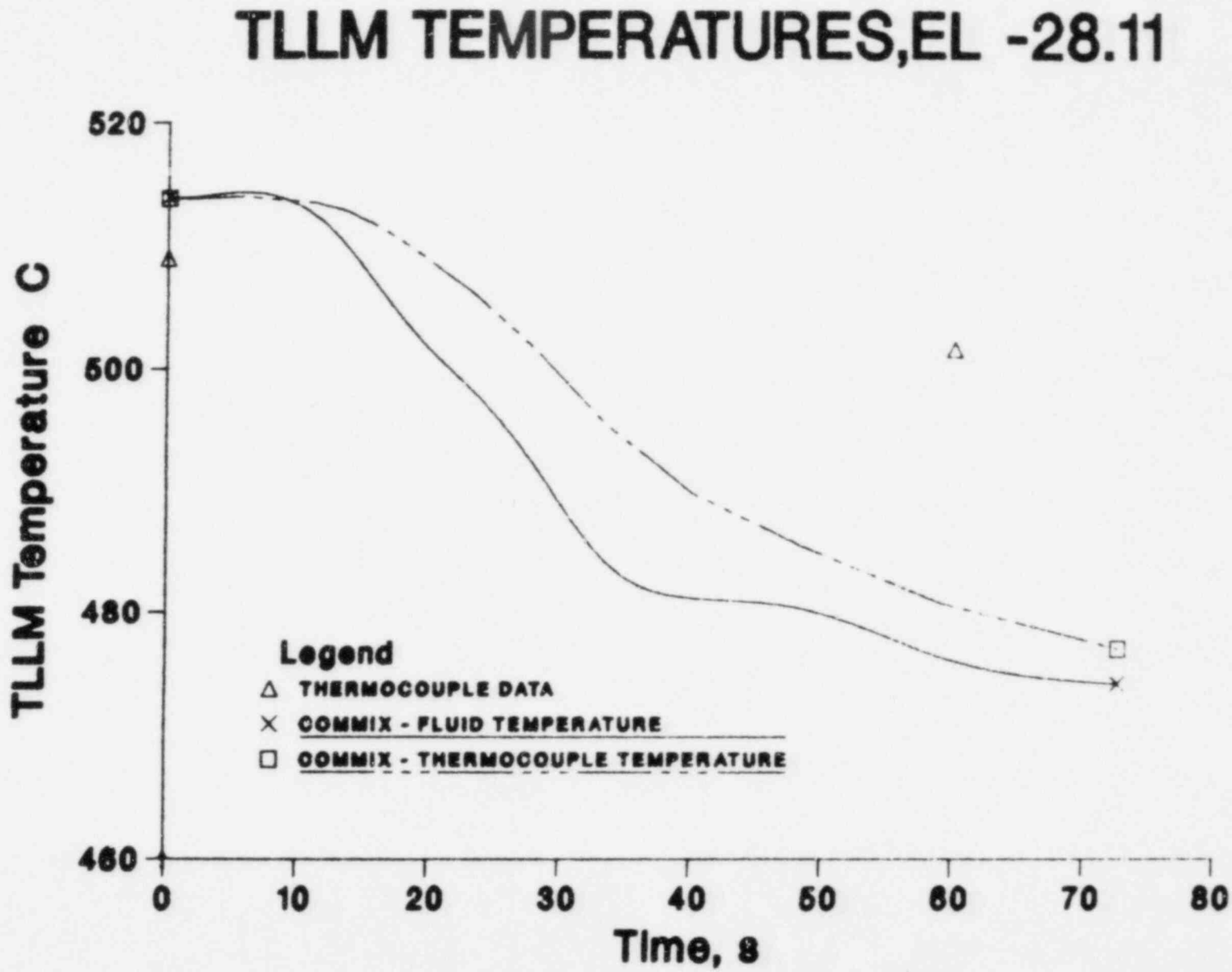

Fig. 17e. Comparison of Calculated and Measured TLLM Temperatures at Elevation -28'11" (-8.81m)

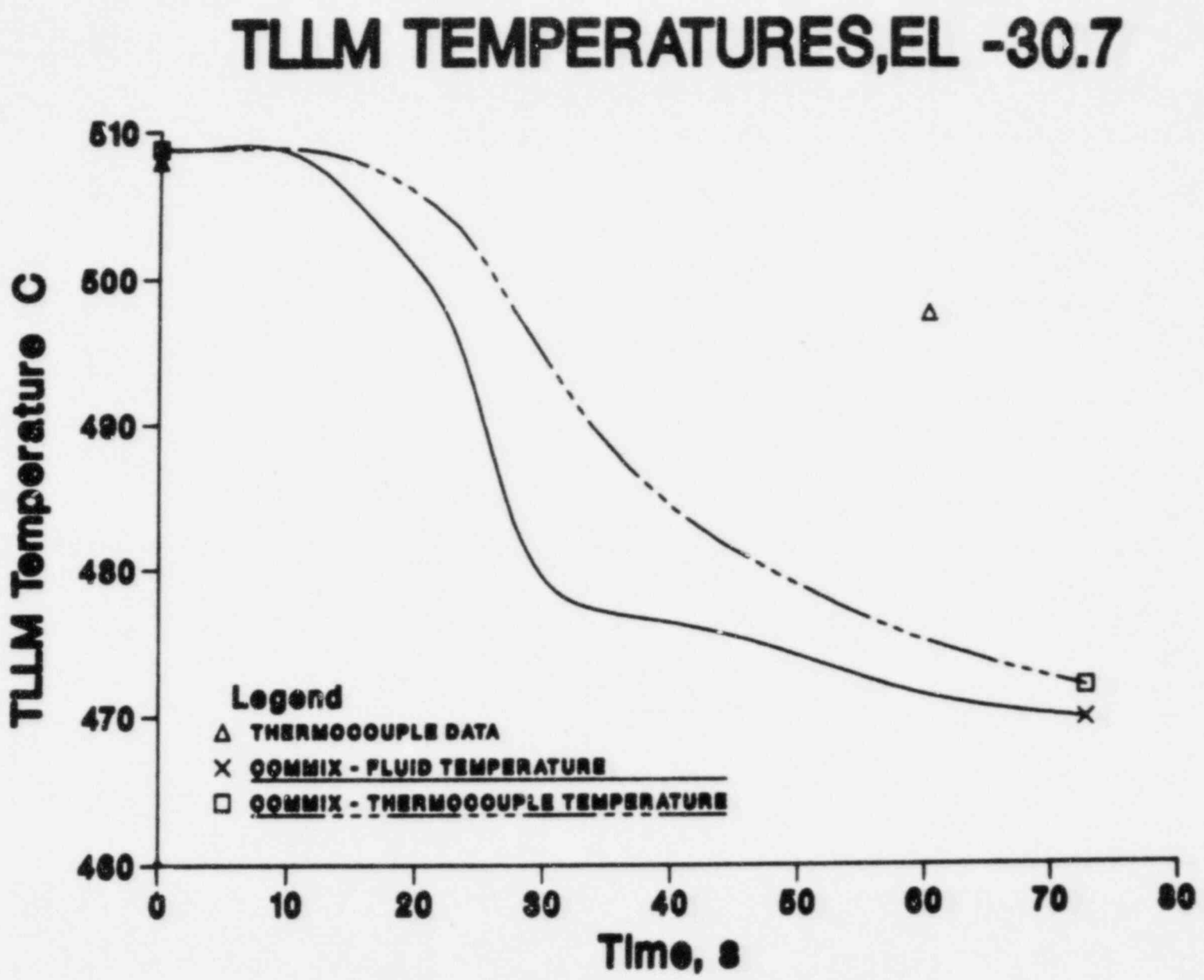

Fig. 17f. Comparison of Calculated and Measured TLLM Temperatures at Elevation -30'7" (-9.32m)

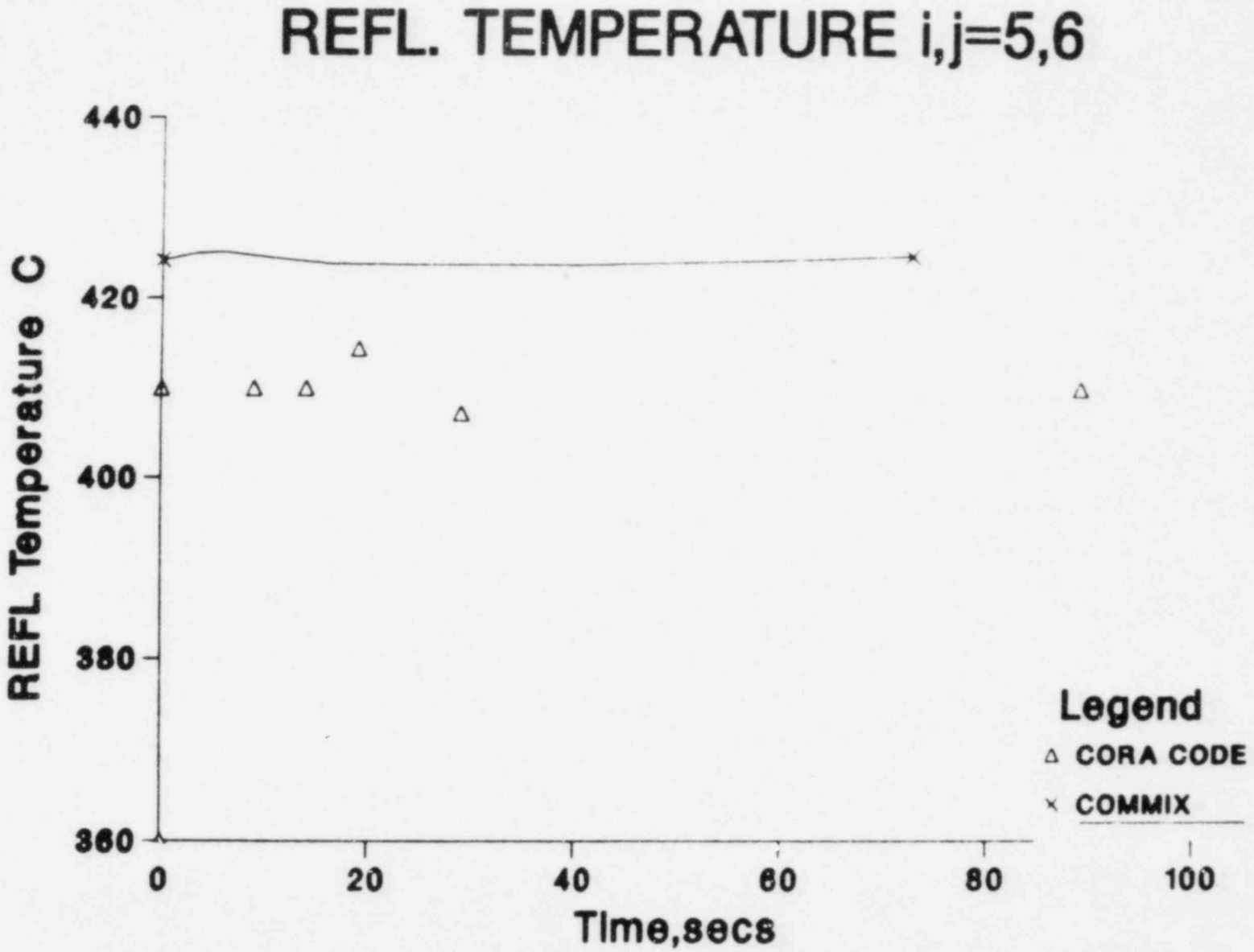

Fig. 18. Variation of Reflector Exit Temperature with Time

APPENDICES

1. RESISTANCE FUNCTIONS FOR ASSEMBLIES

A. Orifice Resistances ($K = C/Re^N$)

Assembly	No. Holes	Dia. in.	Turbulent Range N	Turbulent Range C	Laminar Range N	Laminar Range C
Fuel Zone 1	24	0.364	0.1085	10.53	1.479	256,300
Fuel Zone 2	24	0.343	0.09954	8.962	1.259	50,690
Fuel Zone 3	24	0.278	0.1005	7.814	0.5832	342.7
Absorber	6	0.406	0.0268	19.91	Insufficient Data	
In-Core Shim	3	0.347	0.05336	19.40	0.5583	847.5
Reflector	3	0.320	0.2929	12.38	N O D A T A	

B. Resistance in the Assemblies

The friction factor for fuel assemblies is calculated from the following formulas:

$$f = \frac{84}{Re} \quad \text{for } Re < 1000.0$$

$$f = f^0 \left[1 + \frac{10^6}{Re^2}\left(0.1746 + \frac{10^6}{Re^2} * 0.0745\right)\right] * 1.075 \quad \text{for } Re \geq 1000.0$$

$$\frac{1}{\sqrt{f^0}} = -\left(0.8686 * \ln \frac{2.51}{Re} * \frac{1}{\sqrt{f^0}}\right)$$

For Reflectors and Shield gaps:

$$f = \frac{64}{Re} \quad \text{for } Re < 2000.0$$

and $$f = 0.3164\ Re^{-0.25} \quad \text{for } Re \geq 2000.0$$

2. Nuclear Heat Deposition Rates within Assemblies (WATTS)

		Materials				
Assembly	Total	316 SS Inconel	Na	UO_2	PuO_2	B_4C
2101	.6820 x 10^7	.1426 x 10^6	.3341 x 10^5	.1098 x 10^7	.5452 x 10^7	.0000
1201	.6583 x 10^7	.1395 x 10^6	.3266 x 10^5	.1074 x 10^7	.5245 x 10^7	.0000
1202	.6719 x 10^7	.1486 x 10^6	.3475 x 10^5	.1141 x 10^7	.5297 x 10^7	.0000
2201	.6605 x 10^7	.1405 x 10^6	.3285 x 10^5	.1080 x 10^7	.5259 x 10^7	.0000
2202	.2701 x 10^6	.2192 x 10^6	.2214 x 10^5	.0000	.0000	.0000
3201	.6516 x 10^7	.1343 x 10^6	.3141 x 10^5	.1029 x 10^7	.5232 x 10^7	.0000
3202	.3667 x 10^6	.2995 x 10^6	.2811 x 10^5	.0000	.0000	.0000
1301	.6236 x 10^7	.1298 x 10^6	.3030 x 10^5	.9894 x 10^6	.5000 x 10^7	.0000
1302	.1170 x 10^6	.4756 x 10^5	.5694 x 10^5	.0000	.0000	.0000
1303	.6317 x 10^7	.1354 x 10^6	.3166 x 10^5	.1040 x 10^7	.5020 x 10^7	.0000
1304	.6263 x 10^7	.1340 x 10^6	.3132 x 10^5	.1026 x 10^7	.4983 x 10^7	.0000
2301	.6265 x 10^7	.1345 x 10^6	.3143 x 10^5	.1032 x 10^7	.4978 x 10^7	.0000
2302	.1167 x 10^6	.4746 x 10^5	.5680 x 10^5	.0000	.0000	.0000
2303	.6303 x 10^7	.1314 x 10^6	.3068 x 10^5	.1004 x 10^7	.5050 x 10^7	.0000
2304	.6329 x 10^7	.1335 x 10^6	.3131 x 10^5	.1029 x 10^7	.5047 x 10^7	.0000
3301	.6272 x 10^7	.1328 x 10^6	.3112 x 10^5	.1025 x 10^7	.4995 x 10^7	.0000
3302	.1146 x 10^6	.4656 x 10^5	.5586 x 10^5	.0000	.0000	.0000
3303	.6193 x 10^7	.1285 x 10^6	.3000 x 10^5	.9794 x 10^6	.4970 x 10^7	.0000
3304	.6194 x 10^7	.1282 x 10^6	.2992 x 10^5	.9719 x 10^6	.4978 x 10^7	.0000
1401	.5481 x 10^7	.1160 x 10^6	.2713 x 10^5	.8938 x 10^6	.4367 x 10^7	.0000
1402	.5015 x 10^7	.1073 x 10^6	.2514 x 10^5	.8341 x 10^6	.3978 x 10^7	.0000
1403	.5519 x 10^7	.1172 x 10^6	.2742 x 10^5	.9037 x 10^6	.4393 x 10^7	.0000
1404	.2459 x 10^6	.1996 x 10^6	.2012 x 10^5	.0000	.0000	.0000
1405	.5582 x 10^7	.1210 x 10^6	.2831 x 10^5	.9278 x 10^6	.4425 x 10^7	.0000
1406	.2395 x 10^6	.1944 x 10^6	.1953 x 10^5	.0000	.0000	.0000
2401	.5373 x 10^7	.1139 x 10^6	.2662 x 10^5	.8765 x 10^6	.4281 x 10^7	.0000
2402	.4945 x 10^7	.1051 x 10^6	.2466 x 10^5	.8203 x 10^6	.3925 x 10^7	.0000
2403	.5520 x 10^7	.1162 x 10^6	.2724 x 10^5	.8996 x 10^6	.4400 x 10^7	.0000
2404	.2466 x 10^6	.2000 x 10^6	.2027 x 10^5	.0000	.0000	.0000
2405	.5780 x 10^7	.1257 x 10^6	.2968 x 10^5	.9882 x 10^6	.4554 x 10^7	.0000
2406	.5815 x 10^7	.1289 x 10^6	.3024 x 10^5	.1007 x 10^7	.4565 x 10^7	.0000
3401	.5413 x 10^7	.1160 x 10^6	.2729 x 10^5	.9102 x 10^6	.4283 x 10^7	.0000
3402	.4904 x 10^7	.1035 x 10^6	.2436 x 10^5	.8141 x 10^6	.3893 x 10^7	.0000
3403	.5419 x 10^7	.1138 x 10^6	.2666 x 10^5	.8814 x 10^6	.4322 x 10^7	.0000
3404	.2406 x 10^6	.1953 x 10^6	.1968 x 10^5	.0000	.0000	.0000
3405	.5653 x 10^7	.1216 x 10^6	.2850 x 10^5	.9367 x 10^6	.4486 x 10^7	.0000
3406	.2422 x 10^6	.1966 x 10^6	.1980 x 10^5	.0000	.0000	.0000
1501	.5297 x 10^7	.1179 x 10^6	.2721 x 10^5	.8259 x 10^6	.4747 x 10^7	.0000
1502	.2481 x 10^6	.6836 x 10^5	.3518 x 10^5	.0000	.0000	.1181 x 10
1503	.4805 x 10^7	.9887 x 10^5	.2281 x 10^5	.6944 x 10^6	.3923 x 10^7	.0000
1504	.2499 x 10^6	.6896 x 10^5	.3547 x 10^5	.0000	.0000	.1189 x 10
1505	.5855 x 10^7	.1196 x 10^6	.2759 x 10^5	.8359 x 10^6	.4792 x 10^7	.0000
1506	.6007 x 10^7	.1251 x 10^6	.2888 x 10^5	.8744 x 10^6	.4895 x 10^7	.0000
1507	.5384 x 10^7	.1151 x 10^6	.2658 x 10^5	.8055 x 10^6	.4361 x 10^7	.0000
1508	.5679 x 10^7	.1158 x 10^6	.2660 x 10^5	.8007 x 10^6	.4658 x 10^7	.0000
2501	.5489 x 10^7	.1095 x 10^6	.2513 x 10^5	.7563 x 10^6	.4525 x 10^7	.0000
2502	.2389 x 10^6	.6547 x 10^5	.3360 x 10^5	.0000	.0000	.1144 x 10
2503	.4687 x 10^7	.9535 x 10^5	.2205 x 10^5	.6745 x 10^6	.3832 x 10^7	.0000
2504	.2475 x 10^6	.6775 x 10^5	.3498 x 10^5	.0000	.0000	.1184 x 10
2505	.5941 x 10^7	.1192 x 10^6	.2763 x 10^5	.8439 x 10^6	.4870 x 10^7	.0000
2506	.6233 x 10^7	.1270 x 10^6	.2951 x 10^5	.9051 x 10^6	.5087 x 10^7	.0000
2507	.5718 x 10^7	.1195 x 10^6	.2780 x 10^5	.8552 x 10^6	.4636 x 10^7	.0000
2508	.5756 x 10^7	.1174 x 10^6	.2737 x 10^5	.8460 x 10^6	.4687 x 10^7	.0000
3501	.5421 x 10^7	.1086 x 10^6	.2528 x 10^5	.7814 x 10^6	.4433 x 10^7	.0000

Assembly	Total	Materials				
		316 SS Inconel	Na	UO_2	PuO_2	B_4C
3502	.2351 x 10^6	.6415 x 10^5	.3321 x 10^5	.0000	.0000	.1127 x 10^6
3503	.4629 x 10^7	.9364 x 10^5	.2170 x 10^5	.6660 x 10^6	.3785 x 10^7	.0000
3504	.2427 x 10^6	.6638 x 10^5	.3426 x 10^5	.0000	.0000	.1162 x 10^6
3505	.5763 x 10^7	.1163 x 10^6	.2689 x 10^5	.8189 x 10^6	.4723 x 10^7	.0000
3506	.6006 x 10^7	.1239 x 10^6	.2865 x 10^5	.8715 x 10^6	.4899 x 10^7	.0000
3507	.5556 x 10^7	.1180 x 10^6	.2732 x 10^5	.8333 x 10^6	.4499 x 10^7	.0000
3508	.5983 x 10^7	.1238 x 10^6	.2862 x 10^5	.8697 x 10^6	.4879 x 10^7	.0000
1601	.4724 x 10^7	.9855 x 10^5	.2198 x 10^5	.6568 x 10^6	.3884 x 10^7	.0000
1602	.4319 x 10^7	.8852 x 10^5	.2011 x 10^5	.5994 x 10^6	.3552 x 10^7	.0000
1603	.3870 x 10^7	.8032 x 10^5	.1804 x 10^5	.5289 x 10^6	.3189 x 10^7	.0000
1604	.4357 x 10^7	.8945 x 10^5	.2030 x 10^5	.6045 x 10^6	.3583 x 10^7	.0000
1605	.4799 x 10^7	.9848 x 10^5	.2239 x 10^5	.6674 x 10^6	.3945 x 10^7	.0000
1606	.5096 x 10^7	.1066 x 10^6	.2427 x 10^5	.7232 x 10^6	.4171 x 10^7	.0000
1607	.4779 x 10^7	.9998 x 10^5	.2281 x 10^5	.6830 x 10^6	.3907 x 10^7	.0000
1608	.3714 x 10^7	.7645 x 10^5	.1744 x 10^5	.5226 x 10^6	.3046 x 10^7	.0000
1609	.4200 x 10^7	.8536 x 10^5	.1950 x 10^5	.5857 x 10^6	.3452 x 10^7	.0000
1610	.1243 x 10^6	.8769 x 10^5	.2337 x 10^5	.0000	.0000	.0000
2601	.4457 x 10^7	.8879 x 10^5	.2002 x 10^5	.5921 x 10^6	.3696 x 10^7	.0000
2602	.4120 x 10^7	.8388 x 10^5	.1905 x 10^5	.5685 x 10^6	.3393 x 10^7	.0000
2603	.3754 x 10^7	.7684 x 10^5	.1730 x 10^5	.5107 x 10^6	.3099 x 10^7	.0000
2604	.4299 x 10^7	.8682 x 10^5	.1978 x 10^5	.5934 x 10^6	.3542 x 10^7	.0000
2605	.4833 x 10^7	.9723 x 10^5	.2221 x 10^5	.6680 x 10^6	.3981 x 10^7	.0000
2606	.5251 x 10^7	.1074 x 10^6	.2459 x 10^5	.7404 x 10^6	.4307 x 10^7	.0000
2607	.5089 x 10^7	.1039 x 10^6	.2386 x 10^5	.7220 x 10^6	.4170 x 10^7	.0000
2608	.4393 x 10^7	.8863 x 10^5	.2013 x 10^5	.6019 x 10^6	.3623 x 10^7	.0000
2609	.4590 x 10^7	.9169 x 10^5	.2104 x 10^5	.6384 x 10^6	.3778 x 10^7	.0000
2610	.2203 x 10^6	.5335 x 10^5	.2421 x 10^5	.0000	.0000	.1193 x 10^6
3601	.4246 x 10^7	.8312 x 10^5	.1899 x 10^5	.5731 x 10^6	.3515 x 10^7	.0000
3602	.4065 x 10^7	.8176 x 10^5	.1864 x 10^5	.5605 x 10^6	.3349 x 10^7	.0000
3603	.3679 x 10^7	.7490 x 10^5	.1697 x 10^5	.5004 x 10^6	.3037 x 10^7	.0000
3604	.4209 x 10^7	.8500 x 10^5	.1917 x 10^5	.5813 x 10^6	.3467 x 10^7	.0000
3605	.4677 x 10^7	.9457 x 10^5	.2176 x 10^5	.6476 x 10^6	.3851 x 10^7	.0000
3606	.4901 x 10^7	.1016 x 10^6	.2326 x 10^5	.6972 x 10^6	.4011 x 10^7	.0000
3607	.4701 x 10^7	.9771 x 10^5	.2241 x 10^5	.6744 x 10^6	.3842 x 10^7	.0000
3608	.3868 x 10^7	.7896 x 10^5	.1806 x 10^5	.5448 x 10^6	.3174 x 10^7	.0000
3609	.4453 x 10^7	.9220 x 10^5	.2128 x 10^5	.6476 x 10^6	.3631 x 10^7	.0000
3610	.4949 x 10^7	.1029 x 10^6	.2350 x 10^5	.7041 x 10^6	.4050 x 10^7	.0000
1701	.1426 x 10^6	.1249 x 10^6	.2551 x 10^4	.0000	.0000	.0000
1702	.1363 x 10^6	.1194 x 10^6	.2417 x 10^4	.0000	.0000	.0000
1703	.1218 x 10^6	.1067 x 10^6	.2141 x 10^4	.0000	.0000	.0000
1704	.9390 x 10^5	.8232 x 10^5	.1579 x 10^4	.0000	.0000	.0000
1705	.1247 x 10^6	.1092 x 10^6	.2180 x 10^4	.0000	.0000	.0000
1706	.1414 x 10^6	.1238 x 10^6	.2489 x 10^4	.0000	.0000	.0000
1707	.1509 x 10^6	.1322 x 10^6	.2673 x 10^4	.0000	.0000	.0000
1708	.1469 x 10^6	.1287 x 10^6	.2620 x 10^4	.0000	.0000	.0000
1709	.1238 x 10^6	.1084 x 10^6	.2211 x 10^4	.0000	.0000	.0000
1710	.7674 x 10^5	.6721 x 10^5	.1353 x 10^4	.0000	.0000	.0000
1711	.2108 x 10^6	.4238 x 10^5	.4839 x 10^4	.0000	.0000	.1411 x 10^6
1712	.1119 x 10^6	.9800 x 10^5	.1992 x 10^4	.0000	.0000	.0000
2701	.1271 x 10^6	.1114 x 10^6	.2203 x 10^4	.0000	.0000	.0000
2702	.1299 x 10^6	.1138 x 10^6	.2268 x 10^4	.0000	.0000	.0000
2703	.1167 x 10^6	.1022 x 10^6	.2047 x 10^4	.0000	.0000	.0000
2704	.8952 x 10^5	.7847 x 10^5	.1512 x 10^4	.0000	.0000	.0000
2705	.1187 x 10^6	.1040 x 10^6	.2096 x 10^4	.0000	.0000	.0000
2706	.1365 x 10^6	.1196 x 10^6	.2431 x 10^4	.0000	.0000	.0000
2707	.1489 x 10^6	.1304 x 10^6	.2670 x 10^4	.0000	.0000	.0000
2708	.1497 x 10^6	.1310 x 10^6	.2699 x 10^4	.0000	.0000	.0000

Assembly	Total	Materials				
		316 SS Inconel	Na	UO_2	PuO_2	B_4C
2709	.1352 x 10^6	.1184 x 10^5	.2424 x 10^4	.0000	.0000	.0000
2710	.1015 x 10^6	.8892 x 10^5	.1735 x 10^4	.0000	.0000	.0000
2711	.1283 x 10^6	.1124 x 10^6	.2278 x 10^4	.0000	.0000	.0000
2712	.1233 x 10^6	.1080 x 10^6	.2186 x 10^4	.0000	.0000	.0000
3701	.1210 x 10^6	.1059 x 10^6	.2131 x 10^4	.0000	.0000	.0000
3702	.1243 x 10^6	.1089 x 10^6	.2195 x 10^4	.0000	.0000	.0000
3703	.1118 x 10^6	.9790 x 10^5	.1979 x 10^4	.0000	.0000	.0000
3704	.8393 x 10^5	.7355 x 10^5	.1435 x 10^4	.0000	.0000	.0000
3705	.1155 x 10^6	.1012 x 10^6	.2043 x 10^4	.0000	.0000	.0000
3706	.1340 x 10^6	.1174 x 10^6	.2374 x 10^4	.0000	.0000	.0000
3707	.1398 x 10^6	.1224 x 10^6	.2514 x 10^4	.0000	.0000	.0000
3708	.2890 x 10^5	.2269 x 10^5	.4982 x 10^4	.1223 x 10^4	.0000	.0000
3709	.1215 x 10^6	.1064 x 10^6	.2192 x 10^4	.0000	.0000	.0000
3710	.8287 x 10^5	.7259 x 10^5	.1449 x 10^4	.0000	.0000	.0000
3711	.2257 x 10^6	.4513 x 10^5	.5203 x 10^4	.0000	.0000	.1513 x 10^6
3712	.1267 x 10^6	.1109 x 10^6	.2328 x 10^4	.0000	.0000	.0000
1801	.7637 x 10^5	.6704 x 10^5	.1195 x 10^4	.0000	.0000	.0000
1802	.7019 x 10^5	.6162 x 10^5	.1092 x 10^4	.0000	.0000	.0000
1803	.5769 x 10^5	.5066 x 10^5	.8878 x 10^3	.0000	.0000	.0000
1804	.4235 x 10^5	.3721 x 10^5	.6287 x 10^3	.0000	.0000	.0000
1805	.6307 x 10^5	.5540 x 10^5	.9575 x 10^3	.0000	.0000	.0000
1806	.7843 x 10^5	.6888 x 10^5	.1200 x 10^4	.0000	.0000	.0000
1807	.8660 x 10^5	.7605 x 10^5	.1330 x 10^4	.0000	.0000	.0000
1808	.8640 x 10^5	.7586 x 10^5	.1336 x 10^4	.0000	.0000	.0000
1809	.7552 x 10^5	.6630 x 10^5	.1177 x 10^4	.0000	.0000	.0000
1810	.5301 x 10^5	.4653 x 10^5	.8337 x 10^3	.0000	.0000	.0000
1811	.2641 x 10^5	.2318 x 10^5	.4177 x 10^3	.0000	.0000	.0000
1812	.3772 x 10^5	.3308 x 10^5	.6201 x 10^3	.0000	.0000	.0000
1813	.5341 x 10^5	.4687 x 10^5	.8519 x 10^3	.0000	.0000	.0000
1814	.7292 x 10^5	.6405 x 10^5	.1111 x 10^4	.0000	.0000	.0000
2801	.7718 x 10^5	.6779 x 10^5	.1172 x 10^4	.0000	.0000	.0000
2802	.7147 x 10^5	.6276 x 10^5	.1092 x 10^4	.0000	.0000	.0000
2803	.5872 x 10^5	.5157 x 10^5	.8943 x 10^3	.0000	.0000	.0000
2804	.4014 x 10^5	.3527 x 10^5	.5983 x 10^3	.0000	.0000	.0000
2805	.5591 x 10^5	.4909 x 10^5	.8637 x 10^3	.0000	.0000	.0000
2806	.6975 x 10^5	.6124 x 10^5	.1090 x 10^4	.0000	.0000	.0000
2807	.7874 x 10^5	.6911 x 10^5	.1235 x 10^4	.0000	.0000	.0000
2808	.8172 x 10^5	.7172 x 10^5	.1288 x 10^4	.0000	.0000	.0000
2809	.7678 x 10^5	.6739 x 10^5	.1212 x 10^4	.0000	.0000	.0000
2810	.6318 x 10^5	.5547 x 10^5	.9861 x 10^3	.0000	.0000	.0000
2811	.4526 x 10^5	.3976 x 10^5	.6798 x 10^3	.0000	.0000	.0000
2812	.6489 x 10^5	.5698 x 10^5	.9963 x 10^3	.0000	.0000	.0000
2813	.7562 x 10^5	.6641 x 10^5	.1161 x 10^4	.0000	.0000	.0000
2814	.7764 x 10^5	.6818 x 10^5	.1184 x 10^4	.0000	.0000	.0000
3801	.7459 x 10^5	.6551 x 10^5	.1143 x 10^4	.0000	.0000	.0000
3802	.6578 x 10^5	.5776 x 10^5	.1020 x 10^4	.0000	.0000	.0000
3803	.4956 x 10^5	.4350 x 10^5	.7747 x 10^3	.0000	.0000	.0000
3804	.2859 x 10^5	.2510 x 10^5	.4435 x 10^3	.0000	.0000	.0000
3805	.5116 x 10^5	.4491 x 10^5	.7986 x 10^3	.0000	.0000	.0000
3806	.7027 x 10^5	.6170 x 10^5	.1089 x 10^4	.0000	.0000	.0000
3807	.8105 x 10^5	.7117 x 10^5	.1250 x 10^4	.0000	.0000	.0000
3808	.7886 x 10^5	.6922 x 10^5	.1240 x 10^4	.0000	.0000	.0000
3809	.7304 x 10^5	.6411 x 10^5	.1149 x 10^4	.0000	.0000	.0000
3810	.6152 x 10^5	.5402 x 10^5	.9440 x 10^3	.0000	.0000	.0000
3811	.3859 x 10^5	.3389 x 10^5	.5828 x 10^3	.0000	.0000	.0000
3812	.4357 x 10^5	.3822 x 10^5	.7098 x 10^3	.0000	.0000	.0000
3813	.5542 x 10^5	.4861 x 10^5	.9090 x 10^3	.0000	.0000	.0000
3814	.7284 x 10^5	.6393 x 10^5	.1155 x 10^4	.0000	.0000	.0000

3. IMPORTANT INPUT DATA FOR FFTF SIMULATION

A. Dimensions

The dimensions were obtained either from the FSAR or from the design drawings obtained from HEDL. It is not possible and also not relevant to list all design dimensions that were used to simulate the geometry. However, we shall mention below the most important dimensions, which will enable the reader to obtain a picture of the facility. The input description to COMMIX-1A is also listed at the end of this appendix.

Vessel Radius	2.911 m
Vessel Height (considered for present calculations)	12.18 m
Inlet-pipe diameter	0.4064 m (16 in.)
Outlet-pipe diameter	0.7112 m (28 in.)
Number of pins per assembly	217
Pin diameter	0.00584 m (0.230 in.)
Number of assemblies (including nonfueled)	91

B. Flow Rates and Temperatures

Total inlet flow	2203 kg/s (40,330 gpm)
Inlet temperature	360°C
Outlet temperature	503.3°C

C. Boundary Conditions

Inlet	Prescribed velocity and temperature
Outlet	Zero gradient on outlet velocity and temperature
Walls (outside)	Adiabatic

D. Finite-Difference Grid

The finite-difference grid consisted of 2334 cells, with 19 axial partitions, 15 radial partitions, and 8 azimuthal partitions. The finite-difference grid is sketched in Fig. 4.

E. Input Data Listing

A listing of the complete data is enclosed. The data consist of the grid, the surface identifications, the resistances due to the presence of structures, thermal interaction model between coolant and structure, surface permeabilities, and volume porosities.

4. Listing of Input Data

```
 1.      &GEOM
 2.      NB11 = 2350,NL1=1200,
 3.      NFORCE=20,ISYMCH=3,
 4.      NMATEG=100,NADJCC=700,
 5.      NPAR=260,NSTREL=100,
 6.      NELPAR=400,IFITEN=3, IFREB=1,
 7.      ISTRUC=1,
 8.      IGEOM=-1,LMAGNT=0,IFRES=1,
 9.      IMAX=16,JMAX=8,KMAX=20,NSURF=20,
10.       DX=0.167,0.217,0.109,0.109,0.109,0.166,4*0.222,4*0.285,0.05,0.285,
11.      DY = 8*0.2618,
12.      DZ=0.6096,0.6096,0.6096,0.3302,0.4064,0.7874,0.6096,0.889,0.9144,
13.         1.651,0.1333,0.1333,0.6604,5*0.6096,0.6858,0.1016,
14.      XNORML=0,-1,0,0,0,-1,0,0,0,0,-1,-1,0,0,0,0,-1,-1,1,0,-1.,
15.      YNORML=3*0,1,-1,3*0,-1,1,4*0,1,-1,0,0,0,0,0.,
16.      ZNORML=1,0,-1,0,0,0,-1,1,4*0,-1,1,0,0,0,0,0,-1,0.,
17.      &END
18.     REG      -1.0     1   10   1   8   1   1   1   BOTTOM WALL
19.     REG      -1.0    11   12   1   8   2   2   1   BOTTOM WALL
20.     REG      -1.0    13   15   1   8   3   3   1
21.     REG      -1.0    10   10   1   8   1   1   2   CORE STRC
22.     REG      -1.0    12   12   1   8   2   2   2   CORE SUPPORT STRUC
23.     REG      -1.0    15   15   1   8   3   4   2
24.     REG      -1.0    15   15   1   8   6  10   2
25.     REG      -1.0    15   15   1   8  14  20   2
26.     REG      -1.0     1   15   2   4  20  20   3   TOP WALL
27.     REG      -1.0     1   15   6   8  20  20   3
28.     REG      -1.0     1    7   1   1  20  20   3
29.     REG      -1.0     9   15   1   1  20  20   3
30.     REG      -1.0     1    8   5   5  20  20   3
31.     REG      -1.0    10   15   5   5  20  20   3
32.     REG      -1.0     1   10   1   1   1   1   4
33.     REG      -1.0     1   12   1   1   2   2   4
34.     REG      -1.0     1   15   1   1   3  20   4
35.     REG      -1.0     1   10   8   8   1   1   5
36.     REG      -1.0     1   12   8   8   2   2   5
37.     REG      -1.0     1   15   8   8   3  20   5
38.     REG      0.1393  12   12   2   2   5   5   6   INLET 1
39.     REG      0.0464  13   15   2   2   4   4   7   INLET HOR SIDE
40.     REG      -1.0    13   15   2   2   6   6   8   INLET HOR SIDE
41.     REG      -1.0    13   15   1   1   5   5   9   INLT TANGENT FACE
42.     REG      -1.0    13   15   3   3   5   5  10   INLT TANGENT FACE
43.     REG      -1.0    15   15   1   1   5   5  11   CORE STRUCTURE
44.     REG      -1.0    15   15   3   8   5   5  11
45.     REG      0.3972  16   16   4   4  13  13  12   OUTLET
46.     REG      -1.0    16   16   4   4  13  13  13   OUTLT
47.     REG      -1.0    16   16   4   4  13  13  14   OUTLT HOR FACE
48.     REG      -1.0    16   16   4   4  13  13  15   OUTLET TANGENT FACE
49.     REG      -1.0    16   16   4   4  13  13  16
50.     REG      -1.0    15   15   1   3  13  13  17
51.     REG      -1.0    15   15   5   8  13  13  17
52.     REG      -1.0    15   15   1   8  11  12  18     SIDE INLET
53.     REG      -1.0     1    1   1   8   1  20  19    ORIGIN
54.     REG      -1.0     8    8   1   1  20  20  20
55.     REG      -1.0     9    9   5   5  20  20  20
56.     END
57.      &DATA
58.      EPS5=2.0E-6,IT=1,ITMAXP=200,ITIBUG=1,
59.       IBOIL  =  0 , IDDDP = 0, IDRAG=0,IDTIME=1,
```

```
      IFENER=1,IFPROP=0,
       IFROD=0,INIT=0,
       ISTATE=0,ISWEEP=0,
       ITIMER=0,
       IXNBUG=0,
      IXREB=0, IYREB=0, IZREB=0,
      IENBUG=0,
      HYDALL=2.911,HYDIN=2.911, HYDOUT=2.911,
      CMJ1  = 0.0, CEL1=0.0,
      CDRAGX = 1.0 , CDRAGY=1.0, CDRAGZ=1.0,
      AO = 0.5 , BO=0.0,
      TREST=50.0, TSTART=0.0,
      VELOC=2*0.0,0.00,0.0,0.0,2*3.043,4*0.0,2.040,4*0.0,0.0,0.0,0.0,0.0,0.0,
      KFLOW=3*1,-3,-3,6*1,-5,6*1,-3,1,
      TEMP = 20*360.0,
      KTEMP=2*400,400,400,400,1,1,10*400,400,400,400,
      PRES=20*0.0,
      KPRES=20*0,DPDX=0.0,DPDY=0.0,DPDZ=0.0,
      EPS1=0.0001,EPS2=1.0E-06,EPS3=1.0E-5,
      NTHCON(1)=-1,
       RDTIME=50.0,
       NTMAX=300,TIMAX=3.6E7,
      PRES0 = 1.0135E5,
      XPRES0=3.053 , YPRES0=0.0, ZPRES0=8.0,
      GRAVX= 0.0 , GRAVY=0.0 , GRAVZ= -9.81,
      OMEGA = 1.3 , DLCUT= 0.5 , TEMP0= 360.0,
      OMEGAV=0.8,OMEGAE=0.8,
      TURBV = 0.0 , TURBC=0.0,
      CWIREX= 0.5 , CWIREY=0.5, CWIREZ=0.5,
       NTPRNT=-9999,
      ISTPR=1202,2202,3202,5202,
            1204,2204,3204,5204,
            15201,
      NTHPR=1202,2202,3202,5202,
            1204,2204,3204,5204,
           9202,17202,9204,17204,
      NCORR=15,
      CLENTH=14*-1.0,6.35E-3,2*-1.0,3*-1.0,
      REYLEN=0.010,9.374E-3,2*9.374E-3,2*8.71E-3,2*7.44E-3,2*8.128E-3,
             4*1.0,6.35E-3,5*1.0,
      ICORR=1,2,1,1,5,5,8,8,9,10,2*11,2*12,13,2*12,94,14,15
      ACORRL=1.844E6,1.4563E6,4.44E6,2.483E6,4.84E5,1.061E6,
             1.1469E4,7582.4,4.80E4,7.396E4,1.0E4,0.5,64.0,
             2.1321E4,3120.0,
      ACORRT=75.847,59.91,182.63,102.35,85.56,187.7,261.53,172.88,
             701.45,1080.4,1.0E4,0.5,0.3164,0.0,0.0
      BCORRL=-1.479,-1.479,-1.479,-1.479,-1.259,-1.259,-0.5832,-0.5832,
              -0.1,-0.1,2*0.0,-1.0,0.0,0.0,
      BCORRT=-.1085,-.1085,-.1085,-.1085,-.09954,-.09954,-.1005,-.1005,
              -0.02929,-0.02929,2*0.0,-0.25,0.0,0.0,
      CCORRL=15*0.0,
      CCORRT=15*0.0,
      REYTRN=4*1585.0,4*2228.0,2*0.0,2*1.0E10,2000.0,2*1.0E10,
      FORCEF= 2*0.5,2*0.50,4*0.5,0.5,10.0,4*1.0,0.5,1.0,1000.0,3*1.0,
      NREBRT=6,IREBIT=10,NREBM=525,200,120,120,120,1200,
      NREBX=0,0,0,0,0,1,NREBZ=8,120,120,120,120,0,
      NMATER=2,C0K=2.3,23.0,C1K=0.0,0.0,
      C0RO=1.0,7687.0,C0CP=2.85E6,577.0,
      C1CP=500.0,CK=10*1.0,
      NHEATC=2,HEATC1(2)=1.0,HEATC2(2)=0.0,HEATC3(2)=0.0,
```

```
 120.      &END
 121.        1   1  10   1   8   1   1     REGION 1
 122.        1   1  12   1   8   2   2
 123.        1   1  15   1   8   3   4
 124.        1   7  12   1   8   5   5
 125.        1  11  15   1   8   6   6
 126.        1  13  15   1   1   5   5
 127.        1  13  15   3   8   5   5
 128.        2   1  10   1   8   6   6     REGION 2
 129.        2   1  15   1   8   7   7
 130.        3   1  15   1   8   8   8     REGION 3
 131.        4   1  15   1   8   9   9     REGION 4
 132.        5   1  15   1   8  10  10     REGION 5
 133.        6   1  15   1   8  11  20     REGION 6
 134.        6  15  15   4   4  13  13     NREBX
 135.        1   8   9   1   1   5   5     NREBZ 1
 136.        1   8   9   3   3   5   5
 137.        1   8   9   5   5   5   5
 138.        1   8   9   7   7   5   5
 139.        2   1  15   1   8   7   7     NREBZ 2
 140.        3   1  15   1   8   8   8     NREBZ 3
 141.        4   1  15   1   8   9   9
 142.        5   1  15   1   8  10  10     NREBZ 5
 143.      FORC
 144.      ZFOR   1   1   1   5   8   7   7      CORE1
 145.      ZFOR   2   1   1   1   4   7   7
 146.      ZFOR   3   2   2   1   4   7   7       CORE2
 147.      ZFOR   4   2   2   5   8   7   7       CORE2
 148.      ZFOR   5   3   3   1   4   7   7       CORE3
 149.      ZFOR   6   3   3   5   8   7   7       CORE4
 150.      ZFOR   7   4   4   1   2   7   7       CORE4
 151.      ZFOR   8   4   4   3   8   7   7       CORE4
 152.      ZFOR   9   5   5   1   8   7   7
 153.      ZFOR  10   6   6   1   8   7   7
 154.      ZFOR  11   7  10   1   8   7   7
 155.      ZFOR  12  11  14   1   8   7   7     IVS
 156.      XFOR  13   6   6   1   8   6   6     STRAINER
 157.      ZFOR  14   7  14   1   8  10  10     BAFFLE
 158.      ZFOR  15   5   6   1   8   8  10     REFL
 159.      ZFOR  16   8   9   1   8   5   5       CB INLET
 160.      XFOR  17   1   6   1   8  11  11       ABOVE CORE
 161.      ZFOR  18   1   4   1   8   8  10
 162.      XFOR  19  14  14   1   8  11  11
 163.      XFOR  20  14  14   1   8  20  20
 164.      END
 165.       &STRUCT
 166.       NSTRUC=58,
 167.       NTSEL=6*1,22*1,4*3,6*1,12*1,6*3,2*10,
 168.       NTSMAT=6*1,14*2,8*1,4*1,6*1,12*1,6*1,2*1,
 169.       OUTR=4*0.00292,2*0.0127,14*0.00292,8*0.0127,0.1345,0.1488,
 170.            0.1619,0.1740,4*0.00292,2*0.0127,12*0.0221,0.167,0.384,
 171.             0.493,0.602,0.711,0.877,0.659,0.729,
 172.       RODFR=63.3,190.0,162.75,244.1,33.62,59.41,63.3,63.3,217,217,
 173.             162.75,162.75,108.5,108.5,217,217,271.25,271.25,
 174.             162.75,271.25,4*33.62,4*59.41,4*1.0,63.3,190.0,
 175.             162.75,253.1,33.62,59.41,
 176.             0.875,3.75,4.5,5.25,
 177.             0.875,3.75,4.5,5.25,
 178.             0.875,3.75,4.5,5.25,
 179.             6*0.125,2*0.333,
```

```
180.      IHTSTR=58*1,
181.      HYDRAD=4*0.00292,2*0.0127,
182.             14*0.00292,8*0.0127,0.1345,0.1488,0.1619,0.1740,4*0.00292,
183.             2*0.0127,12*0.0221,0.167,0.384,0.493,0.602,0.711,0877,
184.             0.659,0.729,
185.      IXYZ=58*3,
186.      NTSADJ=6*8,2*4,20*2,4*8,6*8,12*8,6*8,2*3,
187.      MATERL=6*1,2,1,2,1,2,1,2,1,2,1,2,1,2,1,2,1,2,1,2,1,
188.             2,1,2,1,2,1,2,1,
189.             38*1,
190.      NMPAR=6*5,2,3,2,3,2,3,2,3,2,3,2,3,2,3,2,3,2,3,2,3,
191.             2,3,2,3,2,3,2,3,
192.             12*5,4*2,2*5,12*5,6*1,2*5,
193.      DRPAR=4*5.84E-4,2*0.00254,1.905E-4,8.21267E-4,1.905E-4,8.21267E-4,
194.            1.905E-4,8.21267E-4,1.905E-4,8.21267E-4,
195.            1.905E-4,8.21267E-4,1.905E-4,8.21267E-4,
196.            1.905E-4,8.21267E-4,1.905E-4,8.21267E-4,
197.            1.905E-4,8.21267E-4,1.905E-4,8.21267E-4,
198.            1.905E-4,8.21267E-4,1.905E-4,8.21267E-4,
199.            1.905E-4,8.21267E-4,1.905E-4,8.21267E-4,
200.           8*0.00254,0.0269,0.02976,0.03238,0.0348,
201.           4*5.84E-4,2*0.00254,12*0.0044,6*0.001,0.1318,0.1458,
202.      NGAPTY=1,SGAP=7.622E-5,HGAP=7297,IGAP=14*1,44*0,
203.      QSPAR=6*0.0,1.079E8,1.748E9,
204.            1.139E8,1.740E9,
205.            9.19E7,1.493E9,1.15E8,1.435E9,
206.            9.835E7,1.604E9,9.858E7,1.610E9,
207.            8.419E7,1.446E9,8.350E7,1.438E9,
208.            8.793E7,1.438E9,9.358E7,1.504E9,
209.            7.000E7,1.148E9,6.910E7,1.145E9,
210.            6.330E7,1.067E9,7.544E7,1.214E9,
211.            1.3626E7,1.357E7,1.247E7,1.21E7,
212.            3.219E6,4.144E6,4.528E6,4.095E6,30*0.0,
213.            NTSAD2=50*0,6*8,2*0,
214.            HYDRA2=50*0.0,6*0.1206,2*0.0,
215.            IHTST2=50*1,6*2,2*1,
216.      &END
217.        1   1   1   1   8   8   8
218.        2   2   2   1   8   8   8
219.        3   3   3   1   8   8   8
220.        4   4   4   1   8   8   8
221.        5   5   5   1   8   8   8
222.        6   6   6   1   8   8   8
223.        7   1   1   5   8   9   9
224.        8   1   1   1   4   9   9
225.        9   2   2   5   6   9   9
226.       10   2   2   7   8   9   9
227.       11   2   2   1   2   9   9
228.       12   2   2   3   4   9   9
229.       13   3   3   5   6   9   9
230.       14   3   3   7   8   9   9
231.       15   3   3   1   2   9   9
232.       16   3   3   3   4   9   9
233.       17   4   4   5   6   9   9
234.       18   4   4   7   8   9   9
235.       19   4   4   1   2   9   9
236.       20   4   4   3   4   9   9
237.       21   5   5   1   2   9   9
238.       22   5   5   3   4   9   9
239.       23   5   5   5   6   9   9
```

240.	24	5	5	7	8	9	9	
241.	25	6	6	1	2	9	9	
242.	26	6	6	3	4	9	9	
243.	27	6	6	5	6	9	9	
244.	28	6	6	7	8	9	9	
245.	29	7	7	1	8	8	10	
246.	30	8	8	1	8	8	10	
247.	31	9	9	1	8	8	10	
248.	32	10	10	1	8	8	10	
249.	33	1	1	1	8	10	10	
250.	34	2	2	1	8	10	10	
251.	35	3	3	1	8	10	10	
252.	36	4	4	1	8	10	10	
253.	37	5	5	1	8	10	10	
254.	38	6	6	1	8	10	10	
255.	39	1	1	1	8	8	8	
256.	40	2	2	1	8	8	8	
257.	41	3	3	1	8	8	8	
258.	42	4	4	1	8	8	8	
259.	43	1	1	1	8	9	9	
260.	44	2	2	1	8	9	9	
261.	45	3	3	1	8	9	9	
262.	46	4	4	1	8	9	9	
263.	47	1	1	1	8	10	10	
264.	48	2	2	1	8	10	10	
265.	49	3	3	1	8	10	10	
266.	50	4	4	1	8	10	10	
267.	51	2	2	1	8	8	10	1
268.	51	1	1	1	8	8	10	2
269.	52	3	3	1	8	8	10	1
270.	52	2	2	1	8	8	10	2
271.	53	4	4	1	8	8	10	1
272.	53	3	3	1	8	8	10	2
273.	54	5	5	1	8	8	10	1
274.	54	4	4	1	8	8	10	2
275.	55	6	6	1	8	8	10	1
276.	55	5	5	1	8	8	10	2
277.	56	7	7	1	8	8	10	1
278.	56	6	6	1	8	8	10	2
279.	57	6	6	1	1	11	11	
280.	57	8	8	1	1	11	11	
281.	57	7	7	2	2	11	11	
282.	57	6	6	1	1	12	12	
283.	57	8	8	1	1	12	12	
284.	57	7	7	2	2	12	12	
285.	57	6	6	1	1	13	13	
286.	57	8	8	1	1	13	13	
287.	57	7	7	2	2	13	13	
288.	57	6	6	1	1	14	14	
289.	57	8	8	1	1	14	14	
290.	57	7	7	2	2	14	14	
291.	57	6	6	1	1	15	15	
292.	57	8	8	1	1	15	15	
293.	57	7	7	2	2	15	15	
294.	57	6	6	1	1	16	16	
295.	57	8	8	1	1	16	16	
296.	57	7	7	2	2	16	16	
297.	57	6	6	1	1	17	17	
298.	57	8	8	1	1	17	17	
299.	57	7	7	2	2	17	17	

```
300.      57   6   6   1   1  18  18
301.      57   8   8   1   1  18  18
302.      57   7   7   2   2  18  18
303.      57   6   6   1   1  19  19
304.      57   8   8   1   1  19  19
305.      57   7   7   2   2  19  19
306.      57   6   6   1   1  20  20
307.      57   8   8   1   1  20  20
308.      57   7   7   2   2  20  20
309.      58   7   7   5   5  11  11
310.      58   9   9   5   5  11  11
311.      58   8   8   6   6  11  11
312.      58   7   7   5   5  12  12
313.      58   9   9   5   5  12  12
314.      58   8   8   6   6  12  12
315.      58   7   7   5   5  13  13
316.      58   9   9   5   5  13  13
317.      58   8   8   6   6  13  13
318.      58   7   7   5   5  14  14
319.      58   9   9   5   5  14  14
320.      58   8   8   6   6  14  14
321.      58   7   7   5   5  15  15
322.      58   9   9   5   5  15  15
323.      58   8   8   6   6  15  15
324.      58   7   7   5   5  16  16
325.      58   9   9   5   5  16  16
326.      58   8   8   6   6  16  16
327.      58   7   7   5   5  17  17
328.      58   9   9   5   5  17  17
329.      58   8   8   6   6  17  17
330.      58   7   7   5   5  18  18
331.      58   9   9   5   5  18  18
332.      58   8   8   6   6  18  18
333.      58   7   7   5   5  19  19
334.      58   9   9   5   5  19  19
335.      58   8   8   6   6  19  19
336.      58   7   7   5   5  20  20
337.      58   9   9   5   5  20  20
338.      58   8   8   6   6  20  20
339.    END
340.    TL    360.0        1  15   1   8   1   7
341.    TL    527.0        1  15   1   8  11  20
342.    TL    527.0        1   6   1   3   8  10
343.    TL    360.0        7  15   1   8   8  10
344.    ALZ   0.3533       1   1   1   8   7  10
345.    ALZ   0.2826       2   2   5   8   7  10
346.    ALZ   0.2120       2   2   1   4   7  10
347.    ALZ   0.3533       3   3   1   4   7  10
348.    ALZ   0.1765       3   3   5   8   7  10
349.    ALZ   0.3533       4   4   3   8   7  10
350.    ALZ   0.2120       4   4   1   2   7  10
351.    ALZ   0.0935       5   5   1   8   7  10
352.    ALZ   0.1266       6   6   1   8   7  10
353.    ALZ   0.015        7  10   1   8   7  10
354.    ALZ   0.010       11  14   1   8   7  10
355.    ALZ   0.006        7  14   1   8  10  10
356.    AL    0.3533       1   1   1   8   7  10
357.    AL    0.2826       2   2   5   8   7  10
358.    AL    0.2120       2   2   1   4   7  10
359.    AL    0.1765       3   3   5   8   7  10
```

360.	AL	0.3533	3	3	1	4	7	10	
361.	AL	0.3533	4	4	3	8	7	10	
362.	AL	0.2120	4	4	1	2	7	10	
363.	AL	0.0935	5	5	1	8	7	10	
364.	AL	0.1266	6	6	1	8	7	10	
365.	AL	0.015	7	10	1	8	8	10	
366.	AL	0.010	11	14	1	8	8	10	
367.	ALX	0.0	1	6	1	8	7	7	
368.	ALY	0.0	1	6	1	8	7	7	
369.	ALX	0.0	1	10	1	8	8	10	
370.	ALY	0.0	1	10	1	8	8	10	
371.	ALX	0.1237	6	6	1	8	6	6	
372.	ALX	0.0	6	6	1	8	7	7	
373.	ALZ	0.8466	8	9	1	1	5	5	C BASKET INLET
374.	ALZ	0.8466	8	9	3	3	5	5	
375.	ALZ	0.8466	8	9	5	5	5	5	
376.	ALZ	0.8466	8	9	7	7	5	5	
377.	ALZ	0.0	8	9	2	2	5	5	C B INLET
378.	ALZ	0.0	8	9	4	4	5	5	C B INLET
379.	ALZ	0.0	8	9	6	6	5	5	C B INLET
380.	ALZ	0.0	8	9	8	8	5	5	C B INLET
381.	ALZ	0.0	7	7	1	8	5	5	C B INLET
382.	ALZ	0.0	10	10	1	8	5	5	C B INLET
383.	ALZ	0.0	1	6	1	8	4	4	LPLNM WALL
384.	ALZ	0.0	1	6	1	8	5	5	LPLNM WALL
385.	ALZ	0.0	11	15	1	8	6	6	CSS
386.	ALX	0.0	10	10	1	8	6	6	CSS WALL
387.	ALX	0.0	6	6	1	8	5	5	LPLNM SIDE WALL
388.	AL	0.4190	1	4	1	8	11	13	IT IN UPPER PLNM
389.	AL	0.9145	1	4	1	8	15	20	FLOW TUBES
390.	AL	0.9145	1	4	1	8	14	14	FLOW TUBES
391.	ALZ	0.9145	1	4	1	8	14	14	FLOW TUBES
392.	ALZ	0.9145	1	4	1	8	14	20	FLOW TUBES
393.	ALZ	0.940	5	6	1	8	14	20	FLOW TUBES
394.	AL	0.940	5	6	1	8	14	20	FLOW TUBES
395.	AL	0.4428	5	6	1	8	11	13	FLOW TUBES
396.	ALX	0.0	1	6	1	8	12	13	IT OVER CORE
397.	ALX	0.1818	1	6	1	8	11	11	OPEN GAP
398.	ALY	0.0	1	6	1	8	11	13	IT OVER CORE + RFL
399.	ALZ	0.4190	1	4	1	8	11	13	IT OVER CORE
400.	ALZ	0.4428	5	6	1	8	11	13	IT OVER RFL
401.	ALX	0.0	7	8	1	1	12	20	IT STEM
402.	ALY	0.0	8	8	1	1	12	20	
403.	ALY	0.5	9	9	1	1	12	20	
404.	ALZ	0.0	8	8	1	1	12	20	
405.	ALZ	0.5	9	9	1	1	12	20	
406.	AL	1.0	8	8	1	1	12	20	
407.	AL	0.5	9	9	1	1	12	20	
408.	ALZ	0.0	9	9	5	5	13	20	IVHM STEM
409.	AL	1.0	9	9	5	5	13	20	
410.	ALX	0.0	8	9	5	5	13	20	IVHM STEM
411.	ALY	0.0	9	9	4	5	13	20	
412.	ALZ	0.5570	10	10	5	5	13	13	CELL 8 OF IVHM
413.	AL	0.966	10	10	5	5	13	13	
414.	ALX	0.945	10	10	5	5	13	13	IVHM BOTTOM PLATE CELL 8
415.	ALY	0.903	10	10	4	5	13	13	
416.	ALZ	0.5186	11	11	5	5	13	13	IVHM TOE ASSY
417.	AL	0.778	11	11	5	5	13	13	
418.	ALX	0.5717	11	11	5	5	13	13	
419.	ALY	0.2493	11	11	4	5	13	13	

```
420.     ALZ     0.8       11  11   5   5  14  20    IVHM TOE ASSY
421.     AL      0.8       11  11   5   5  14  20
422.     ALX     0.6186    11  11   5   5  14  20
423.     ALY     0.3315    11  11   4   5  14  20
424.     ALZ     0.422      1   3   1   8  14  14     IT.TUBES
425.     ALZ     0.422      4   6   1   8  15  15
426.     ALZ     0.2647     7   7   1   1  15  20
427.     AL      0.2647     7   7   1   1  15  20
428.     ALZ     0.0        1  13   1   8  19  19      SUPPR PLATE
429.     ALZ     0.018     14  14   1   8  19  19      SUPPR PLATE
430.     ALX     0.0       14  14   1   8   8  19      SOLID WALL
431.     ALX     0.1       14  14   1   8  11  11      BOTT INJ
432.     ALX     0.1       14  14   1   8  20  20      TOP INJ
433.     ALX     1.0       14  14   4   4  13  13      OUTLET
434.     ALZ     0.0       15  15   4   4  12  12      OUTLET
435.     ALZ     0.0       15  15   4   4  13  13
436.     ALY     0.0       15  15   4   4  13  13
437.     ALY     0.0       15  15   3   3  13  13      OUTLET
438.     ALX     0.0       13  13   1   8  20  20      BLOCKED S P
439.     END
```

5. EVALUATION OF THERMOCOUPLE TEMPERATURES FROM CALCULATED FLUID TEMPERATURES

The thermocouple temperatures differ from the fluid temperatures because of the thermal inertia of the thermocouples. The calculated fluid temperatures have been used to evaluate the implied thermocouple temperatures by solving the following (first order) differential equation.

$$mC_p \frac{dT_{TC}}{dt} = hA(T_F - T_{TC}) \tag{1}$$

where

mC_p = Thermal capacity of the thermocouple,

h = Heat transfer coefficient,

A = Surface area,

T_F = Temperature of the fluid, and

T_{TC} = Temperature of the thermocouple.

For fixed T_F, the solution to Eq. 1 is

$$T_{TC} = T_F(1 - e^{-t/\tau})$$

where $\tau = \frac{mC_p}{hA}$ is the response time.

For time varying T_F however, we have to numerically integrate Eq 1. A simple differencing in time was used to obtain

$$T_{TC}^{n+1} = \frac{T_{TC}^{n} + \Delta t \left(\frac{hA}{mC_p} T_F^{n+1}\right)}{1 + \Delta t \left(\frac{hA}{mC_p}\right)} \tag{2}$$

Given T_F^{n+1} from COMMIX calculations, T_{TC}^{n+1} was evaluated with starting conditions as $T_{TC}^{o} = T_F^{o}$ = steady state value. Δt is the time step. The value of mC_p/hA was taken to be 10 secs.

ACKNOWLEDGMENT

We are indebted to Drs. R. Stover, W. T. Nutt, and H. Johnson of Westinghouse Hanford Engineering Development Laboratory for their help in providing information on the FFTF. We are also indebted to Drs. R. T. Curtis and C. N. Kelber and Mr. P. M. Wood of the U. S. Nuclear Regulatory Commission for their support, without which this work would not have been possible.

REFERENCES

1. S. P. Vanka, H. M. Domanus, and W. T. Sha, "COMMIX-1A Three-Dimensional Invessel Simulation of the FFTF Thermal Hydraulics," NUREG/CR-2535, ANL-CT-82-1 (1982).

2. W. T. Sha, H. M. Domanus et al., "COMMIX-1: A Three-Dimensional Transient Single-Phase Component Computer Program for Thermal Hydraulic Analysis," NUREG/CR-0785, ANL-77-96 (Sept 1978).

3. W. T. Sha, "An Overview on Rod-Bundle Thermal-Hydraulic Analysis," Nucl. Eng. Des. 62, (Dec 1980).

4. Experimental data supplied by HEDL to Argonne National Laboratory, W. T. Sha. Letter from J. Ziff to W. T. Sha, dated April 28, 1981.

5. Harry Johnson to S. P. Vanka and W. T. Sha. Personal Communications (1981).

6. "FFTF Final Safety Analysis Report," Hanford Engineering Development Laboratory (1975).

7. F. H. Harlow and A. A. Amsden, "Numerical Calculation of Multiphase Fluid Flow," J. Comp. Phys. 17, 19-52 (1975).

8. Private Communications with Drs. R. Stover, W. T. Nutt, and H. Johnson of HEDL, 19(80-81).

Distribution for NUREG/CR-2773 (ANL-CT-82-14)

Internal:

E. S. Beckjord
C. E. Till
R. S. Zeno
P. R. Huebotter
G. S. Rosenberg
W. L. Baumann
B. C. Chen
T. H. Chien
H. M. Domanus
C. C. Miao
R. C. Schmitt
W. T. Sha (6)
V. L. Shah
S. P. Vanka
M. Weber
P. B. Abramson
F. E. Dunn
D. R. Ferguson
H. H. Hummel
D. Mohr
R. M. Singer
ANL Contract File
ANL Libraries (2)
TIS Files (4)
ANL Patent Dept

External:

NRC, for distribution per R7 (275)
DOE-TIC (2)
Manager, Chicago Operations Office, DOE
President, Argonne Universities Association
Components Technology Division Review Committee:
A. A. Bishop, U. of Pittsburgh, Pittsburgh, Pa. 15261
F. W. Buckman, Consumers Power Co., 1945 Parnall Rd., Jackson, Mich. 49201
R. Cohen, Purdue U., West Lafayette, Indiana 47907
R. A. Greenkorn, Purdue U., West Lafayette, Indiana 47907
W. M. Jacobi, Westinghouse Electric Corp., Pittsburgh, Pa. 15230
E. E. Ungar, Bolt Beranek and Newman Inc., 50 Moulton St., Cambridge, MA 02138
J. Weisman, U. of Cincinnati, Cincinnati, Ohio 45221
K. Absher, Richland Operations Office, USDOE, Richland, Washington 99352
S. S. Chang, Hanford Engineering Development Lab., P. O. Box 1970, Richland, Washington 99352
M. H. Cooper, Westinghouse Advanced Reactors Div., P. O. Box 158, Madison, Pennsylvania 15663
A. E. Dubberley, General Electric Co., c/o Argonne National Laboratory
G. Drucker, Atomics International, 8900 DeSoto Ave., Canoga Park, California 91303
J. A. Ford, Office of Reactor Research and Technology, USDOE, Washington
F. X. Gavigan, Office of Reactor Research and Technology, USDOE, Washington
E. L. Gluekler, General Electric Co., 310 DeGuigne Dr., Sunnyvale, California 94086
J. Mangus, Westinghouse Advanced Reactors Div., P. O. Box 158, Madison, Pennsylvania 15663
J. C. Mills, Atomics International, 8900 DeSoto Ave., Canoga Park, California 91306
E. Moody, Atomics International, 8900 DeSoto Ave., Canoga Park, California 91303
E. H. Novendstern, Westinghouse Advanced Reactors Div., P. O. Box 158, Madison, Pennsylvania 15663
W. T. Nutt, Hanford Engineering Development Lab., P. O. Box 1970, Richland, Washington 99352
S. C. Rose, General Electric Co., 310 DeGuigne, Sunnyvale, California 94086
R. L. Stover, Hanford Engineering Development Lab., P. O. Box 1970, Richland, Washington 99352
J. L. Wantland, Oak Ridge National Lab., P. O. Box Y, Oak Ridge, Tennessee 37830